

University of Naples “FEDERICO II”



Department of Industrial Engineering – Aerospace Section  
Doctorate School in Industrial Engineering  
Ph.D. Course in Aerospace, Naval and Quality Engineering  
XXVII cycle

**Design of composite stiffened panels by new design  
criteria and progressive failure analysis**

Research Supervisor:

**Prof. Leonardo Lecce**

Candidate:

**Eng. Fulvio Romano**

Assistant Supervisor:

**Eng. Umberto Mercurio**

The Chairman of the Ph.D. School:

**Prof. Luigi de Luca**

---

Thesis submitted in March 2015

*To my parents Rosario  
and Silvana  
with love*

*To my wife Carmina  
and my children Silvana and Rosario  
with love*

## ACKNOWLEDGEMENTS

I would especially like to thank my corporate tutor **Eng. Umberto Mercurio** for giving me the opportunity to perform this research under his leadership. His wide technical experience, encouragement and support made this experience possible and successful and were very helpful for me throughout my time at CIRA (Italian Aerospace Research Centre).

I am also grateful to my academic tutor **Prof. Leonardo Lecce** for his availability in supporting this activity and for giving me great freedom in my scientific work carried out during these three years. I hope we will have further occasions to work together in the next future.

I wish to extend my thanks to my colleagues of the Italian Aerospace Research Centre, Francesco Di Caprio, Rosario Borrelli, Stefania Franchitti; they always encouraged and sustained me during my Ph.D. period.

Finally, on a more personal note, I wish to express my immense gratitude to all my family: to my parents Rosario and Silvana, for their unquestioning faith in me; to my wife Carmina, whose love and ever-lasting support made me possible to complete this work; to my children Silvana and Rosario, because I dedicated so much time to my research without spending it with them. I am proud to be a part of them and hope that I can make them proud, too.

# INDICE

1	INTRODUCTION.....	1
2	TRADITIONAL AND NEW DESIGN APPROACHES FOR COMPOSITE STRUCTURES ..	4
2.1	Current design practise and criticalities .....	4
2.1.1	Effect of damage .....	6
2.2	New design approaches and criteria for low weight .....	11
2.2.1	Design with SHM.....	11
2.2.2	Residual Strength prediction.....	13
2.2.3	Simplified design model and new criteria.....	15
3	LOW WEIGHT DESIGN USING INFORMATION GIVEN BY SHM SYSTEMS.....	19
3.1	Reference panels.....	19
3.1.1	Design requirements and criteria .....	21
3.1.2	Methodology .....	21
3.1.3	Material properties .....	22
3.1.4	Design of the reference panels .....	24
3.2	Weight sensitivity analysis by new design approach with SHM .....	24
3.2.1	Weight reduction evaluation without BVID knock-down factor.....	25
3.2.2	Weight reduction evaluation by several sensitivity levels of the SHM systems versus classical visual inspection .....	30
4	PROGRESSIVE FAILURE ANALYSIS METHODOLOGY .....	34
4.1	Nonlinear analysis .....	36
4.2	Failure analysis.....	39
4.3	Material degradation.....	41
4.4	Re-establishment of equilibrium .....	42
4.5	MSC Nastran <sup>®</sup> PFA capability .....	43
5	DISCRETE DAMAGE MODEL ANALYSIS .....	45
5.1	PFA of the panel critical at strength.....	45
5.1.1	FE Model validation.....	46
5.1.2	PFA for the panel with hole .....	50
5.2	Sensitivity of the total failure to damage density for the panel critical at strength.....	57
5.2.1	PFA results for the panels with one hole .....	59
5.2.2	PFA results for the panels with multi-hole maps.....	60
5.2.3	Resume of the PFA results.....	63

5.3	Influence of post-buckling on the total failure of the panel with discrete damages.....	66
5.3.1	Nonlinear and PFA results for the UDA panel .....	68
5.3.2	PFA results for the discrete damage model .....	71
5.3.3	Resume of the PFA results.....	80
6	CAI TESTS AND EQUIVALENCE HOLE-BVID.....	84
6.1	Test description and results .....	84
6.2	Numerical simulation by PFA.....	90
6.2.1	Residual strength of the impacted coupons.....	90
6.2.2	Residual strength of the open hole coupons.....	95
6.2.3	Hole size equivalent to the impact damage.....	98
7	INFLUENCE ON THE CAPABILITY OF A STIFFENED PANEL IN PRESENCE OF AN IMPACT DAMAGE OBTAINED ON CAI COUPON .....	101
7.1.1	Comparison impact damage – hole at panel level.....	104
7.1.2	Design at panel level .....	105
8	CONCLUSIONS AND FUTURE DEVELOPMENTS .....	110
	APPENDIX A: POST-BUCKLING ANALYSIS IN HYPERSIZER® .....	112
	BIBLIOGRAPHY .....	114

## List of Acronyms

ADL	Allowable Damage Limit
BUCK	Buckling
BVID	Barely Visible Impact Damage
CAI	Compression After Impact
CBI	Compression Before Impact
DA	Damaged
FPF	First Ply Failure
FE	Finite Element
FI	Failure Index
FE	Finite Element
FEA	Finite Element Analysis
FEM	Finite Element Method
FHC	Filled Hole Compression
FI	Failure Index
HS	Hypersizer <sup>®</sup>
L.L.	Limit Load
MS	Margin of Safety
NDI	Non Destructive Inspection
NL	Nonlinear
OHC	Open Hole Compression
QI	Quasi-Isotropic
SHM	Structural Health Monitoring
PFA	Progressive Failure Analysis
RTD	Room Temperature Dry
UDA	Undamaged
U.L.	Ultimate Load
TF	Total Failure
VID	Visible Impact Damage

## List of Figures

Figure 1: percentage of composite materials on airplanes .....	4
Figure 2: schematic diagram of building block tests for a fixed wing [1] .....	5
Figure 3: knock-down factors on design strains [3].....	6
Figure 4: sensitivity of compression strength of composites to various types of damage [4] .....	7
Figure 5: schematic diagram showing design load levels versus categories of damage severity [1]....	9
Figure 6: Category 1 description [1] .....	9
Figure 7: large aircraft wing box – typical upper skin thickness distribution (mm).....	10
Figure 8: higher compressive strain design allowable by SHM .....	13
Figure 9: progressive failure analysis of an impact damaged stiffened panel .....	14
Figure 10: discrete damage map .....	14
Figure 11: equivalence between 6.35 mm hole and BVID .....	16
Figure 12: scheme of the current and of the simplified design approach and analysis.....	18
Figure 13: wing box example.....	20
Figure 14: locations of the panels (a); panel section (b).....	20
Figure 15: panel dimensions and loads .....	20
Figure 16: Hypersizer <sup>®</sup> software.....	22
Figure 17: lamina material properties .....	23
Figure 18: panel 1 reference baseline .....	24
Figure 19: panel 2 reference baseline .....	24
Figure 20: panel 1 redesign – weight saving analysis.....	26
Figure 21: panel 1 redesign with a weight reduction of 24.45% .....	27
Figure 22: panel 2 redesign – weight saving analysis.....	28
Figure 23: panel 2 redesign with a weight reduction of 3% .....	29
Figure 24: increment of the compressive design value for the weight reduction evaluation.....	30
Figure 25: panel 1 – weight vs compressive design value.....	31
Figure 26: panel 2 – weight vs compressive design value.....	31
Figure 27: panel 1 – weight vs compressive design value considering also CAI knock-down factor .....	33
Figure 28: flowchart of a typical Progressive Failure Analysis.....	35
Figure 29: basic concept of nonlinear analysis .....	37
Figure 30: Newton Raphson method .....	39
Figure 31: post-failure degradation behaviour in composite laminate [15].....	42
Figure 32: reference panel critical at strength (panel 1) .....	46

Figure 33: FE model of the panel.....	46
Figure 34: Reaction vs Applied Strain – Linear and Nonlinear analysis – Hypersizer <sup>®</sup> results.....	48
Figure 35: Reaction vs Applied Strain – PFA and Nonlinear analysis.....	49
Figure 36: FE model of the panel with one hole in the middle of the central stringer bay.....	50
Figure 37: Reaction vs Applied Strain – panel with hole in the middle of the central stringer bay ..	51
Figure 38: progressive failure of the panel UDA_1H.....	52
Figure 39: Reaction vs Applied Strain – PFA – panel with hole and DA panel.....	53
Figure 40: panel 1H vs DA panel.....	54
Figure 41: OHC test simulation – failure strain vs W/D for different layups.....	54
Figure 42: reference panel – W/D ratio .....	55
Figure 43: total failure of the stiffened panel on the base of OHC test .....	56
Figure 44: total failure – reference panel (6 stringers) vs panel with 2 stringers .....	56
Figure 45: schemes of the hole locations .....	58
Figure 46: Reaction vs Applied Strain – panels with all the hole locations 1H .....	60
Figure 47: Reaction vs Applied Strain – panels with 3 holes .....	61
Figure 48: Reaction vs Applied Strain – panels with 3 holes, 5 holes, and 7 holes .....	62
Figure 49: collapse of the panel 5H – without deformed shape.....	62
Figure 50: total failure of all the panel configurations.....	64
Figure 51: total failure of all the panels vs design allowable obtained at coupon level .....	65
Figure 52: design considerations.....	65
Figure 53: panel geometry and boundary conditions.....	66
Figure 54: FE model of the UDA panel.....	67
Figure 55: UDA panel – linear buckling analysis: first mode. ....	68
Figure 56: Reaction vs Applied Strain – UDA panel – Linear and Nonlinear analysis .....	69
Figure 57: Reaction vs Applied Strain – UDA panel – Nonlinear analysis and PFA.....	70
Figure 58: deformed panel at the collapse point. Displacements (left side) and damaged elements (right side) contour plot.....	71
Figure 59: schemes of the hole locations .....	72
Figure 60: FE models of the UDA panel with a single hole .....	73
Figure 61: Reaction vs Applied Strain – panel with hole 1Hc.....	74
Figure 62: progressive failure of the panel with hole 1Hc (without deformed shape) .....	75
Figure 63: progressive damage around the hole – panel with hole 1Hc.....	75
Figure 64: deformed panel at the collapse point. Displacements (left side) and damaged elements (right side) contour plot.....	76
Figure 65: Reaction vs Applied Strain – panels with all the hole locations 1H .....	77

Figure 66: Reaction vs Applied Strain – panels with 3 holes .....	79
Figure 67: collapse of the panel 3H3 – without deformed shape.....	79
Figure 68: Reaction vs Applied Strain – panels with 3 holes and 5 holes .....	80
Figure 69: total failure of all the panel configurations.....	82
Figure 70: total failure of all the panels vs design allowable obtained at coupon level .....	83
Figure 71: design considerations.....	83
Figure 72: coupon dimensions (mm) and sketch of the impact test.....	85
Figure 73: impact machine and fixture .....	86
Figure 74: MTS 810 servo hydraulic testing machine.....	86
Figure 75: sketch of the CAI test (dimensions in mm).....	87
Figure 76: CAI coupon before impact and with the hole.....	87
Figure 77: 28-ply laminate – impact test at 50 joule.....	89
Figure 78: 28-ply laminate – C-SCAN image, impact at 50 joule.....	89
Figure 79: 28-ply laminate – open hole CAI coupon after compression test .....	90
Figure 80: laminate 28-ply – FE model of the impacted coupon at 50 joule.....	91
Figure 81: laminate 28-ply – numerical damage envelop at 50 joule.....	92
Figure 82: laminate 28-ply – numerical damage envelops at 50 joule for the different failure modes .....	93
Figure 83: boundary conditions for the numerical simulation of the CAI test .....	94
Figure 84: Reaction vs Applied Strain – laminate 28-ply impacted at 50 joule .....	95
Figure 85: laminate 28-ply – FE model of the coupon with hole 6.35 mm in diameter.....	96
Figure 86: Reaction vs Applied Strain – laminate 28-ply with hole 6.35 mm .....	97
Figure 87: laminate 28-ply with hole 6.35 mm – progressive damage.....	98
Figure 88: hole diameters investigated .....	99
Figure 89: Reaction vs Applied Strain – laminate 28-ply with holes vs 50 joule impact test .....	100
Figure 90: 50 joule impact damage introduction into 2-stringer skin panel .....	101
Figure 91: 2-stringer panel.....	102
Figure 92: FE model of the 2-stringer panel with 50 joule impact damage.....	102
Figure 93: 2-stringer panel – damaged elements .....	103
Figure 94: 2-stringer panel with central hole 25.4 mm in diameter.....	103
Figure 95: Reaction vs Applied Strain – 2-Stringer panel – impact damage vs hole 25.4 mm .....	105
Figure 96: design implications for the 2-stringer panel .....	106
Figure 97: scheme of the impact damage locations .....	107
Figure 98: FE models – different damage locations .....	108
Figure 99: Reaction Force vs Applied Strain – for different damage locations .....	109

Figure 100: typical load-strain curve for nonlinear analysis in post-buckling regime ..... 112  
Figure 101: effective width of the panel ..... 113  
Figure 102: effective width of the panel vs load..... 113

## List of Tables

Table 1: summary of the most critical values of the Total Failure load for the different damage scenarios.....	63
Table 2: comparison between the most critical values of the Total Failure load for the different damage scenarios .....	63
Table 3: UDA panel – linear buckling and failure analysis results .....	67
Table 4: summary of the most critical values of the Total Failure load for the different damage scenarios.....	80
Table 5: comparison between the most critical values of the Total Failure load for the different damage scenarios .....	81
Table 6: compression test results at RTD .....	88
Table 7: laminate 28-ply impacted at 50 joule – numerical TF vs experimental TF.....	95
Table 8: laminate 28-ply with hole 6.35 mm – numerical TF vs experimental TF .....	97
Table 9: numerical TF of notched CAI coupons vs 50 joule impact test.....	100
Table 10: 2-Stringer panel – TF load comparison .....	105

## 1 INTRODUCTION

Composite materials have been increasingly used in aerospace applications over the last three decades. The use of composite materials is very attractive because of their outstanding strength, stiffness, and light-weight properties. An additional advantage of using composites is the ability to tailor the stiffness and strength to specific design loads. But the fulfilment of these advantages is often compromised by certification constraints that, due to the lack of knowledge about the real mechanical behaviour of composite structures during their operative life, *are more restrictive and conservative than those ones of metallic materials*. The *traditional design approach* applied by the civil aircraft manufacturers, in order to satisfy the current certification requirements of composite structures (EASA AMC 20-29, [1]), is prevalently based on

- First Ply Failure criteria (FPF),
- no damage growth,
- no-buckling onset up to the ultimate design loads,
- etc.

Due to the high sensitivity to damage and defects, in particular low energy impact damage (*BVID, Barely Visible Impact Damage*), the full potential of composite materials is not exploited resulting in increased structural mass.

*New appropriate design approaches and criteria are necessary* in order to *exploit the effective potential and benefits of composite materials for aircraft applications*. Investigations on the buckling and post-buckling behaviour, damage onset and its propagation, and investigations also on the possible benefits of using Structural Health Monitoring (SHM) systems, are important issues to assure at the same time the structural integrity of this kind of structures and significant weight reductions, with respect to the composite structures obtained by the traditional design.

Currently there is a wide consciousness of the conservatism of the traditional design, and this work has been focused on the evaluation of the amount of the weight reduction potentially achievable releasing the traditional limitations and constraints of the traditional design.

The objective of this work is the investigation of a new design methodology for the design of composite stiffened panels aiming to reduce the conservatism of the traditional design and to obtain lighter structures respect to the current ones. This methodology is based on the assumption of the presence of *SHM* systems, and on the application of the *progressive failure analysis (PFA)* methodology, that can allow to release some of the traditional design criteria.

With reference to a typical regional aircraft wing box (EASA CS-25, [2]), it has been evaluated the benefit on the weight reduction achievable by redesigning, under compressive load, two stiffened panels representative of the upper skin of the wing box (at wing root and toward the wing tip), releasing some of the conservatisms of the traditional design, because resolved by SHM systems. The identification of the design variables that more affect the weight saving, and definition of the design requirements for the SHM systems, have been performed.

The PFA has been applied in order to evaluate the actual residual strength, under compressive load, of impact damaged stiffened panels, considering several discrete damage models with the full mechanical strength properties of the material. The results of these analyses have been compared with those ones of the traditional design; the latter is based on the FPF criteria and on the use of material design allowables degraded because of BVID evaluated at coupon level (panel wholly damaged). A simplified design approach, based on the equivalence between the BVID and the hole 6.35 mm (1/4 inch) in diameter, as suggested by industrial guidelines for the preliminary design, has been investigated. All the numerical activities of this study have been supported and verified by correlation with experimental results of CAI (Compression After Impact) tests. In conclusion, in order to assess the real degradation of the load carrying capability at panel level in the presence of BVID, the impact damage induced on CAI coupon has been substituted to an equivalent portion of the skin of a stiffened panel. These analyses have had the scope to evaluate the benefits of a design allowable obtained at panel level rather than at coupon level.

In the following, a short description of the content of each chapter is reported:

## **Chapter 2**

This chapter provides an overview of the current traditional design practises and criticalities related to the design of composite structures, and illustrates the features of the new design approaches performed in this work.

## **Chapter 3**

This chapter illustrates the weight reduction that is potentially achievable by designing the wing stiffened panels by using the information given by SHM systems, and furnishes the design requirements for this kind of systems.

**Chapter 4**

This chapter provides an overview of the progressive failure analysis methodology.

**Chapter 5**

This chapter provides the results of the PFA performed on the stiffened panels by using discrete damage models. Discrete damages, simulated by holes 1/4 inch in diameter, have been introduced in the skin of the panels keeping the mechanical strength properties of the material without degradation for BVID, in contrast to the traditional design that is based on the assumption of the whole panel uniformly damaged by applying a knock-down factor for BVID to the material strength properties. Two panels have been considered: one critical at strength and the other one with a buckling load lower than the failure load (post-buckling regime).

**Chapter 6**

In order to verify the equivalence between the hole 1/4 inch in diameter and the BVID, this chapter provides, for two selected laminates, the results of CAI tests for different impact energy levels, and the results of the compression tests executed on coupons of the same geometry of CAI ones but with the central hole 1/4 inch in diameter.

Moreover the hole equivalent to the BVID has been evaluated numerically by the PFA.

**Chapter 7**

This chapter provides the results of the design approach performed by substituting the impacted CAI coupon to an equivalent portion of the skin of a stiffened panel. These results have been compared to those ones obtained by the traditional design.

**Chapter 8**

This chapter summarises the conclusions of the work and suggests future activities.

The activities hereafter reported have been basically performed at the Italian Aerospace Research Centre (CIRA), where the author is employed in the field of the structural design and stress analysis of composite aerospace structures, and with the collaboration, advice and support of the University “Federico II” that hosted the Ph.D. period.

## 2 TRADITIONAL AND NEW DESIGN APPROACHES FOR COMPOSITE STRUCTURES

This chapter provides a summary of the current traditional design practises and criticalities related to the design of composite structures, and illustrates the key features of new design approaches performed in this work finalised to a low weight design of this kind of structures, through the use of information given by SHM systems (Structural Health Monitoring), the application of progressive failure analysis methodology, and the realising of some traditional design criteria.

### 2.1 Current design practise and criticalities

The use of composite materials in aircraft structures is mainly dictated by the need to achieve lighter structures and less expensive than the aluminium ones. Never in the history of civil aviation so many composite materials have been used on an airplane as in the last decade, Figure 1.

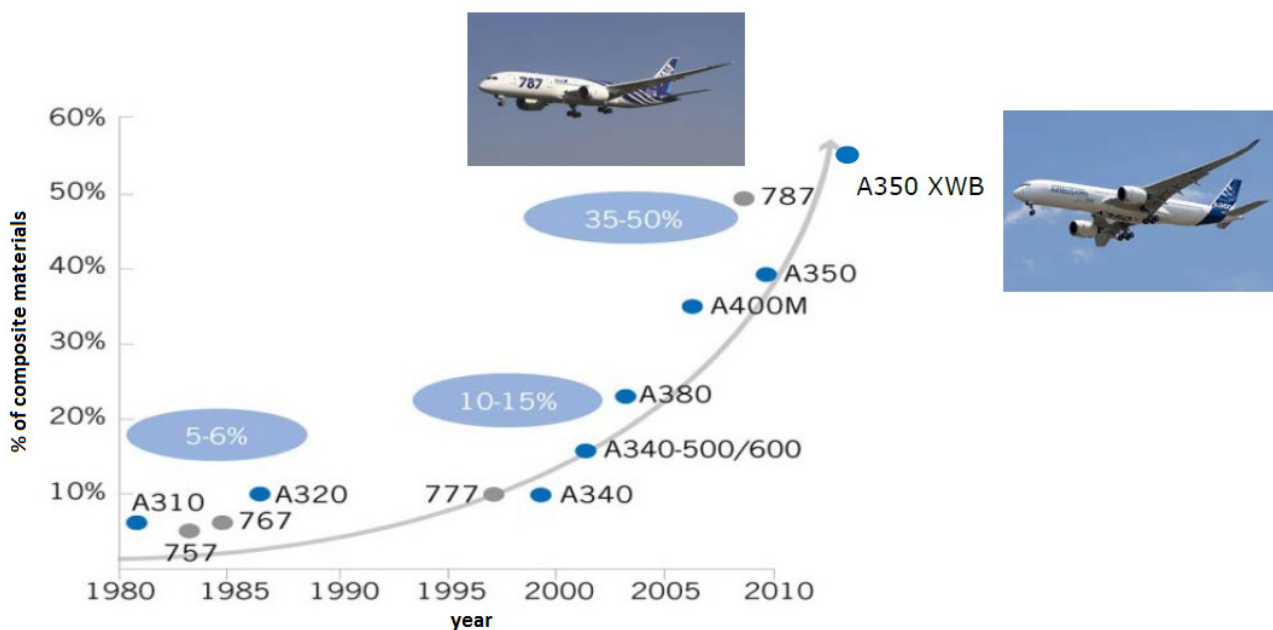


Figure 1: percentage of composite materials on airplanes

But the goal of the low weight reduction, particularly for primary structures, is compromised by certification requirement constraints that are more restrictive than those applicable to metal structures. This conservatism is principally attributable to the incomplete knowledge of the actual mechanisms of failure of composite structures especially during the operational life of the aircraft.

The certification compliance of composite structures, according to the current airworthiness regulations, **EASA AMC 20-29 - Composite Aircraft Structures - 27 July 2010** [1], is traditionally accomplished from the civil aircraft manufacturers by applying:

- building block approach, Figure 2, that implies expensive and long test campaigns: typically, tests on thousands of coupons, hundreds of elements, dozens of subcomponents lead up to one or two full scale tests;
- no-growth design approach for nonvisual damage, implying that structures with this type of damage will carry design ultimate loads for the operational life of the aircraft;
- high knock-down factors to the material strength properties (design values) to take into account the effects of temperature, moisture, B-basis statistical reduction, notch and low energy impact damages; the structure is considered uniformly damaged;
- first-ply-failure design criteria; composite damage is described by the First Ply Failure concept: failure index or strength ratio is properly calculated for each ply and the structure is considered as damaged when at least in one ply it reaches the unit value; it is a very conservative method but all the design processes are currently based on it;
- usually no buckling onset up to design ultimate loads;
- etc.

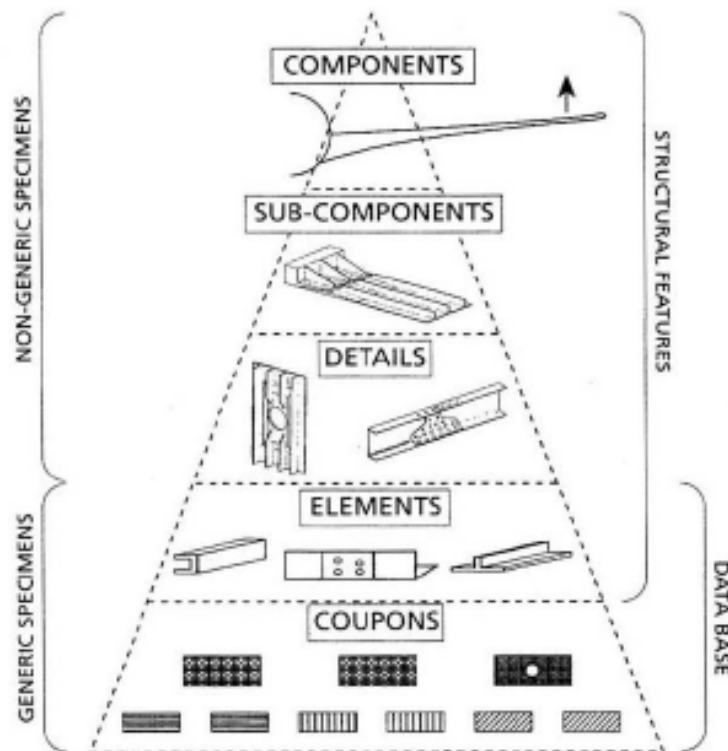


Figure 2: schematic diagram of building block tests for a fixed wing [1]

The result of the above approach is that the allowable design strain in composite structures is limited to approximately 1/3 of the limiting value for a pristine material. This approach leads to oversized composite structures and therefore to a very conservative design. Figure 3, [3], illustrates the contribution of the various knock-down factors to the design strain.

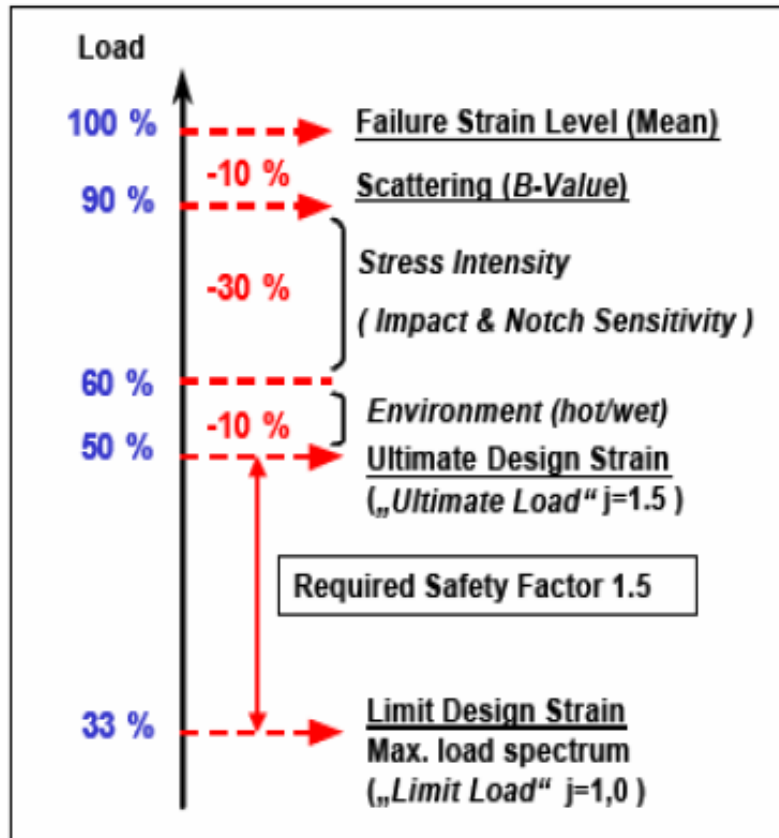


Figure 3: knock-down factors on design strains [3]

### 2.1.1 Effect of damage

Due to the high sensitivity of composite materials to damage and defects, the full potential of residual strength of composite materials is not exploited resulting in increased structural mass.

The strength in the presence of damage, such as impact or crack or cutout, is significantly lower and varies with the damage size and type [4]. The influence of damage on compression strength is more significant than the influence of damage on tension strength; hence, more attention is restricted to response to compression loading.

Typical trends of compression strength in presence of damage are shown in Figure 4: minor manufacturing imperfections such as porosity and small delaminations have little effect on strength, relative to the effects of holes and impacts; *the most critical damage is the impact damage*.

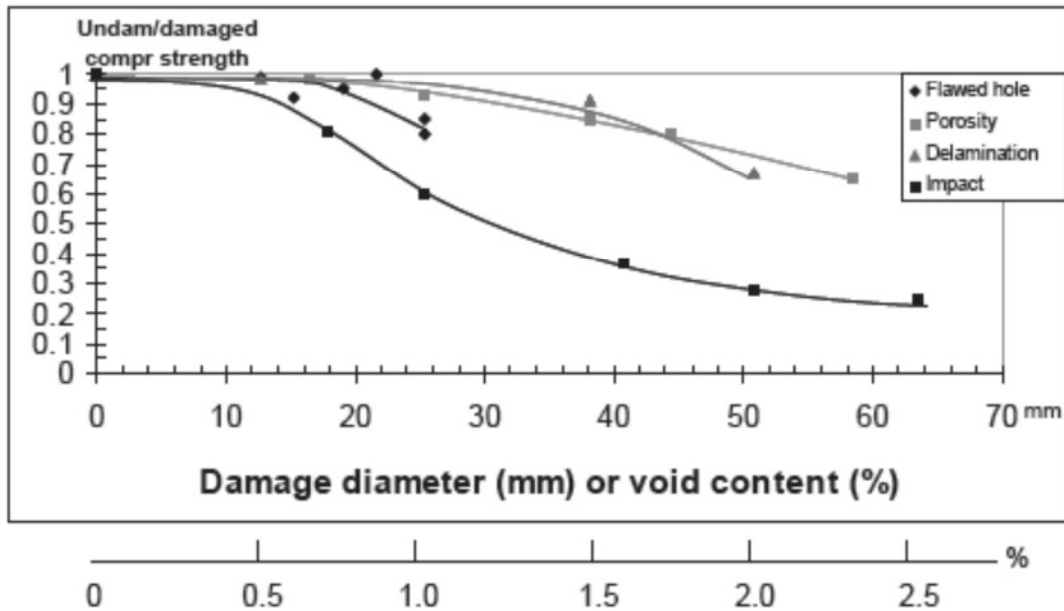


Figure 4: sensitivity of compression strength of composites to various types of damage [4]

The impact damage is caused by a large variety of sources, ranging from tool drops, runway or ground debris, and foot traffic to impact with large objects (e.g. luggage) and hail damage. *The strength reduction in the presence of damage must be taken into account in the design process; the approach is dependent on the inspection method used and its reliability*, [4].

First, the type and size of damage or flaw that the selected inspection method can find consistently and reliably, must be determined.

Then, the *threshold of detectability*, named *ADL (allowable damage limit)*, is defined: *it is the damage size above which all damages can be found by the inspection method with a certain confidence (e.g. 99% of the time)*. The ADL definition depends on inspection technique sensitivity.

The ADL divides the damage that may occur during manufacturing or service in two categories:

- non detectable damage;
- detectable damage.

These categories are then tied to specific load levels that the structure must withstand: the two main load levels of interest in structural design of airframe structures are the *limit* and *ultimate* load.

The limit load is the highest load the structure is ever expected to encounter during service. The ultimate load is the limit load multiplied by 1.5.

A structure with damage below the threshold of detectability of the selected inspection method must be capable of withstanding ultimate load without failure.

A structure with damage above the threshold of detectability level of the selected inspection method must be capable of withstanding limit load without failure, and must be repaired in order to restore its load carrying capability up to ultimate load.

In practice, the most common inspection method currently used is *visual inspection (i.e. walking around inspection)*. This is because it combines low cost with ease of implementation [4]. This does not mean that more accurate and more reliable inspection techniques such as ultrasound, X-rays, etc. are not used at different times in the life of an aircraft. Usually, however, these methods are applied during planned detailed inspections at the depot level where an aircraft is taken out of service and specially trained personnel with appropriate equipment conduct a thorough inspection of the structure. *On a more regular basis, the structure is inspected visually.*

According to the airworthiness certification requirements for composite aircraft structures (EASA AMC 20-29, [1]):

*“When using a visual inspection procedure, the likely impact damage at the threshold of reliable detection, ADL, has been called **barely visible impact damage (BVID)**”.*

With visual inspection, the structural requirements in the presence of damage become:

- structure with damage up to barely visible impact damage (BVID) must withstand ultimate load without failure;
- structure with damage greater than BVID, i.e. structure with visible damage (VID), must withstand limit load without failure.

Therefore, *the structural substantiation for BVID damage includes demonstration of a reliable service life, while retaining ultimate load capability*, as illustrated in Figure 5.

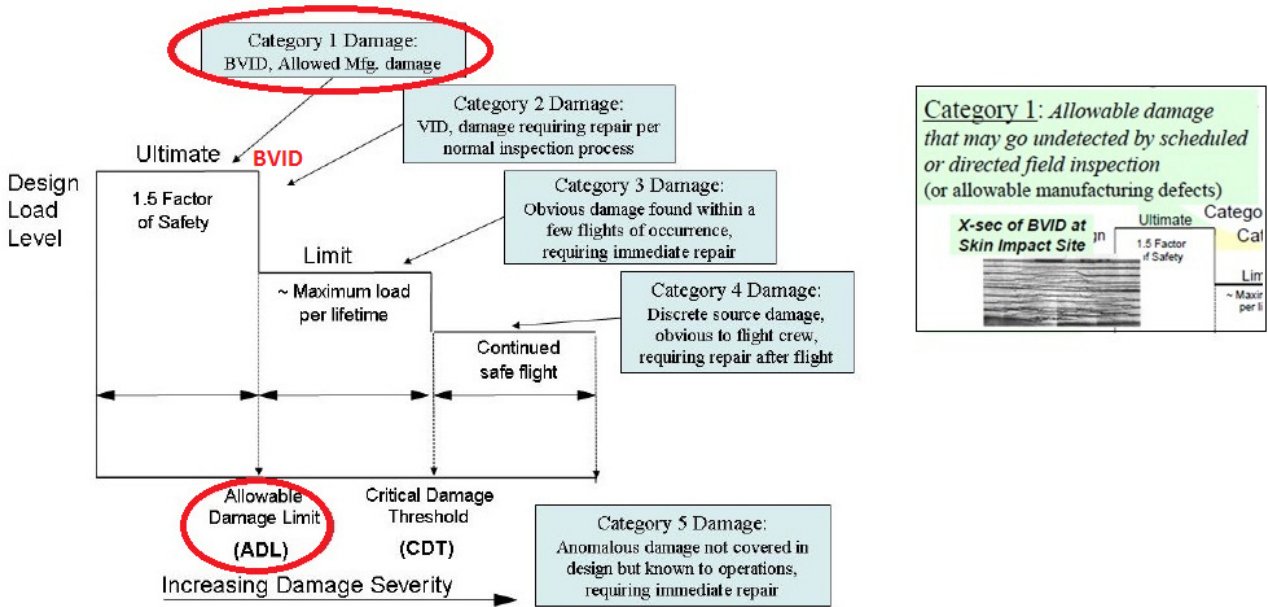


Figure 5: schematic diagram showing design load levels versus categories of damage severity [1]

The *BVID* is usually defined as damage that is “barely” visible from a distance of 1.5 meters under ambient light conditions [4, 5].

The BVID is the upper limit of **Category 1 of damages**, Figure 5:

ADL, i.e BVID, does not require repair contrary to the other categories of damage. Figure 6 summarizes what is specified for Category 1 of damage by EASA certification requirements [1].

Category 1: Allowable damage that may go undetected by scheduled or directed field inspection and allowable manufacturing defects. Structural substantiation for Category 1 damage includes demonstration of a reliable service life, while retaining ultimate load capability. By definition, such damage is subjected to the requirements and guidance associated with paragraph 7 of this AMC. Some examples of Category 1 damage include BVID and allowable defects caused in manufacturing or service (e.g., small delamination, porosity, small scratches, gouges, and minor environmental damage) that have substantiation data showing ultimate load is retained for the life of an aircraft structure.

Figure 6: Category 1 description [1]

It is recognized that the definition of BVID is *subjective and dependent on the inspector and his/her experience level*. For this reason attempts to more accurately define BVID have been made by tying the BVID to a specific indentation size. *Usually, 0.8-1 mm deep indentation is considered to correspond to BVID* [4, 5].

The reduced strength of a laminate in presence of BVID is a function of

- the impact energy level,
- thickness,
- stacking sequence.

In view of a lot of experimental tests to measure the strength reductions due to BVID (usually the worst type of damage) for different laminates that characterize a composite structure, the design/analysis process must use reliable analytical and numerical methods that allow determination of the reduced strength in the presence of this kind of damage.

Habitually, a conservative approach is used:

- determine the BVID knock-down factor by execution of CAI (Compression After Impact) tests according to the standard regulation ASTM D 7137/D 7137M – 07 [6] on a limited but significant range of layups, by comparing the undamaged and damaged tests results;
- apply the most critical value of this factor to all the laminates of the structure, whatever is the thickness and the stacking sequence of the laminate;

this avoids a lot of tests on thousands of specimens to determine the BVID resistance of a large number of laminates, with consequent large and expensive test campaigns.

The BVID knock-down factor is conservatively selected even up to a value of about **0.4**, thus the material strength properties are reduced up to **60%**.

This is the approach that is traditionally applied for the design of the wing of an aircraft, regardless of the real thickness distribution of the skin along the span: as illustrated in Figure 7 the thickness of a typical composite wing of a large aircraft (EASA CS-25, [2]) can also change from 10 mm at root up to 2 mm at tip. This design approach surely leads to oversized wings.

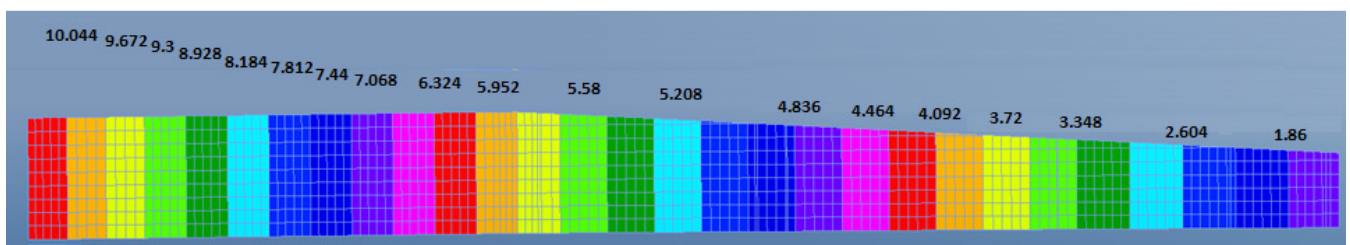


Figure 7: large aircraft wing box – typical upper skin thickness distribution (mm)

## 2.2 New design approaches and criteria for low weight

As described in § 2.1, the high sensitivity of composite materials to low energy impact damage (BVID) penalizes the design of composite structures, in terms of thickness and weight of the final structure, because often the reduction of the material design allowable due to the BVID is affected by conservatisms linked essentially to the limitations of current techniques for the inspection and measurement of the BVID, including visual inspection.

On the other hand the design of composite structures based on:

- material allowables reduced for BVID at coupon level,
- first ply failure criteria (not considering damage evolution after first ply failure),

means for example a stiffened panel is wholly damaged. This has as consequence the not exploitation of the full potential capability of the real structure in presence of discrete damage scenario. Therefore the extensive use of analysis methods based on PFA approaches is necessary to evaluate the real capability of the structure to obtain more realistic design allowables.

The new design methodologies investigated in this work, are finalised to

- reduce many of the uncertainties of the classical design;
- increase the design allowables thinking to a coupled use with SHM;
- provide preliminary requirements to the SHM systems;
- relax some traditional design criteria;
- evaluate the real capability of the structures.

This investigation has supposed the presence of a Structural Health Monitoring system, and the extensive application of progressive failure analysis methodology.

### 2.2.1 Design with SHM

SHM systems are currently conceived for maintenance purposes of airplanes.

Incorporation of SHM has the potential to reduce through-life costs by the adoption of **Condition Based Maintenance** and to reduce operating costs by the design of more structurally efficient aircraft [7-13]. SHM technology can remotely monitor the physical condition of the components, reducing the costly requirement for aircraft downtime for component disassembly and inspection. This capability opens the potential to move away from traditional “Time Based Maintenance” to “Condition Based Maintenance”:

- *the aircraft structural maintenance can be optimally planned given the actual condition of the aircraft components and not controlled primarily by flight hours irrespective of component condition.*

In many cases it is also impossible to access certain areas and consequently considerable additional cost is sustained to ensure an ultraconservative design in recognition of the inability to access the component.

In the last decade the SHM systems are also under investigation as support to the design of composite structures to achieve consistent weight reductions. This work is dedicated to this latter aspect. The use of SHM, as considered by many aircraft manufactures, can dramatically change future design and operation of aircraft.

As described in § 2.1 many aircraft composite structures are currently overdesigned due to the requirement for safe operation with undetected damage. With **reliable monitoring** of the structural parts some of the **over-designs can be removed** and this will lead to reduced aircraft weight, new design concepts and increased performance. One of the major benefits of SHM is its ability to **detect damage at an early stage** and to monitor its progression throughout the life of the structure, leading to improved diagnostic capabilities, more efficient repair strategies and ultimately more optimised structural designs.

Incorporation of SHM into composite structures has therefore the potential to reduce many of the current uncertainties and permit increased design allowables leading to lighter and more efficient structures; *it can detect the presence of defects and damage in the structure at sizes smaller than those currently assumed for design and certification (BVID).*

In detail SHM systems can allow to design with higher design allowables thanks to a more reliable detection of the current BVID (0.8-1 mm deep indentation, § 2.1.1), **improving the static strength (compression after impact)** of the composite structures for a reduced damage size detection.

As illustrated in Figure 8, the detection by SHM of a BVID smaller than that one identified by visual inspection (0.8/1 mm) and applied in the traditional design, implies the adoption of a higher material allowable for the design of the composite structure with a consequent reduction in weight.

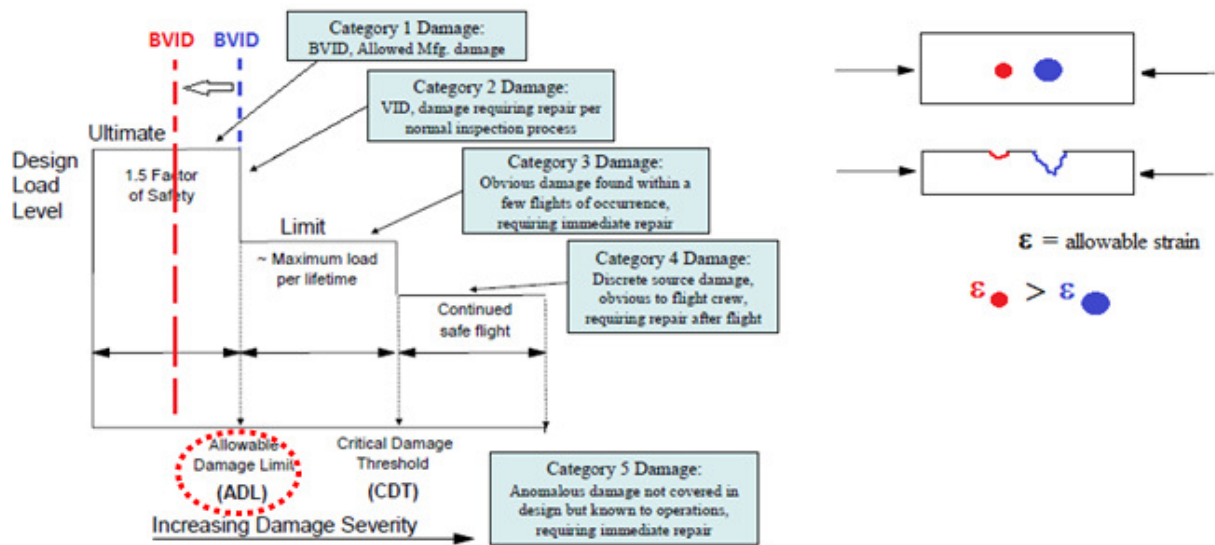


Figure 8: higher compressive strain design allowable by SHM

Through the use of these systems it could be possible also to monitor the initiation of more damages in the structure and their evolutions, up to reaching the **map of damage** that exhausts the residual strength of the structure (i.e. *most critical damage scenario*).

### 2.2.2 Residual Strength prediction

Composite structures are traditionally designed supposing that any damage up to the ADL size will not grow under fatigue design loads during all the operative life of the aircraft. This is verified at final test at component level; this assumption is made on the base of the fact that the ultimate static design allowables are very low as illustrated in § 2.1. Consequently the composite structure is verified by static analysis.

The necessity to exploit the full potential of composite materials foresees the use of the Progressive Failure Analysis (PFA) methodology able to predict the real capability of complex structures in presence of discrete damages.

The PFA methodology [14-16], founded on implicit solution methods and nonlinear analysis, is finalized to predict in addition to the damage initiation (FPF), the damage propagation up to the collapse load of a composite structure, in order to fully exploit the real residual strength of impact damaged structures, Figure 9.

This kind of analysis foresees a discrete damage model that is introduced in the FE model of the structure and preserving the full mechanical strength properties of the material (no BVID degradation).

In particular the PFA methodology allows to analyse also discrete maps of damages, representatives of real damage scenarios of the structure, Figure 10. This capability will allow to identify, among more damage scenarios, that one that really exhausts the residual strength of the structure and therefore the real ultimate design value of the structure; this value will probably be higher than that one assumed by the traditional design which is based on a uniformly damaged model of the structure by using design allowables reduced for BVID obtained at coupon level.

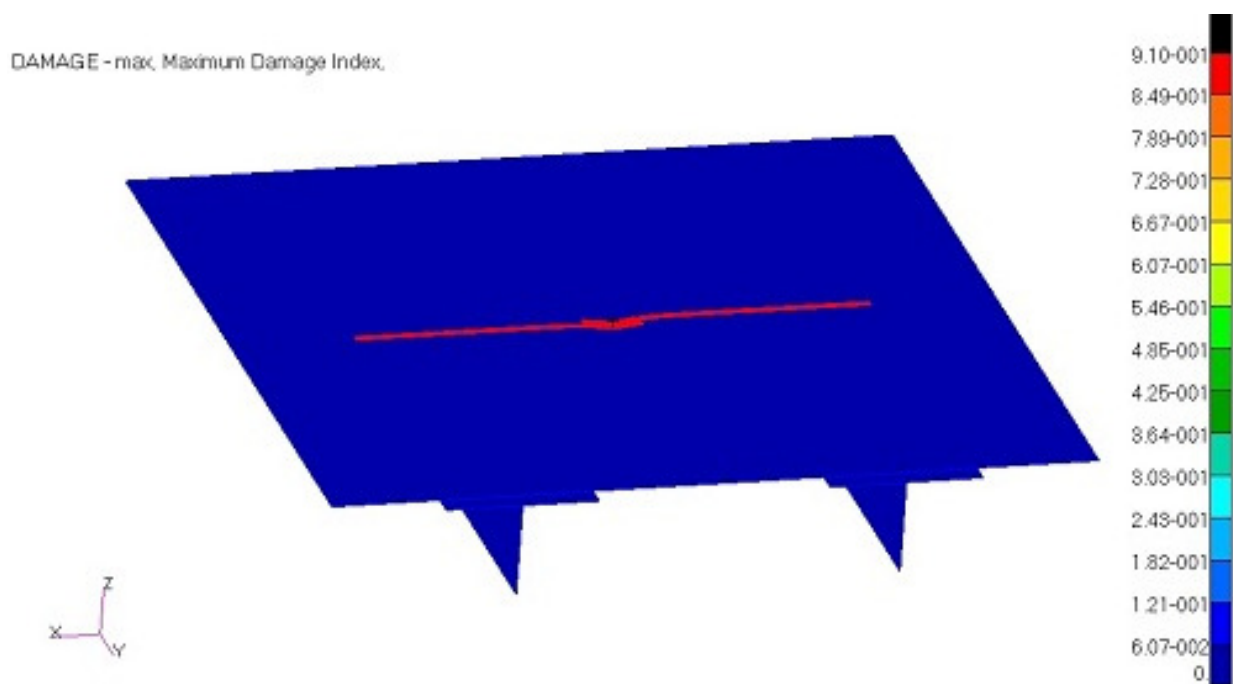


**Figure 9: progressive failure analysis of an impact damaged stiffened panel**

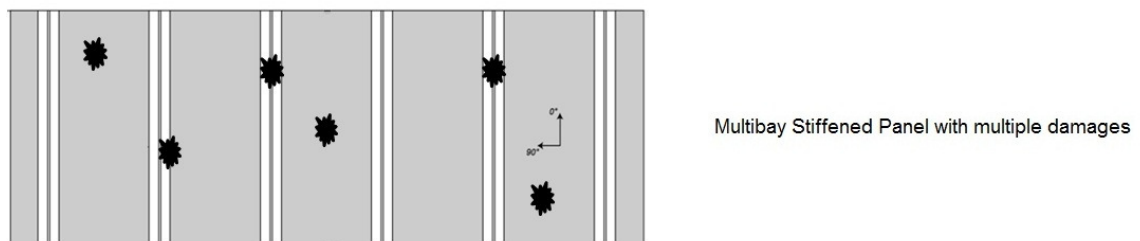


**Figure 10: discrete damage map**

The residual strength analysis represents the prognosis evaluation of the structure and in conjunction with a SHM system it constitutes the highest level of a comprehensive SHM system [7]. The monitoring of the real health condition of the structure and of the related residual strength would allow besides a reduction of the structural weight also a greater amplitude of the inspection intervals expected for the structural part in question.

### 2.2.3 Simplified design model and new criteria

Due to the complexity of the FE models and of the analysis for determining the strength of a structure in the presence of damage, simplified methods are commonly used in the *preliminary design phase* [4, 17-23]. A conservative approach is usually followed to avoid computational intensive analysis methods that model damage initiation and its evolution under load; this approach consists of using a simplified design model of BVID by simulating it with a hole 1/4 inch (6.35 mm) in diameter, as suggested also by some industrial design guidelines issued by Northrop Grumman [23]:

*“design of damage tolerant composite structures: **initial design** laminated composite structures **must account** for the presence of fastener holes, typically 1/4 inch in diameter”.*

The rationale of this guideline is based on the following considerations, [23]:

- a) A majority of the laminates in service today are less than 3/8-inches thick (9.525 mm). Hence, a vast majority of fasteners used to join these laminates are approximately 1/4 inches in diameter. Therefore, mechanically-fastened laminates may contain a large number of 1/4-inch holes.
- b) The fidelity of nondestructive inspection techniques lead to the conclusion that (undetected) rogue flaws had to be accepted in production flight hardware. These rogue flaws included porosity, damaged fibers, small inclusions, and impact damage from dropped tools.
- c) There are many databases for military aircraft containing data on the relationship between strength degradation and damage detectability. These data support the idea that an impact causing barely visible impact damage (BVID) produced a level of strength loss close to that one caused by the presence of a 1/4 inch diameter hole. This similarity of the effect on strength of BVID and a 1/4-inch hole is by no means precise. Laminate thickness, lay-up, planform, edge support, fibers, resin matrices, impactor shape, impact location, and

environment all influence the correlations between the effect on strength of BVID with that of a 1/4-inch hole.

- d) Measurements of the strength of laminates containing a 1/4-inch hole are generally repeatable and consistent. Use of impacted laminates to measure strength requires careful control of many more independent variables and results in data exhibiting excessive scatter. Hence, the effects of damage are investigated separately on a case-by-case basis.

Based on the above considerations, material design allowables used for **initial design** can be based on coupon tests of laminates with 1/4 inch holes, Figure 11.

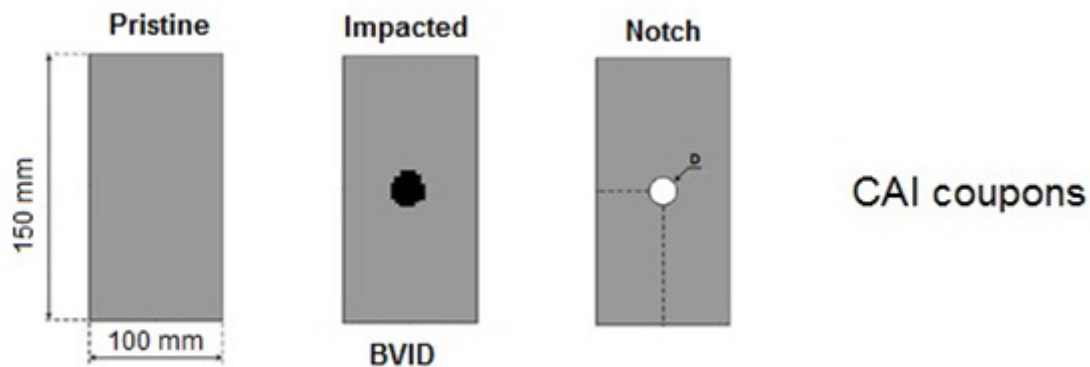


**Figure 11: equivalence between 6.35 mm hole and BVID**

The strengths of the structural laminates with impact damage are then checked after the structural design matures, [23]:

*“Final Design of Composite Laminates Must Provide Sufficient Post-Impact Strength”.*

The frequently used concept to determine the uniaxial strength,  $N_{x,a}$ , of laminates containing holes and impact damage is the following:

$$N_{x,a} = E_x t \varepsilon_{x,a}$$

where

$N_{x,a}$  = ultimate strength (force/unit length)

$E_x$  = laminate Young's modulus, derived from carpet plots or classical lamination theory, of the pristine (unnotched, undamaged) laminate

$t$  = laminate thickness

$\epsilon_{x,a}$  = B-basis allowable strain for the appropriate material, layup, and environment derived from coupon tests of laminates containing a 1/4 inch diameter hole or BVID (should screening tests indicate BVID yields significantly lower  $\epsilon_{x,a}$ )

Modulus and thickness are predictable with entirely acceptable accuracy. The main difficulty is in the estimation, using a minimum amount of experimental data, of the allowable strain.

It is important to note that accounting for a 1/4 inch hole is just the first, basic step in the structural design process; this approach has its limitations because it could be not applicable to all threat scenarios. For example, it can be extremely conservative in cases of thick composite structures. The typical damage scenarios based on common threats during manufacturing and service should not include a 6.35 mm through hole for example because it is a very unlikely event. Designing for damage must be done with care on a case-by-case basis after careful examination of threats and requirements. And, most importantly, it should be supported by tests that verify the analysis method and its applicability to the loading, layups, and configurations under consideration.

But the possibility to simulate the BVID with an equivalent hole, probably of diameter not equal to 6.35 mm (as suggested by the above guidelines), if demonstrated, is aimed at simplifying in the next future, the numerical models simulating the low energy impact effects with high computational time savings; in particular it could allow the evaluation of the residual strength after impact avoiding the implementation of induced damage models (explicit codes), but simply modelling the laminate with a hole of appropriate diameter in the same BVID location, as illustrated in Figure 12.

Another design criteria investigated in this work, also illustrated in Figure 12, is based on the following consideration:

the traditional use for the design of complex structures (for instance stiffened panels) of the reduced allowable for BVID determined at coupon level, could be more conservative respect to what really happens in terms of residual strength for a panel with two or more stringers both for the panel geometry (presence of the stringers, alternative load paths, etc.) and for the different boundary conditions.

If the impacted skin is part of a stiffened panel, the stiffeners may provide in fact an alternative load path and may be strong enough to carry load after the panel has been impact damaged.

Therefore the stiffened panel could have a higher residual strength respect to that one predicted by the traditional design based on a uniformly damaged model of the structure by using the design allowable reduced for BVID obtained at coupon level. This awareness could suggest, respect to the

traditional design, to consider a design approach at element level (stiffened panel), or to design with a reduced allowable for BVID higher respect to that one obtained by CAI tests on coupon, with consequent benefit in terms of weight reduction and/or higher load carrying capability.

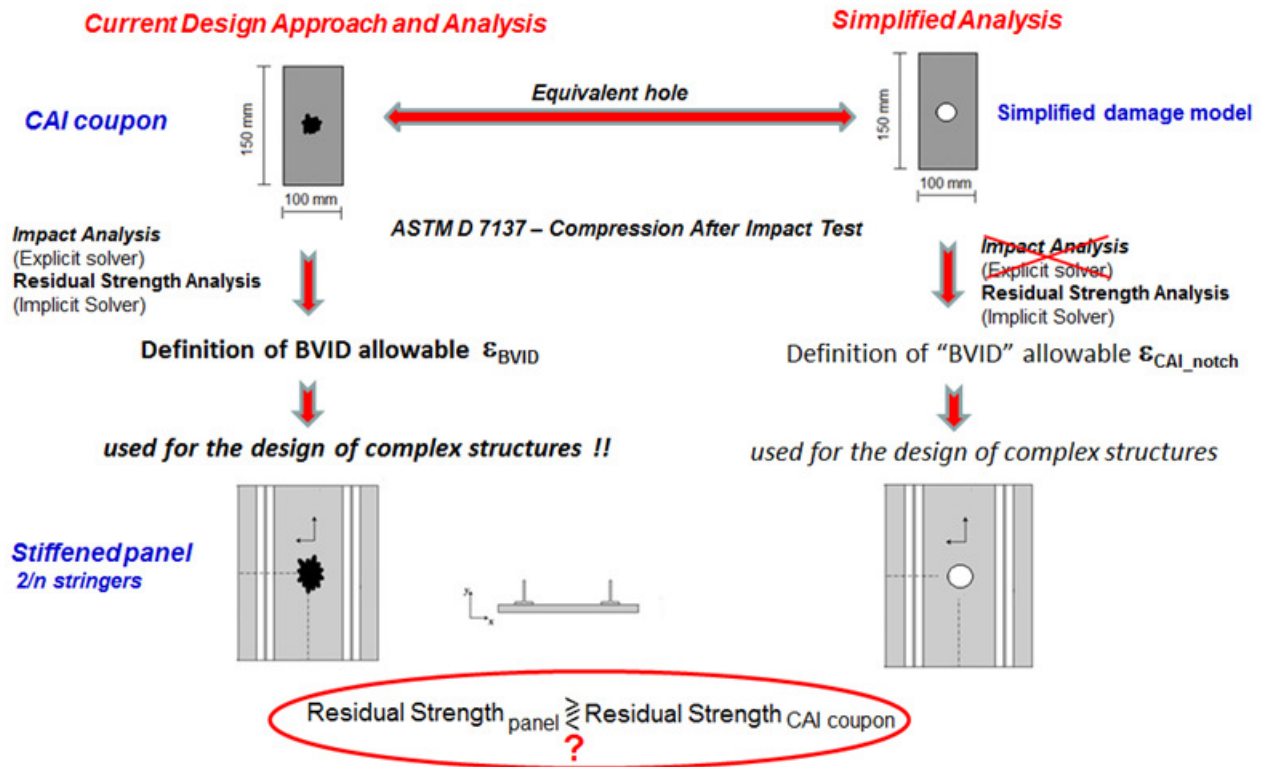


Figure 12: scheme of the current and of the simplified design approach and analysis

### 3 LOW WEIGHT DESIGN USING INFORMATION GIVEN BY SHM SYSTEMS

The activities of this work have been performed assuming as reference baseline a typical wing box of a regional aircraft (EASA CS-25, [2]), in particular two panels representatives of the upper skin: one located at the wing root (sized according to strength criteria) and the other one toward the wing tip (sized according to buckling criteria).

These panels have been initially designed according to the current industrial design approach; the panels so designed, and in particular their structural weight, represent the *reference baseline*.

Then the panels have been redesigned according to new design criteria based on the potential exploitation of the information given by a reliable SHM system.

In particular, it has been evaluated the benefit on weight reduction achievable by redesigning the reference panels by relaxing some of the traditional conservatisms, because resolved by SHM systems, in order to identify the design variables that more affect the weight saving of the panels.

A weight sensitivity analysis, finalized to assess the influence on the panel weight of the application of the knock-down factor for BVID on material allowables, has been performed.

In detail, the two reference panels have been redesigned not considering the BVID knock-down factor on material allowables because of monitoring of SHM. This approach has been used in some cases on the whole panel and in some cases only on the skin or stringers alone thinking to partial monitoring conditions. Furthermore other analyses have been performed using intermediate values of BVID knock-down factor related to the different SHM sensitivity (change the ADL, § 2.1.1, respect to different SHM capabilities). The analyses have been performed to evaluate the weight reduction respect to different knock-down factors scenarios and with and without post-buckling regime.

The results of these analyses have provided fundamental requirements for the SHM system definition in terms of “*where, which parameters and their amount it is necessary to monitor*”.

#### 3.1 Reference panels

The stiffened panels are representative of the upper skin of a typical regional aircraft wing box, Figure 13; *panel 1* is located at wing root, *panel 2* toward the wing tip, Figure 14-(a). They are characterised by T-shaped stringers, Figure 14-(b), with a ratio between length (span dimension) and width (chord dimension) equal to 0.32 for *panel 1* and 0.375 for *panel 2*.

For the research objectives, the panels have been supposed flat and only compressive loads have been considered for their design; 1128 N/mm and 600 N/mm are the design limit compressive loads (L.L.) for *panel 1* and *panel 2* respectively. Figure 15 summarises the panel dimensions and the design loads.

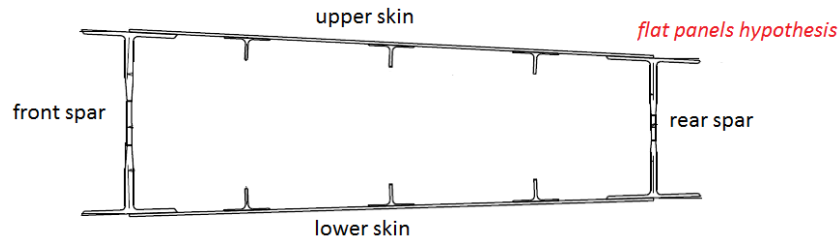


Figure 13: wing box example

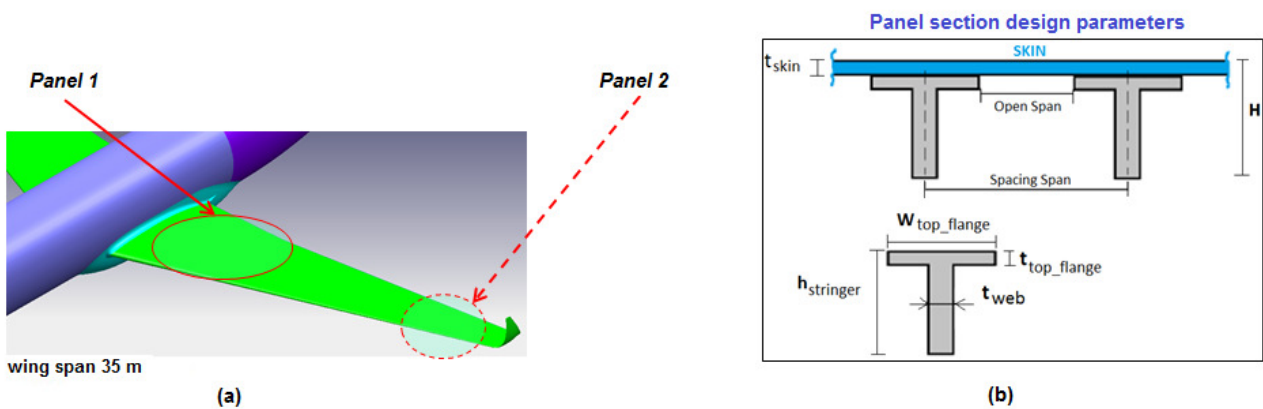


Figure 14: locations of the panels (a); panel section (b)

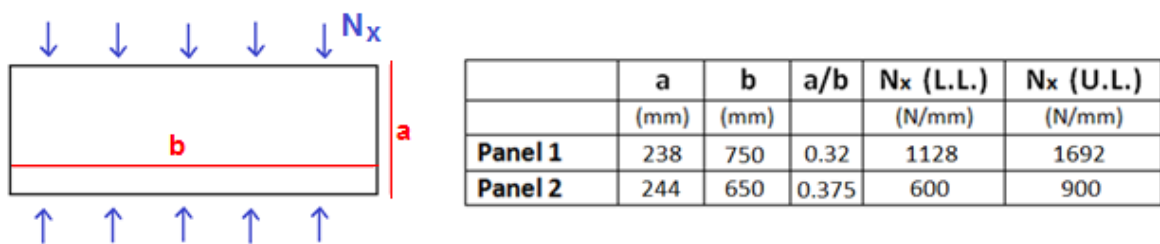


Figure 15: panel dimensions and loads

The design of these panels, according to the current conservative design criteria, has furnished the reference baseline respect to compare the weight reduction achievable by applying a new design approach (§ 2.2.1) exploiting the potentiality of SHM systems.

### 3.1.1 Design requirements and criteria

The panels have been sized by linear analysis according to

- minimum weight requirement

and according to the following design criteria:

- no strength failure and no onset of buckling up to ultimate load (U.L.).

Furthermore, as foreseen by the traditional sizing approach,

- FPF criteria

and

- material allowables, reduced by knock-down factors for BVID, temperature, moisture, and B-basis statistical reduction, and applied homogeneously on the whole panel,

have been applied in design.

About the layups, they satisfy all the conventional rules:

- symmetric and balanced (minimum gauge of 8 plies),
- standard orientations ( $0^\circ$ ,  $\pm 45^\circ$ ,  $90^\circ$ ) with minimum 10% of plies in each orientation,
- external plies  $\pm 45^\circ$ ;
- stacking sequence suitable for mechanical joints and repairs.

### 3.1.2 Methodology

The design of the reference panels, and also of the new ones supposing the presence of a SHM system, has been developed by means of a stand-alone approach (no finite element solver), based on the use of a dedicated structural sizing code for composite structures, Hypersizer<sup>®</sup> [24], typically used in the preliminary design phase by civil aircraft industries.

Hypersizer<sup>®</sup> is able to compute the load distribution that satisfies the condition of FBD (Free Body Diagram) force equilibrium for imposed geometry, shape, material, layup. The external loads per unit length are resolved internally into stress resultants on each analysed object (e.g. flanges, webs, etc). Furthermore, the FBD state of internal stresses and strains for all panel segments is used to verify the equilibrium of forces and strain compatibility for the panel/beam as a whole. The strength

and stability of these panels are analysed for the applied loads and boundary conditions using both analysis approaches based on traditional industry methods and modern analytical/computational solutions (over 100 different failure analyses).

The objective of the panel design and sizing is to minimize the weight with the added constraint to have all the margins of safety (stability and strength) positive, Figure 16.

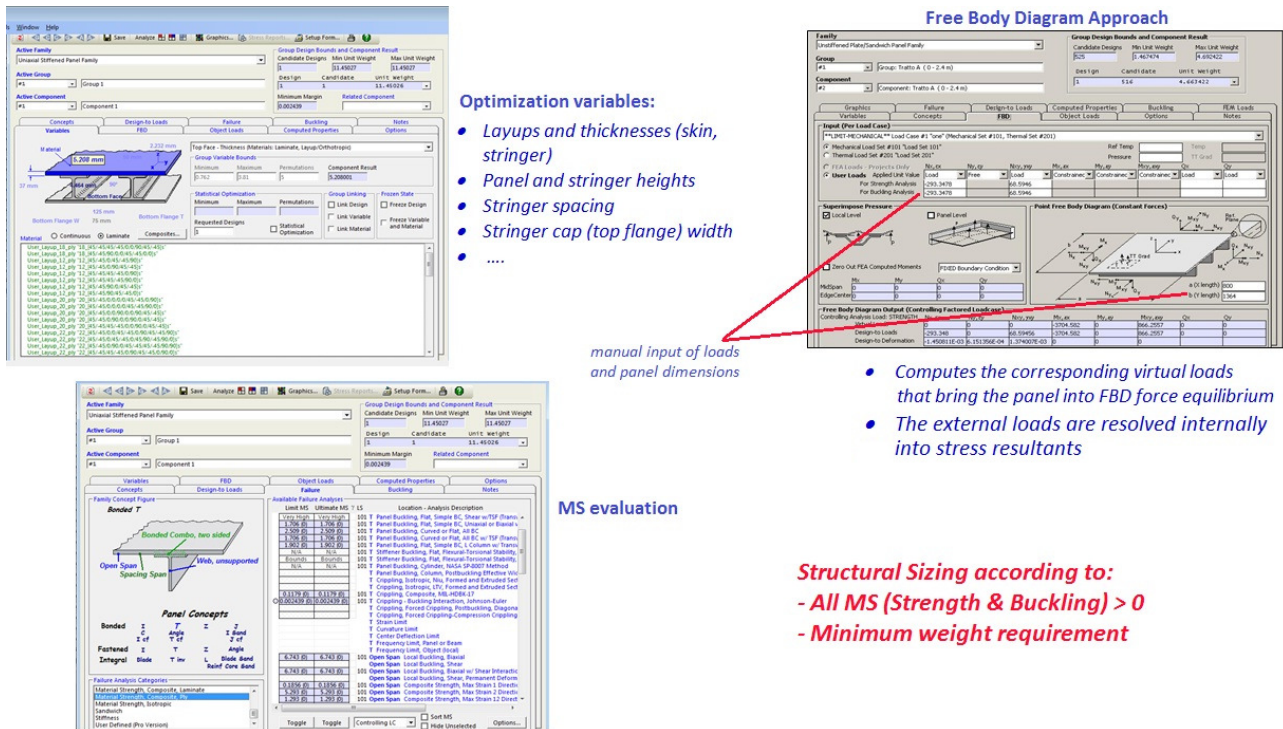


Figure 16: Hypersizer® software

### 3.1.3 Material properties

About the composite material, a carbon fiber resin epoxy system, commonly used for aeronautical applications, have been considered in the design of the panels. It is a unidirectional prepreg tape, with a nominal cured ply thickness of 0.186 mm.

According to the current traditional design approach, the material allowables are degraded by appropriate knock-down factors to take into account temperature and moisture effects ( $K_{T,M}$ ), B-basis statistical reduction ( $K_{B-basis}$ ), and low energy impact damage ( $K_{BVID}$ ). Figure 17 illustrates the lamina material allowables without  $K_{BVID}$  (Figure a), and with  $K_{BVID}$  (Figure b).

According to the design guideline issued by **Northrop Grumman** regarding the preliminary design of composite structure (§ 2.2.3. [23]),  $K_{BVID}$  has been assumed equal to that one of the open hole

compression test,  $K_{OHC}$  (compressive test on quasi-isotropic laminate with a hole 6.35 mm in diameter [25]). Therefore the design value of  $K_{BVID}$  applied to the compressive allowable is the following one

$$K_{BVID} = K_{OHC} = \epsilon_{OHC} / \epsilon_{cu\_unnotched} = 0.70.$$

Material properties - $K_{B\text{-basis}}$ $K_{T,M}$		
Longitudinal Young's modulus, Tension	$E_{t1}$	163 GPa
Longitudinal Young's modulus, Compression	$E_{c1}$	137.5 GPa
Transverse Young's modulus, Tension	$E_{t2}$	8.35 GPa
Transverse Young's modulus, Compression	$E_{c2}$	8.50 GPa
In-plane shear modulus	$G_{12}$	3.95 GPa
Poisson's ratio	$\nu_{12}$	0.35
Longitudinal Tensile strength	$F_{1t}$	1764.44 MPa
Longitudinal Tensile strain	$\epsilon_{1t}$	10825 $\mu\epsilon$
Longitudinal Compressive strength	$F_{1c}$	740.14 MPa
Longitudinal Compressive strain	$\epsilon_{1c}$	5383 $\mu\epsilon$
Transverse Tensile strength	$F_{2t}$	55.72 MPa
Transverse Tensile strain	$\epsilon_{2t}$	6795 $\mu\epsilon$
Transverse Compressive strength	$F_{2c}$	170.15 MPa
Transverse Compressive strain	$\epsilon_{2c}$	20750 $\mu\epsilon$
In-plane Shear strength	$S_{12}$	66.33 MPa
In-plane Shear strain	$\epsilon_{12}$	16792 $\mu\epsilon$
Interlaminar shear strength	$\tau_{ILSS}$	51.29 MPa
Interlaminar shear strain	$\epsilon_{ILSS}$	12986 $\mu\epsilon$
Ply thickness	$t$	0.186 mm

(a)

Material properties - $K_{B\text{-basis}}$ $K_{T,M}$ $K_{BVID}$		
Longitudinal Young's modulus, Tension	$E_{t1}$	163 GPa
Longitudinal Young's modulus, Compression	$E_{c1}$	137.5 GPa
Transverse Young's modulus, Tension	$E_{t2}$	8.35 GPa
Transverse Young's modulus, Compression	$E_{c2}$	8.50 GPa
In-plane shear modulus	$G_{12}$	3.95 GPa
Poisson's ratio	$\nu_{12}$	0.35
Longitudinal Tensile strength	$F_{1t}$	896.72 MPa
Longitudinal Tensile strain	$\epsilon_{1t}$	5501 $\mu\epsilon$
Longitudinal Compressive strength	$F_{1c}$	518.10 MPa
Longitudinal Compressive strain	$\epsilon_{1c}$	3768 $\mu\epsilon$
Transverse Tensile strength	$F_{2t}$	55.72 MPa
Transverse Tensile strain	$\epsilon_{2t}$	6795 $\mu\epsilon$
Transverse Compressive strength	$F_{2c}$	170.15 MPa
Transverse Compressive strain	$\epsilon_{2c}$	20750 $\mu\epsilon$
In-plane Shear strength	$S_{12}$	40.13 MPa
In-plane Shear strain	$\epsilon_{12}$	10159 $\mu\epsilon$
Interlaminar shear strength	$\tau_{ILSS}$	31.03 MPa
Interlaminar shear strain	$\epsilon_{ILSS}$	7856 $\mu\epsilon$
Ply thickness	$t$	0.186 mm

(b)

Figure 17: lamina material properties

The design of the reference panels, according to the current design approach, has been designed applying all the knock-down factors, Figure 17-b).

In detail, referring to the data of the cured ply available in the material datasheet, the classical design approach has been performed

- assuming as basic allowable in compression,  $\epsilon_{cu}$ , the result of the compression test executed on the unnotched laminate (24 ply QI, available in the material datasheet),  $\epsilon_{cu\_unnotched}$ , instead of the material allowable deriving from the standard compression test on unidirectional laminate, in order to consider the in-situ strain effect:  $\epsilon_{cu} = \epsilon_{cu\_unnotched} = 7333 \mu\epsilon$ ;
- applying to the unnotched allowable the knock-down factors  $K_{T,M}$ ,  $K_{B\text{-basis}}$ ,  $K_{BVID}$ ,

$$\epsilon_{cu} = \epsilon_{cu\_unnotched} K_{T,M} K_{B\text{-basis}} K_{BVID}.$$

### 3.1.4 Design of the reference panels

Figure 18 and Figure 19 show the results of the design of the two reference panels according to the above requirements and design criteria, and the design parameters illustrated in Figure 14-(b).

As expected, *panel 1* and *panel 2* are characterized by minimum margin of safety ( $MS_{min}$ ) at ultimate load (U.L.), at strength and local buckling respectively.

<b>PANEL 1</b>			Skin		t_skin (mm)	Weight W/A (Kg/m <sup>2</sup> )	MS U.L.
Spacing Span (mm)	n. Stringers	H (mm)	n. plies Skin - [% 0°, ±45°, 90°]				
125	6	37	28 plies [45/-45/45/-45/0/0/90/0/0/45/-45/0/90/0]s [42.86% 0°, 42.86% ±45°, 14.28% 90°]		5.21		
Stringer					Weight	MS U.L.	
H_stringer (mm)	Top Flange Wt (mm)	n. plies Top Flange - [% 0°, ±45°, 90°]		t_topflange (mm)	t_web (mm)	W/A (Kg/m <sup>2</sup> )	
31.792	50	12 plies [45/-45/0/0/90/0]s [50% 0°, 33.33% ±45°, 16.67% 90°]		2.232	4.464	11.45	0.5258 # Web, Local Buckling 1.706 # Panel Buckling 0.1179 # Crippling, Method Mil Hdbk 17 0.1395 # Composite Strength, Tsai-Wu Strain

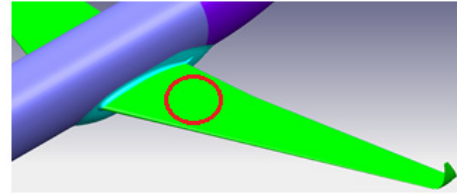


Figure 18: panel 1 reference baseline

<b>PANEL 2</b>			Skin		t_skin (mm)	Weight W/A (Kg/m <sup>2</sup> )	MS U.L.
Spacing Span (mm)	n. Stringers	H (mm)	n. plies Skin - [% 0°, ±45°, 90°]				
108.33	6	31	14 plies [45/-45/0/0/90/45/-45]s [28.57% 0°, 57.14% ±45°, 14.29% 90°]		2.6		
Stringer					Weight	MS U.L.	
H_stringer (mm)	Top Flange Wt (mm)	n. plies Top Flange - [% 0°, ±45°, 90°]		t_topflange (mm)	t_web (mm)	W/A (Kg/m <sup>2</sup> )	
28.396	50	10 plies [45/-45/0/0/90]s [40% 0°, 40% ±45°, 20% 90°]		1.86	3.72	7.0	0.007571 # Spacing Span Local Buckling 1.644 # Panel Buckling 0.945 # Buckling Stiffener 0.05235 # Crippling, Method Mil Hdbk 17 0.0648 # Composite Strength, Tsai-Wu Strain

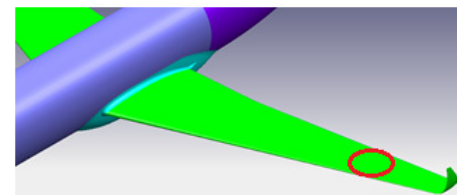


Figure 19: panel 2 reference baseline

## 3.2 Weight sensitivity analysis by new design approach with SHM

The reference panels have been redesigned relaxing some of the current conservative design criteria (§ 3.1) and according to a new design philosophy supposing the presence of an SHM system, aiming at exploiting the full potential of composite materials in terms of weight reduction.

By detecting the presence or development of critical defects and damages by SHM systems, the structure could be designed with a higher design allowable improving the static strength (compression after impact) for a reduced damage size detection (§ 2.2.1).

The work developed in this chapter consists of two parts.

In the first part some traditional design criteria have been relaxed:

- No BVID knock-down factor,  $K_{\text{BVID}}$ , has been applied in the new design on the whole panels and/or on skin and stringers alone;
- post-buckling regime between limit and ultimate load has been allowed.

In the second part of this chapter, different sensitivity limits of the SHM system to detect the BVID have been taken into account, assuming different values of the BVID knock-down factor by increasing the compressive design value.

The new design of the panels has been developed, as the reference ones, by using Hypersizer<sup>®</sup> code in stand-alone approach, but in this case also applying in some cases nonlinear analysis for post-buckling (Appendix A).

### ***3.2.1 Weight reduction evaluation without BVID knock-down factor***

The reference panels have been redesigned to estimate the potential weight reduction achievable releasing some traditional criteria because resolved by the use of SHM systems.

For this purpose, a numerical test matrix has been defined and executed in order to evaluate the weight benefit arising from this design approach.

This test matrix includes, for each of the two panels, many tests as many as the released design criteria considered, as for instance no buckling up to U.L. and no application of  $K_{\text{BVID}}$ , their combination, and also the application of these new criteria only to different panel sub-elements:

for instance, no application of BVID knock-down factor

- only on the skin (i.e. only the skin is supposed monitored by SHM systems)
- or only on the stringer,
- or on both,

with or without allowing the onset of buckling between limit and ultimate load.

The numerical analyses developed in this part of the work have supplied, for each reference panel and for each test case, new panel configurations; they are different in terms of

- layups, thicknesses, stringer spacing

and therefore

- weight,
- with respect to the reference ones (§ 3.1.4).

### Panel 1

Figure 20 summarizes the results obtained by redesigning *panel 1*.

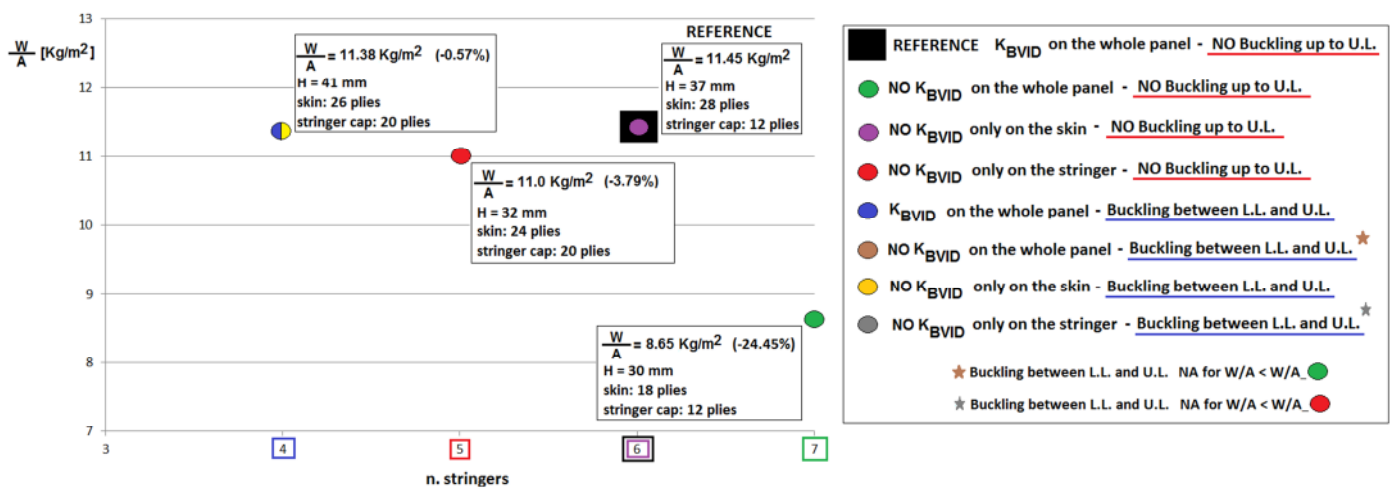
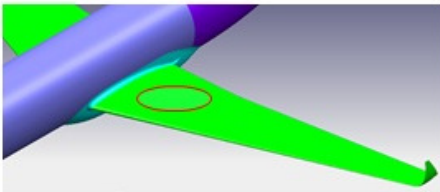


Figure 20: panel 1 redesign – weight saving analysis

According to the above figure, the results obtained by redesigning the panel are the following ones:

- the **maximum weight reduction** achievable (*vs reference* – Figure 18) is of **24.45%**, and it is achievable for the following panel:
  - **NO K<sub>BVID</sub> on the whole panel - NO Buckling up to U.L.**
    - without applying BVID knock-down factor (NO K<sub>BVID</sub>) on the whole panel (i.e. *SHM applied on both the skin and the stringers*) and according to the design criteria of NO Buckling up to U.L.
    - the *new panel 1*, Figure 21, is characterised by the following new design values (Figure 14-(b)):
      - ✓ H: 30 mm *vs* 37 mm;
      - ✓ n. stringers: 7 *vs* 6;
      - ✓ skin plies: 18 *vs* 28;
      - ✓ stringer cap plies not changed.

- NO weight reduction is achievable if NO  $K_{BVID}$  is applied only on the skin (i.e. *SHM applied only on the skin*)
- weight reduction of only **4%** is achievable if NO  $K_{BVID}$  is applied only on the stringers (i.e. *SHM applied only on the stringers*)
- NO weight reduction is achievable allowing the panel to enter the post-buckling regime between L.L. and U.L.



<b>PANEL 1</b>			Skin		Weight		Post Buckling
Spacing Span (mm)	n. Stringers	H (mm)	n. plies Skin - [% 0°, ±45°, 90°]	t_skin (mm)	W/A (Kg/m <sup>2</sup> )	% reduction vs reference	
107.14	7	30	18 plies [45/-45/90/45/0/0/0/-45]s [44.44% 0°, 44.44% ±45°, 11.11% 90°]	3.348	8.65	-24.45%	NA
Stringer					MS U.L.		
H_stringer (mm)	Top Flange Wt (mm)	n. plies Top Flange - [% 0°, ±45°, 90°]		t_topflange (mm)	t_web (mm)		
26.652	50	12 plies [45/-45/0/0/90/0]s [50% 0°, 33.33% ±45°, 16.67% 90°]		2.232	4.46	0.09928 # Spacing Span Local Buckling 0.7878 # Panel Buckling 0.2188 # Crippling, Method Mil Hdbk 17 0.2318 # Composite Strength, Tsai-Wu Strain	

Figure 21: panel 1 redesign with a weight reduction of 24.45%

**Panel 2**

Figure 22 summarizes the results obtained by redesigning *panel 2*

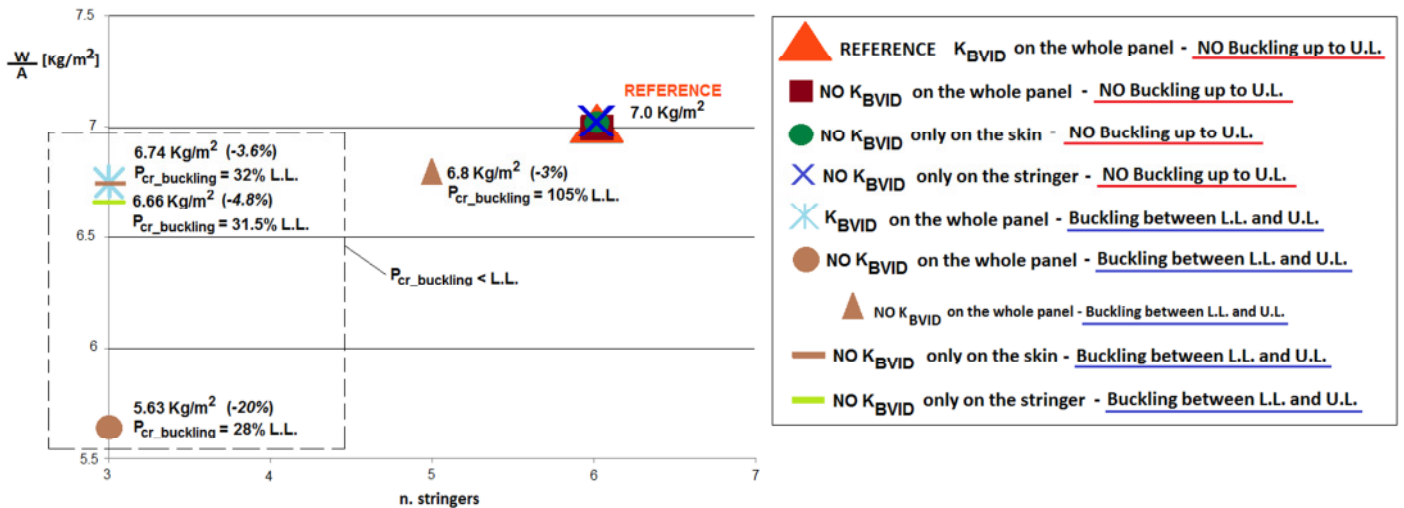


Figure 22: panel 2 redesign – weight saving analysis

According to the above figure, the results obtained by redesigning the panel are the following ones:

- the maximum weight reduction achievable (*vs reference* – Figure 19) is of **3%**, and it is achievable for the following panel:

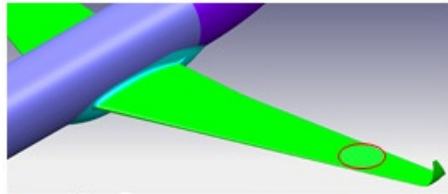
▲ **NO  $K_{BVID}$  on the whole panel - Buckling between L.L. and U.L.**

- without applying BVID knock-down factor (NO  $K_{BVID}$ ) on the whole panel (i.e. *SHM applied on both the skin and the stringers*), and post-buckling regime between L.L. and U.L..  $P_{cr\_buckling}=105\%$  L.L.

- the *new panel 2*, Figure 23, is characterised by the following new design values (Figure 14-(b)):

- ✓ H: 30 mm vs 31 mm;
- ✓ n. stringers: 5 vs 6;
- ✓ skin plies: 12 vs 14;
- ✓ stringer cap plies: 14 vs 10.

- greater weight reductions are achievable, but for post-buckling regime for loads lower than L.L. (not applicable for skin wing cover panels)



<b>PANEL 2</b>			<b>Skin</b>		<b>Weight</b>		<b>Post Buckling</b>
Spacing Span (mm)	n. Stringers	H (mm)	n. plies Skin - [% 0°, ±45°, 90°]	t <sub>skin</sub> (mm)	W/A (Kg/m <sup>2</sup> )	% reduction vs reference	
130	5	30	12 plies [45/-45/0/90/45/-45] <sub>s</sub> [16.67% 0°; 66.67% ±45°; 16.67% 90°]	2.232	6.8	-3%	105% L.L.
<b>Stringer</b>					<b>MS U.L.</b>		
H <sub>stringer</sub> (mm)	Top Flange Wt (mm)	n. plies Top Flange - [% 0°, ±45°, 90°]		t <sub>topflange</sub> (mm)	t <sub>web</sub> (mm)		
27.768	50	14 plies [45/-45/0/0/90/45/-45] <sub>s</sub> [28.57% 0°; 57.14% ±45°; 14.29% 90°]		2.604	5.21	1.98 # Web, unsupported Local Buckling 1.186 # Panel Buckling 0.0609 # Crippling, Method Mil Hdbk 17 <b>0.0592 # Composite Strength, Tsai-Wu Strain</b>	

Figure 23: panel 2 redesign with a weight reduction of 3%

The maximum weight reduction achievable for the two panels, *panel 1* and *panel 2*, as illustrated in the figures above is the maximum reduction achievable in the “ideal case” of complete absence of BVID knock-down factor thanks to the application of accurate and reliable SHM systems.

The *maximum value of the weight reduction* is achievable for the *panel sized according to the strength criteria* rather than the panel sized according to the buckling criteria: **24.45% versus 3%**.

Moreover panel weight reductions are potentially achievable monitoring

- or the whole panel,
- or monitoring only the stringers (NO  $K_{BVID}$  only on the stringers),
- but not monitoring only the skin.

In general, the load carrying capability of both the panels, with and without BVID damage, is resulted not so influenced by post-buckling regime, therefore

- no consistent weight reduction is achievable if panels enter the post-buckling regime between L.L. and U.L.

The above results give useful design requirements to the SHM systems in terms of design parameters and panel subparts (skin, stringers) to which the panel weight saving is more sensitive, and also the influence of post-buckling regime; in detail:

“*what monitor and where for a low weight design*”.

### 3.2.2 Weight reduction evaluation by several sensitivity levels of the SHM systems versus classical visual inspection

Lower design weight of the stiffened panels is related to a specific capability to identify damages by using SHM systems, with respect to visual inspection (*walking around inspection*).

The evaluation performed in this chapter supposes that different sensitivity levels of the SHM systems are linked to different amounts of damage that have as consequence different residual strength levels. At this purpose the analyses have been performed using different values of the compressive strain allowable as if we were in presence of different SHM capabilities.

$K_{BVID}$  has been incremented from the design value ( $K_{BVID} = 0.70$ , § 3.1.3) up to the ideal case of NO  $K_{BVID}$  (i.e.  $K_{BVID} = 1$ , as analysed in § 3.2.1), by increasing the compressive failure strain.

Figure 24 illustrates the levels of the compressive failure strain that have been applied for the redesign of the panels.

	$K_{BVID}$	$K_{BVID\_1}$	$K_{BVID\_2}$	$K_{BVID\_3}$	NO $K_{BVID}$
	0.70	0.81	0.89	0.96	1
$\epsilon_{cu}$ [ $\mu\epsilon$ ]	3768	4172	4576	4979	5383
		+10.72%	+21.44%	+32.14%	+42.86%

$\epsilon_{cu}$  = allowable compressive strain

$\epsilon_{cu} > \epsilon_{cu}$

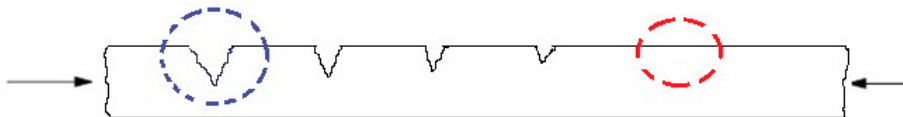


Figure 24: increment of the compressive design value for the weight reduction evaluation

Figure 25 and Figure 26 illustrates the results obtained for *panel 1* and *panel 2* respectively.

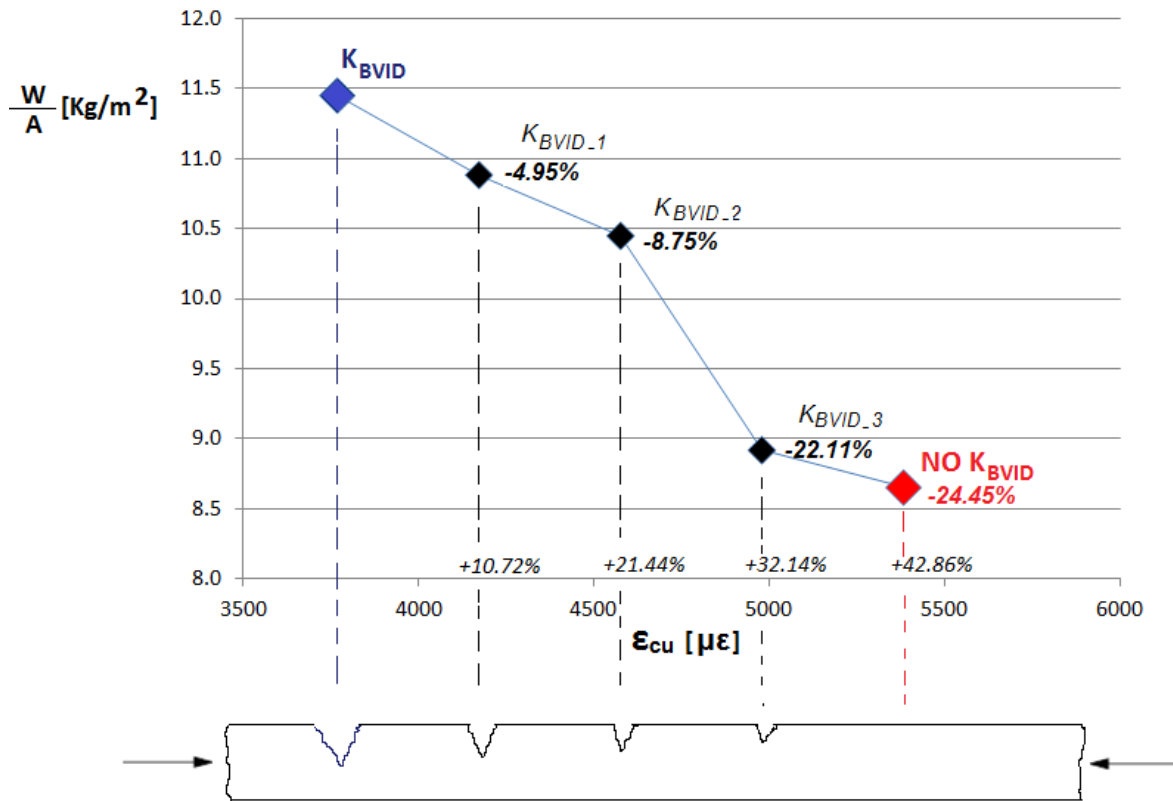


Figure 25: panel 1 – weight vs compressive design value

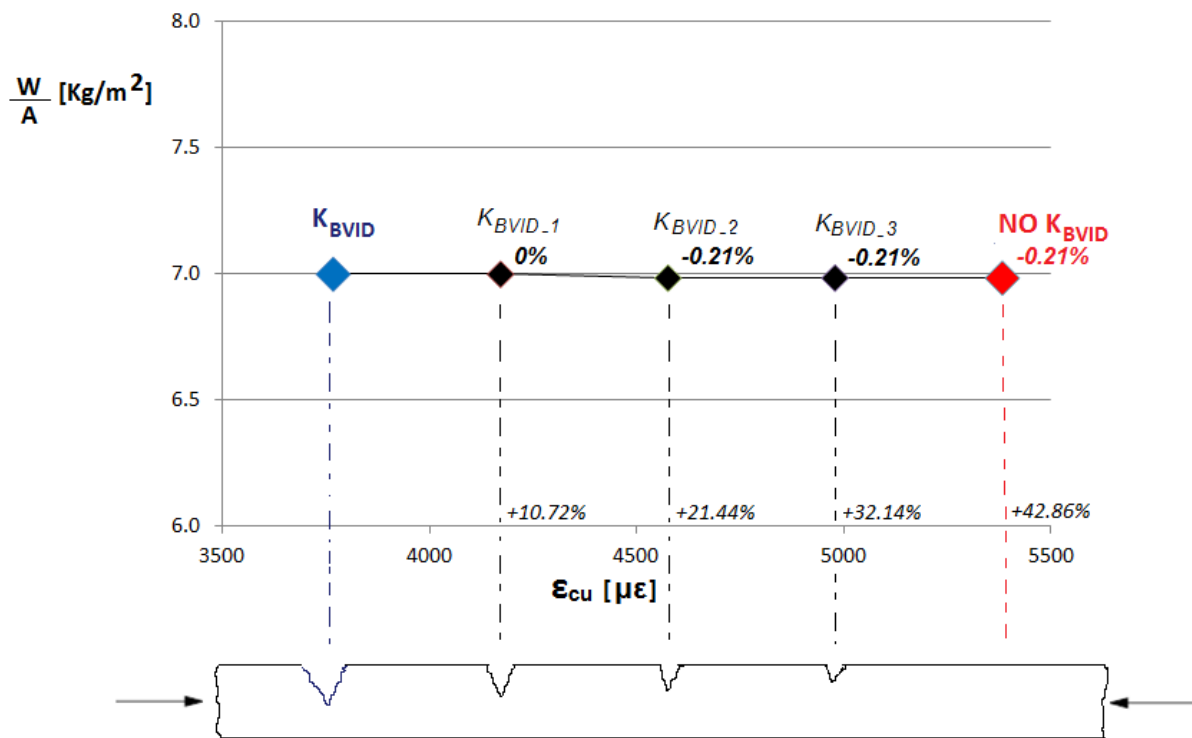


Figure 26: panel 2 – weight vs compressive design value

- For the *panel 1*, critical at strength, the results of the redesign show that weight reduction is achievable up to a reduction of **24.45%** (ideal case of no degradation for BVID) by incrementing the design allowable. Therefore *the use of a SHM system could allow the design of lighter panels depending on its specific capability and accuracy.*
- The results obtained for the *panel 2*, critical at buckling, show instead that *no weight reduction is achievable* by incrementing the design allowable, and consequently also by using SHM systems able to detect damages smaller than the damage detected by the visual inspection (BVID).

It's important to highlight that these results are sensitive to panel geometry and loads. For example, for not high loaded structures the weight reduction could be limited by minimum gage conditions and no further advantages could be obtained by increasing the material design allowable.

Further FE analyses, in particular progressive failure analyses, have been successively performed to investigate the real effects, on the total failure of the panel, of the interaction between the reduction of the panel stiffness due to buckling onset and the initiation and propagation of local failures (§ 5.3).

For sake of completeness, taking into account the results of the CAI tests, available from the material datasheet, on laminate 24-ply QI according to the ASTM standard regulation [6], the knock-down factor due to the impact damage (BVID) is equal to 0.41:

$$K_{CAI} = \frac{CAI(50J)}{CAI(0J)} = 0.41$$

This factor has been evaluated considering conservatively the static compression strength of the 50 joule impacted CAI coupon. 50 joule, according to the possible threats to the composite wing, is commonly accepted as **cut-off energy level** for the definition of the BVID.

Assuming the above factor as  $K_{BVID}$ ,

$$K_{BVID} = K_{CAI}$$

and applying it, as illustrated in § 3.1.3, to the unnotched compressive allowable, the final design allowable in compression,  $\epsilon_{cu}$ , is:

$$\epsilon_{cu} = \epsilon_{cu\_unnotched} K_{T,M} K_{B\text{-basis}} K_{BVID} = 2120 \mu\epsilon$$

This value is lower of about 43% than the design allowable of 3768  $\mu\epsilon$  based on the assumption  $K_{BVID} = K_{OHC}$  (§ 3.1.3).

Figure 27 shows, for the *panel 1* critical at strength, the weight vs compressive design allowable in the range 2120 ( $K_{BVID}$ )  $\mu\epsilon$  and 5383  $\mu\epsilon$  (NO BVID degradation).

The maximum weight reduction achievable is resulted equal to about 50% (ideal case of NO BVID).

But, as illustrated in the figure, the increment of the compressive design allowable from the CAI value up to higher values thanks to the use of SHM systems, can be limited, for designs with mechanical joints, by other critical allowables: the open hole compression (OHC) and the filled hole compression (FHC) allowables. These allowables become the new design values in place of the BVID/CAI allowable.

The use of bonding joints in place of mechanical ones, if monitored by SHM systems, could avoid this limitation and fully exploit the potential increment of the compressive design allowable up to values higher than the OHC and FHC values.

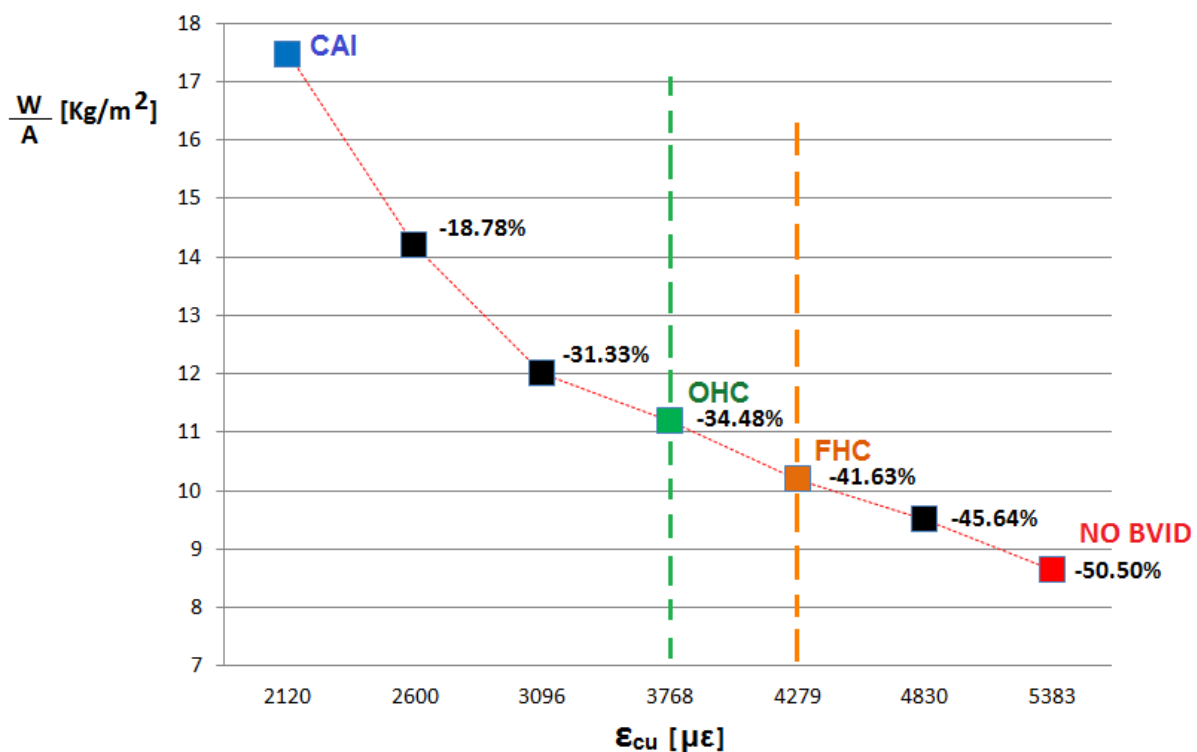


Figure 27: panel 1 – weight vs compressive design value considering also CAI knock-down factor

## 4 PROGRESSIVE FAILURE ANALYSIS METHODOLOGY

Laminated composite structures can develop local failures or exhibit local damage such as matrix cracks, fiber breakage, fiber-matrix debonds, and delaminations under normal operating conditions which may contribute to their failure. The ability to predict the initiation and growth of such damage is essential for predicting the performance of composite structures and developing reliable, safe designs which exploit the advantages offered by composite materials. The catastrophic failure of a composite structure, i.e. its ultimate load-carrying capability, rarely occurs at the load corresponding to the first-ply failure; composite structures usually fail due to the propagation or accumulation of local failures as the load is increased. Initial failure of a layer within the laminate can be predicted by applying an appropriate failure criterion; the subsequent evaluation of the failure propagation requires the use of advanced failure propagation models. The need for a reliable methodology for predicting failure initiation and propagation in composite laminated structures is of great importance.

During the years, new advanced numerical methodologies, named Progressive Failure Analysis (PFA) methodologies, based on the Finite Element Method (FEM), have been developed and employed in order to simulate the real capability of composite structures [26-32].

PFA methodologies are finalized to predict, in addition to the damage initiation (FPF), the damage propagation up to the collapse load of a composite structure. These methodologies have been implemented both in many commercial FE codes and in-house codes [14, 33-35].

PFA results obtained in a work developed at CIRA [36], concerning the assessment of PFA capability of several commercial FE codes by applying them to simple experimental test cases extracted from literature (flat and rectangular graphite-epoxy specimens with an hole and loaded in axial compression), have confirmed the capability of the current FE codes (B2000++<sup>®</sup>, ANSYS<sup>®</sup>, ABAQUS<sup>®</sup> and MSC NASTRAN<sup>®</sup>) to capture the collapse load, also in post-buckling regime, with a good accuracy.

The flowchart of a typical progressive failure analysis [15] is illustrated in Figure 28.

At each load step, a nonlinear analysis is performed until a converged solution is obtained assuming no changes in the material model. Then, using this equilibrium state, the stress distribution in each lamina is computed and stored. The computed stresses are introduced into specified failure criteria; they are compared with material allowables to determine whether any failures have occurred or not. If the adopted failure criterion indicates that lamina failure has occurred, the related lamina properties are degraded according to a particular degradation model. Since the initial nonlinear

solution no longer corresponds to an equilibrium state due to the fact that the material properties have been degraded, equilibrium of the structures needs to be re-established utilizing the modified lamina properties for the failed lamina while keeping the current load level. This iterative process, of obtaining nonlinear equilibrium solutions each time a local material model is changed, is continued until no additional lamina failures are detected. The load step is then incremented until catastrophic failure of the structure is detected (converged solution is no more obtained).

Hence PFA is based on the appropriate selection of two ingredients: the type of the failure criterion utilized to evaluate the failure initiation, and the material degradation model implemented to decrease the load carrying capability of the damaged structure.

In the following subparagraphs the fundamental key features of a typical progressive failure analysis are shown [15].

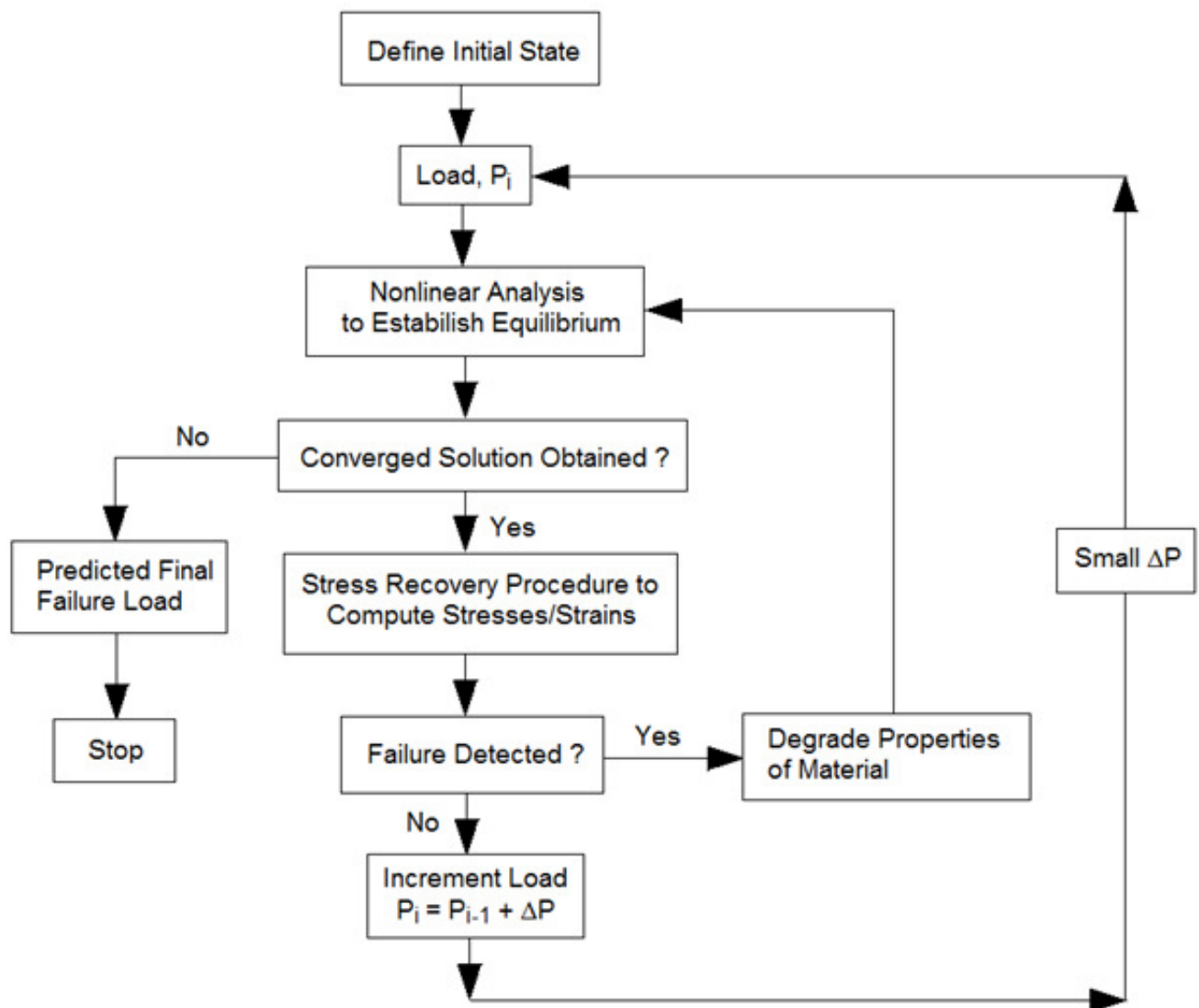


Figure 28: flowchart of a typical Progressive Failure Analysis

## 4.1 Nonlinear analysis

A nonlinear analysis is performed to take in account the geometrical nonlinear behaviour in the progressive failure analysis.

The basic concept of nonlinear analysis illustrated in Figure 29, can be summarized in the following *MultiStep* Approach:

1. Determine an increment (e.g. load, displacement)
2. Determine an estimate of the tangent stiffness matrix (default). The user can request that the stiffness matrix remains the same or will be updated exactly (tangent stiffness matrix).
3. Determine the displacement increment
4. Calculate the element forces
5. Calculate the unbalanced load and check for convergence.
  - If converged, go to Step 1
  - If not converged, continue as follows:
6. Determine an estimate of tangent stiffness matrix
7. Determine the displacement increment due to the unbalanced load
8. Calculate the element resisting forces
9. Calculate the unbalanced load and check for convergence.
  - If converged, go to Step 1.
  - If not converged, go to Step 6 or start the divergence procedure.

The update of the stiffness matrix is one of the most time-consuming calculation; this step is optional: in some cases the stiffness matrix is not updated for each iteration.

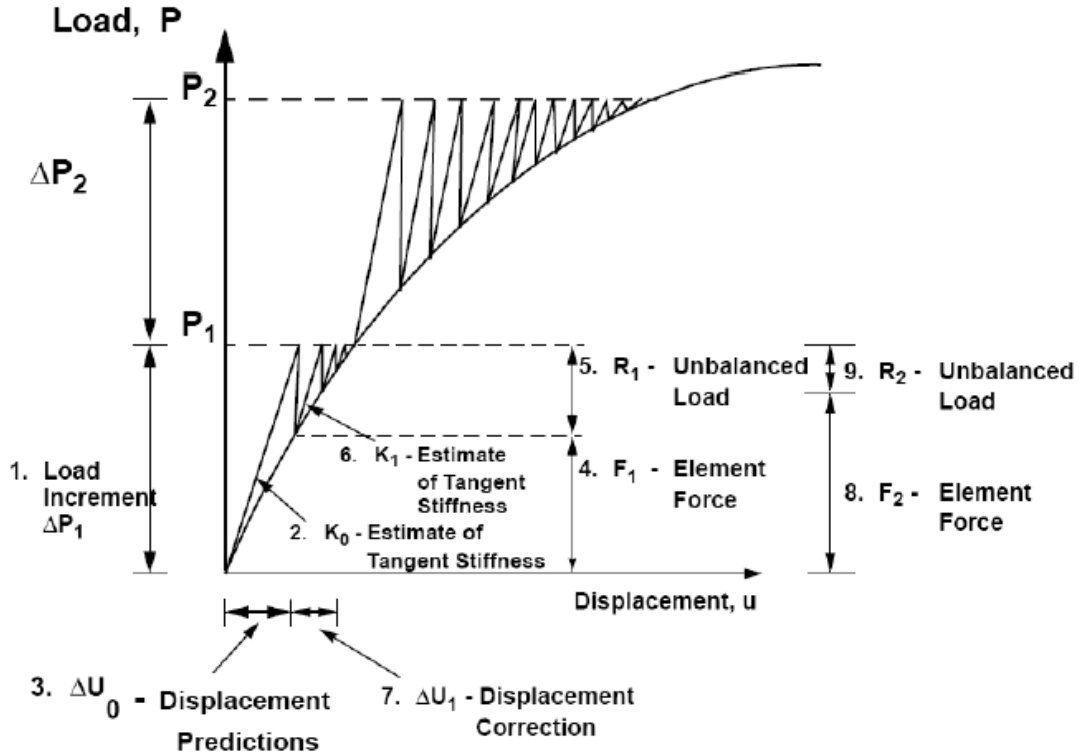


Figure 29: basic concept of nonlinear analysis

In detail, the assembled finite element equations are given by

$$[K_T(\{D\})]\{D\} = \{P\}$$

in which  $\{D\}$  is the displacement vector,  $\{P\}$  is the applied load vector, and  $[K_T]$  is the assembled tangent stiffness matrix. Composite laminates typically behave in a linear elastic manner until a local failure happens. The local failure within the laminate changes the global stiffness, and in particular the global stiffness decreases. Hence, the tangent stiffness matrix  $[K_T]$  depends on the material properties as well as the unknown displacement solution  $\{D\}$ . In the progressive failure analysis, a nonlinear analysis is performed until a converged solution is obtained for a constant set of material properties. The nonlinear analysis involves solving the linearized finite element equations for the  $k^{\text{th}}$  iteration

$$[K_T]^{(k)}\{\Delta D\} = \{R\}^{(k)}$$

$$\{D\}^{(k+1)} = \{D\}^{(k)} + \{\Delta D\}$$

where the tangent stiffness matrix  $[K_T]^{(k)}$  and force imbalance vector  $\{R\}^{(k)}$  are functions of the displacements  $\{D\}^{(k)}$ . Solving the equilibrium equations is an iterative process where the  $k^{th}$  step requires computing the displacement increment  $\{\Delta D\}$  for the  $k + 1$  load step using the  $k^{th}$  tangent stiffness matrix. Then the  $k^{th}$  displacement vector  $\{D\}$  is updated using  $\{\Delta D\}$ . Having a new displacement solution, the force imbalance vector  $\{R\}$  and possibly the tangent stiffness matrix  $[K_T]$  are updated, and the process is continued for the next iteration. The solution process is continued until convergence is achieved by reducing the force imbalance  $\{R\}$ , and consequently  $\{\Delta D\}$  to within some tolerance.

Using this nonlinear solution corresponding to a given load step, the lamina stresses are determined and used with a failure criterion to determine whether any failures have occurred during this load increment. If no failures are detected, then the applied load is increased, and the analysis continues. When a failure in the laminate occurs, a change in the stiffness matrix due to a localized failure is calculated considering the material degradation model. If the load step size is too large, static equilibrium needs to be re-established by repeating the nonlinear analysis at the current load step using the new material properties in the tangent stiffness matrix. This process is repeated until no additional failures are detected. Alternatively, small load step sizes can be used thereby minimizing the effect of not re-establishing equilibrium at the same load level. This incremental iterative process is performed until a lack of convergence in the nonlinear solution occurs.

The most popular iterative scheme for the solution of nonlinear finite element equations is the Newton-Raphson procedure, Figure 30, which is widely used because it generally converges quite rapidly.

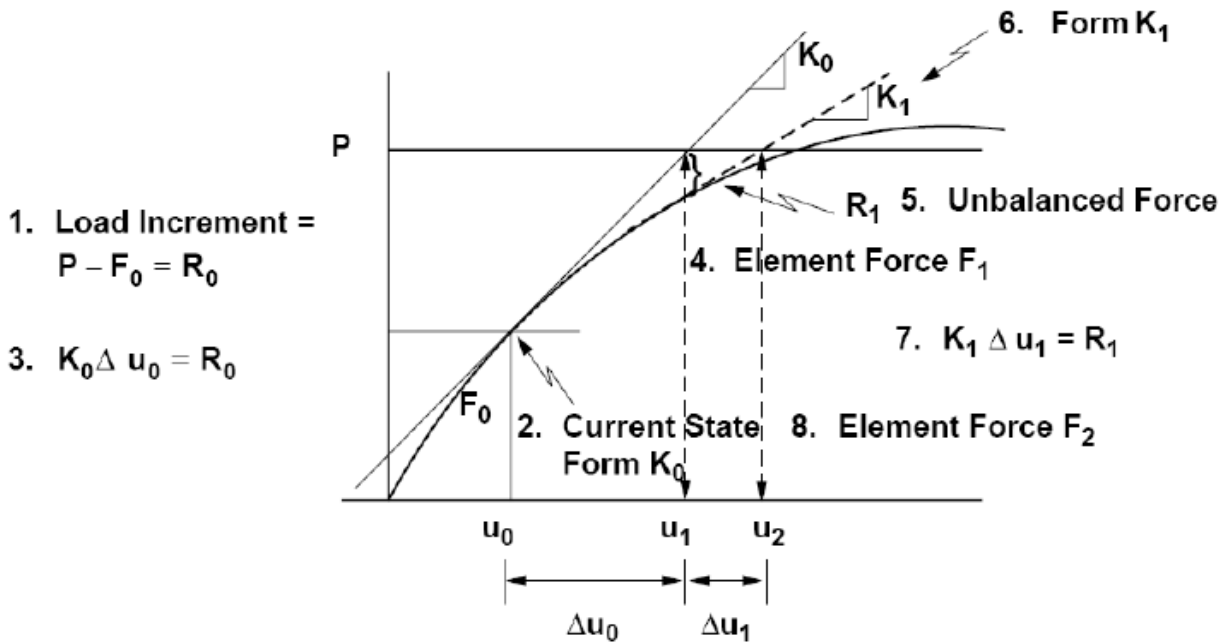


Figure 30: Newton Raphson method

However, one of the drawbacks of the Newton-Raphson procedure is the large amount of computational resources needed to evaluate, assemble, and decompose the tangent stiffness matrix at each iteration.

To reduce the computational effort, a Modified Newton-Raphson procedure is commonly used. The modified Newton-Raphson procedure differs from the Newton-Raphson method because the tangent stiffness matrix is not updated on each iteration but periodically during the analysis, such as at the beginning of each new load step.

## 4.2 Failure analysis

The catastrophic failure of a composite structure rarely occurs at the load corresponding to the initial or first-ply failure. Instead, the structure collapses due to the propagation or accumulation of local failures (or damage) as the load is increased. Initial failure of a layer within the laminate of a composite structure can be predicted by applying an appropriate failure criterion or first-ply failure theory. The subsequent failure prediction requires an understanding of failure modes and failure propagation. Composites may fail by fiber breakage, matrix cracking, or by delamination of layers. The failure mode, among several factors, depends upon the loading, stacking sequence, and specimen geometry. These failure modes depend on the constituent's strength properties, whereas

delamination may be due to manufacturing anomalies during lay-up or curing or out-of-plane effects. However, the progressive failure methodology applied in this work only includes predictions for fiber breakage and matrix cracking. Various failure criteria have been proposed in literature to predict the intralaminar damage in composite laminate; a good review of composite failure theories and related failure criteria was given in [37]. Most failure criteria are based on the stress state in a lamina. Ideally, a three-dimensional model is desirable to obtain accurate stresses and strains. However, due to the extensive amount of computational time required for a three-dimensional analysis, two-dimensional failure analyses are usually performed using plate and shell finite element models. Failure criteria are intended to predict macroscopic failures in the composite laminate and are based on the tensile, compressive, and shear strengths of the individual lamina. If a stress limit within a lamina/layer is not exceeded, the material properties in the layer are not changed and then the other layers within the laminate are checked. When a material allowable value is exceeded in a layer, the engineering material constants corresponding to the related failure mode are reduced in according to the material degradation model.

Often, failure criteria for composite materials are classified into two groups [15]:

- Non-Interactive Failure Criteria: they don't include interactions between the stress or strain components. These criteria, sometimes called independent failure criteria, compare the individual stress or strain components with the corresponding material allowable strength values. The maximum stress and maximum strain criteria belong to this category. Both failure criteria indicate the type of failure mode. The failure surfaces for these criteria are rectangular in stress and strain space, respectively [38].
- Interactive Failure Criteria: they involve interactions between stress and strain components. Interactive failure criteria are mathematical in their formulation. Interactive failure criteria fall into three categories: (1) polynomial theories, (2) direct-mode determining theories, and (3) strain energy theories. The polynomial theories use a polynomial based upon the material strengths to describe a failure surface [39]. The direct-mode determining theories are usually polynomial equations based on the material strengths and use separate equations to describe each mode of failure. Finally, the strain energy theories are based on local strain energy levels determined during a nonlinear analysis.

The most popular polynomial failure criterion for composite materials is the tensor polynomial criterion proposed by Tsai and Wu [40]. Other quadratic failure criteria includes Tsai-Hill [41, 42], Azzi and Tsai [43], Hoffman [44]. One of the disadvantages of these quadratic failure criteria is that they predict the failure but say nothing about the failure mode or how the composite fails.

Direct-mode determining failure criteria are very useful in progressive failure analysis because, respect to the other two categories, they also describe the failure mode of the composite laminate, i.e. how the composite fails. Hashin criterion [45] belongs to this category and it has been applied in this work. This criterion distinguishes four failure modes: **tensile fiber**, **compressive fiber**, **tensile matrix** and **compressive matrix**. The **Hashin** failure indices ( $FI_i$ ) are the following ones:

*tensile fiber mode*

$$FI_1 = \left(\frac{\sigma_1}{F_{1t}}\right)^2 + \frac{\sigma_{12}^2 + \sigma_{13}^2}{F_{12}^2} \quad \text{if } \sigma_1 > 0$$

*compressive fiber mode*

$$FI_2 = \left(\frac{\sigma_1}{F_{1c}}\right)^2 \quad \text{if } \sigma_1 \leq 0$$

*tensile matrix mode*

$$FI_3 = \left(\frac{\sigma_2 + \sigma_3}{F_{2t}}\right)^2 + \frac{\sigma_{23}^2 - \sigma_2 \sigma_3}{F_{23}^2} + \frac{\sigma_{12}^2 + \sigma_{13}^2}{F_{12}^2} \quad \text{if } (\sigma_2 + \sigma_3) > 0$$

*compressive matrix mode*

$$FI_4 = \frac{1}{F_{2c}} \left[ \left(\frac{F_{2c}}{2F_{23}}\right)^2 - 1 \right] (\sigma_2 + \sigma_3) + \left(\frac{\sigma_2 + \sigma_3}{2F_{23}}\right)^2 + \frac{\sigma_{23}^2 - \sigma_2 \sigma_3}{F_{23}^2} + \frac{\sigma_{12}^2 + \sigma_{13}^2}{F_{12}^2} \quad \text{if } (\sigma_2 + \sigma_3) \leq 0$$

where  $\sigma_{ij}$  is the stress in the material directions, and  $F_{lm}$  are the lamina allowable stresses.

Failure occurs if  $FI_i \geq 1$ . In this work Hashin formulation for shell elements has been used.

### 4.3 Material degradation

If failure is detected in a lamina of the composite material, the properties of that lamina have to be degraded in according to a material property degradation model; in general three categories can be identified [15], Figure 31: instantaneous unloading [46], gradual unloading [47, 48] and constant stress at ply failure [49]. For the instantaneous unloading case, the material property associated with

that mode of failure is degraded instantly to zero. For the gradual unloading case, the material property associated with that mode of failure is degraded gradually (linearly or exponentially) until it reaches zero. For the constant stress case, the material properties associated with that mode of failure are degraded such that the material cannot sustain additional load. The behaviour of the lamina as it fails, as well as which elastic constants are degraded, depends on the failure mode of the composite laminate.

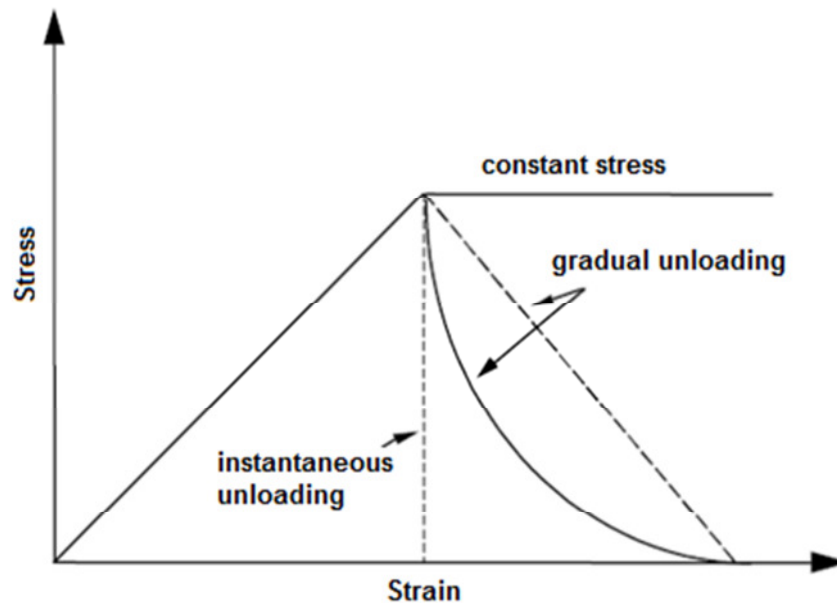


Figure 31: post-failure degradation behaviour in composite laminate [15]

#### 4.4 Re-establishment of equilibrium

Once a lamina fails and the stiffness properties have been degraded, it is often necessary to recalculate the element stiffness matrices and update the tangent stiffness matrix of the model. This new tangent stiffness matrix accounts for the local changes in material stiffness as well as any large deformation effects associated with geometric nonlinearities. The nonlinear analysis procedure described earlier is then used to re-establish equilibrium at the same load level for the composite structure with localized failures. To establish equilibrium, additional iterations may be required until a new converged solution is reached. Once obtained, checks for subsequent lamina failures are necessary. If the load steps are restricted to be small, such a procedure may not be needed.

## 4.5 MSC Nastran<sup>®</sup> PFA capability

PFA is carried out in MSC Nastran<sup>®</sup> by using SOL 400 solution sequence, [50]. The progressive failure mechanism implemented in MSC Nastran<sup>®</sup> foresees:

- linear elastic behaviour of the composite laminate up to a local failure happens;
- the composite laminate is failed on layer-by-layer basis;
- upon failure, the elastic properties are scaled down;
- the degradation model is selective (if matrix fails, the fiber properties do not change);
- the degradation model can be immediate or gradual.

In particular, in this work the PFA has been executed in MSC Nastran<sup>®</sup> software by selecting:

- ✓ Hashin criteria, to detect the lamina failure (§ 4.2).
- ✓ the immediate (instantaneous unloading) degradation model: when failure occurs, the respective material moduli are set to a fraction of the original value (*residual stiffness factor,  $K$* ); in particular, when lamina failure is detected by using Hashin criteria, if the failure mode is the fiber mode, the lamina property  $E_1$  is reduced; if the failure mode is the matrix one,  $E_2$ ,  $G_{12}$ ,  $G_{23}$  and  $G_{13}$  are reduced. For sake of clarity, the stiffness material property associated with that mode of failure ( $E_j$ ) is degraded instantly to a fraction  $K$  of the initial value:  $E_{j\_new} = K E_{j\_old}$ .
- ✓ Pure Full Newton-Raphson iteration method for the solution of nonlinear finite element equations.
- ✓ automatic adaptive load stepping procedure in order to minimize the time step dependence.

The immediate degradation model has been preferred to the gradual one. This choice is due to previous results of progressive failure analyses performed by using MSC Nastran<sup>®</sup> code to simulate simple experimental test cases ([36]): the residual strength obtained by using the gradual degradation model was quite overestimated respect to the experimental results, while the results obtained with the immediate model better fitted the experimental data.

About the finite element used for the discretization of the composite structure illustrated in this work, a four-node layered shell element has been applied: *Element 75*. This element is a four-node, thick-shell element with global displacements and rotations as degrees of freedom, with a full integration scheme. Bilinear interpolation is used for the coordinates, displacements and the

rotations. It is a very efficient and simple element which exhibits correct behaviour in the limiting case of thin shells. Due to its simple formulation when compared to the standard higher order shell elements, it is less expensive and, therefore, very attractive in nonlinear analysis.

## 5 DISCRETE DAMAGE MODEL ANALYSIS

According to the new design criteria and approaches illustrated in § 2.2.2 and § 2.2.3, in order to evaluate the real capability of the stiffened panels, discrete damages have been introduced in the panel and keeping the mechanical strength properties of the material without degradation for BVID (Figure 17-a), in contrast to the traditional design based on the assumption of the whole panel uniformly damaged by applying a knock-down factor  $K_{BVID}$ . For this purpose, according to the simplified design approach illustrated in § 2.2.3 and in particular to the indications enclosed in the guidelines for the preliminary design of composite structures issued by Northrop Grumman [23], a hole 6.35 mm (1/4 ") in diameter has been selected as equivalent to the BVID.

For the research objectives of the present work discrete damages only in the skin of the panel have been analysed, and no delaminations and disbonding skin-stringers have been considered. In a future research activity it is foreseen to analyse the panel response in presence of delaminations and skin-stringer disbondings.

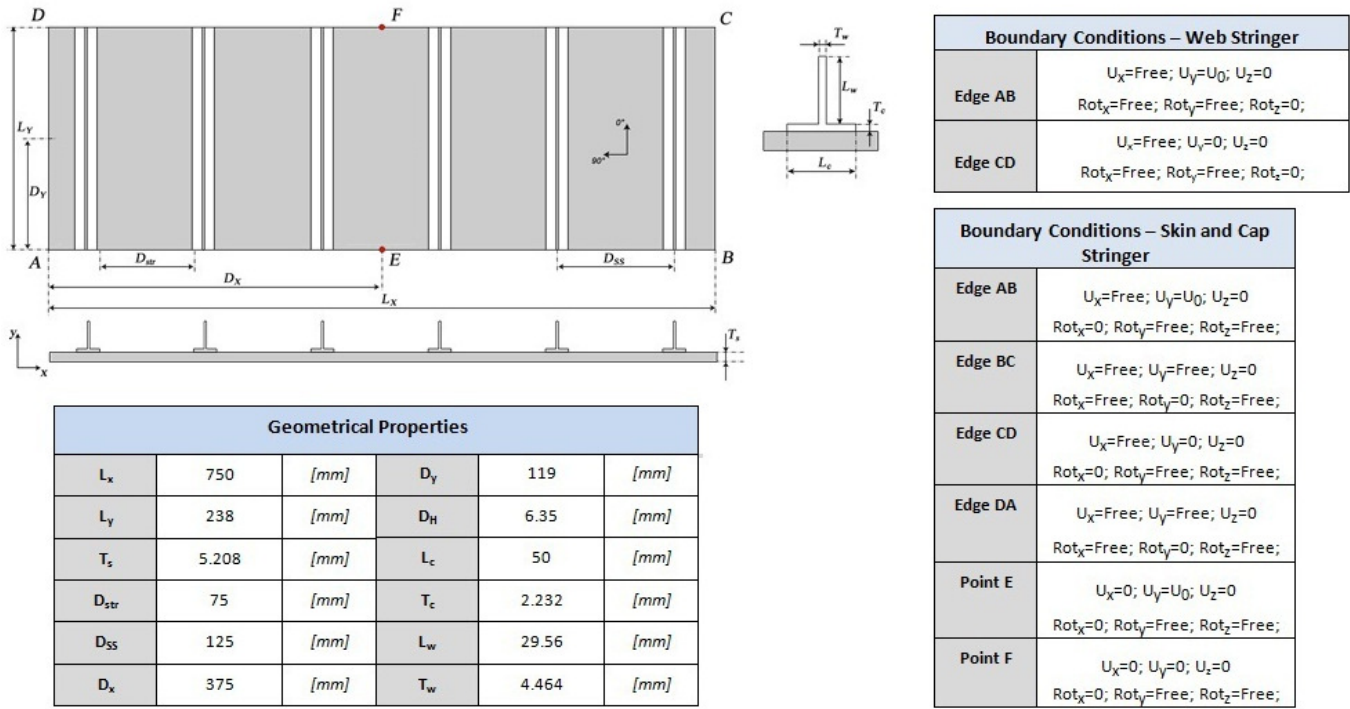
The entire panels are discretized by means of four-node layered shell element with a full integration scheme (§ 4.5) and the linkage between the skin and the stringers is modelled by contact elements with multi-point constraints option.

PFA has been performed according to the methodology illustrated in § 4.

### 5.1 PFA of the panel critical at strength

PFA has been performed for the panel located at wing root and sized at strength, *panel 1* (Figure 18) with a hole of 6.35 mm in the skin, in the middle of the central stringer bay, and without the application of the knock-down factor  $K_{BVID}$ .

The boundary conditions of the panel are the same ones applied for its design by means of Hypersizer<sup>®</sup> in stand-alone approach (§ 3.1.4); Figure 32 summarizes its geometry and boundary conditions. The panel is loaded in axial compression: a uniform displacement along the y-axis is applied to the edge AB.



skin: 28\_[45/-45/45/-45/0/0/90/0/0/45/-45/0/90/0]s  
 stringer\_cap: 12\_[45/-45/0/0/90/0]s

Figure 32: reference panel critical at strength (panel 1)

5.1.1 FE Model validation

Before performing PFA on the panel with the hole under compressive load, FE analyses have been initially developed on the reference panel (Figure 18) with and without  $K_{BVID}$  (Figure 17); Figure 33 shows the FE model.

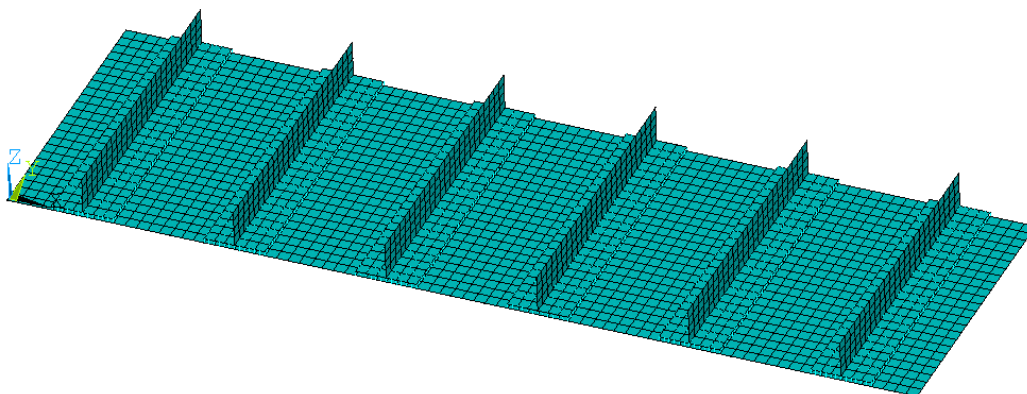


Figure 33: FE model of the panel

This model has been used in order to evaluate both the rightness of the FE model and to compare the FEA results with those ones obtained with Hypersizer<sup>®</sup> code (§ 3.1).

In detail, the following FE analyses have been performed on the model of Figure 33:

- a) linear buckling,
- b) nonlinear static with and without  $K_{BVID}$ ,
- c) PFA with and without  $K_{BVID}$ .

and the following nomenclature has been used

- BUCK: buckling;
- DA: damaged – BVID degradation of the material strength allowables by  $K_{BVID}$ , Figure 17-b;
- HS: Hypersizer<sup>®</sup>/stand-alone design;
- LB: linear buckling
- NL: nonlinear analysis;
- UDA: undamaged – no BVID degradation of the material strength allowables (NO  $K_{BVID}$ ), Figure 17-a;
- TF: Total Failure (collapse load)

Figure 34 illustrates the Reaction Force vs the Applied Strain for the analysis of the above point a) and b) and the results obtained with Hypersizer<sup>®</sup>.

According to the results of the nonlinear analysis illustrated in Figure 34, it has been not necessary the introduction of a buckling trigger (perturbed mesh) to evaluate the buckling load.

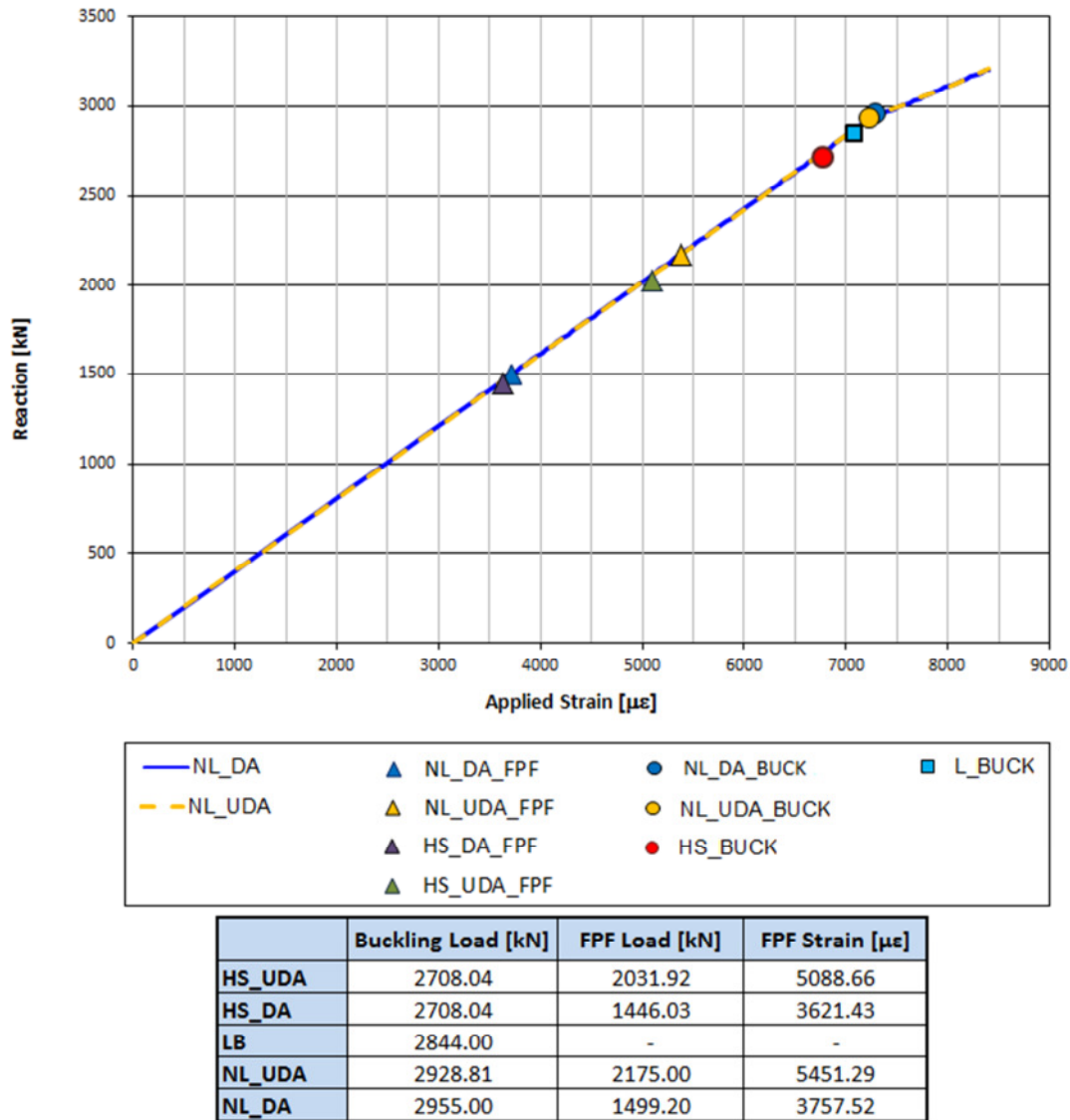


**Figure 34: Reaction vs Applied Strain – Linear and Nonlinear analysis – Hypersizer® results**

The results of the FE analyses are well correlated to those ones of the stand-alone design by Hypersizer®. The result of the FE linear buckling analysis is higher of about +5% with respect to that one of the stand-alone design, HS\_BUCK. FPF values obtained by nonlinear FE analyses, DA and UDA models, are higher of about +3.5% and +7% respectively. Hypersizer® is slightly more conservative.

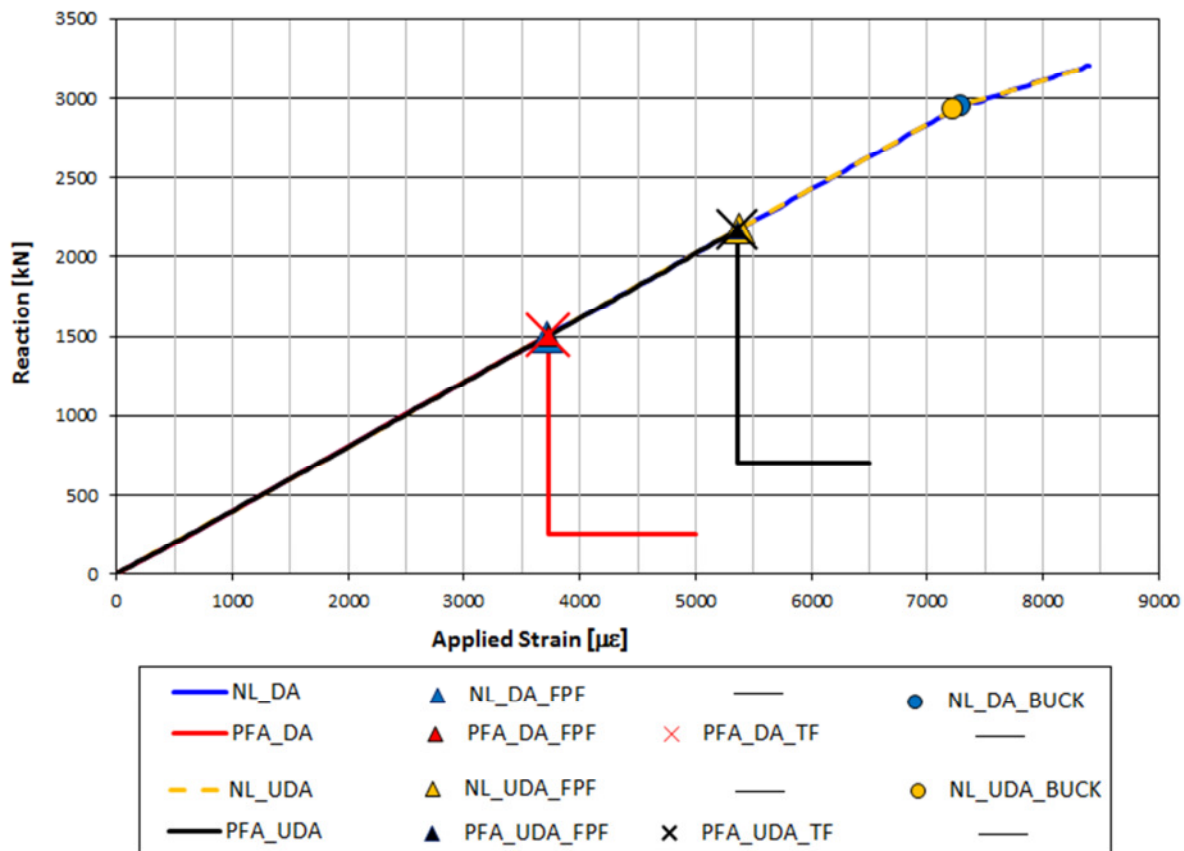
The FE linear buckling and nonlinear buckling analyses, with and without  $K_{BVID}$  (DA and UDA), are as expected very close to each other.

For the nonlinear analysis without PFA, as expected the FPF load is coincident with the total failure load TF, i.e. collapse load of the panel; the PFA is not activated, so *the damage of the panel does*

not trigger the degradation of material causing a stiffness reduction of the structure; the slope changing is only due to the buckling phenomena and it is the same for the UDA and DA panels.

Figure 35 shows the Reaction Force vs the Applied Strain for the analysis of the above point c): PFA for DA and UDA panels and the comparison with the results of the nonlinear analysis.

PFA has been performed to verify if there is a difference in the total failure evaluation of the panel respect to the nonlinear analysis.



	FPF Load [kN]	%	FPF Strain [μϵ]	%	Total Failure [kN]	%	FAILURE Strain [μϵ]	%	Buckling Load [kN]
NL_DA	1499.20	-	3757.52	-	-	-	-	-	2955.00
PFA_DA	1499.15	0%	3757.38	0%	1499.15	-	3757.38	-	-
NL_UDA	2175.00	-	5451.29	-	-	-	-	-	2928.81
PFA_UDA	2166.42	-0.39%	5429.79	-0.39%	2166.42	-	5429.79	-	-

Figure 35: Reaction vs Applied Strain – PFA and Nonlinear analysis

The results of the PFA illustrated in Figure 35 confirm that the panel is sized at strength: the total failure, i.e. collapse load of the panel, is lower than the buckling load for both the panels UDA and DA.

The values of the FPF and the TF loads obtained by the PFA are coincident for both the UDA and DA panels, and they are coincident with the results obtained with the nonlinear analysis (FPF), therefore as happens for the results of the nonlinear analysis, *no damage evolution occurs*.

This is due to the following consideration:

because of the type of load (pure compressive load), because of the boundary conditions and the geometry of the panel (panel without hole), it is reasonable to assume that the distribution of stress is the same in each section of the panel orthogonal to the load direction; therefore, for a given lamina, the value of stress will be the same in each point of the panel; when the failure is reached in the lamina oriented at  $0^\circ$  (load direction), the panel is not able to withstand additional loads, and then collapses: this confirms that the FPF load and the TF load are the same and therefore no residual strength is available.

Furthermore, the values of the failure strains obtained by the PFA analysis (equal to those ones of the nonlinear analyses),  $3757.38 \mu\epsilon$  for the DA panel and  $5451.79 \mu\epsilon$  for the UDA panel, are as expected practically coincident with the allowable compressive design values respectively of the material with  $K_{BVID}$  (Figure 17-b,  $\epsilon_{cu}=3768 \mu\epsilon$ ) and of that one without  $K_{BVID}$  (Figure 17-a,  $\epsilon_{cu}=5383 \mu\epsilon$ ). The slight differences are only due to purely numerical aspects.

### 5.1.2 PFA for the panel with hole

PFA has been performed on the panel with one hole in the middle of the central stringer bay, Figure 36. In this case, the allowable compressive design values are degraded taking into account only temperature and moisture effects and B-basis statistical reduction; no BVID knock-down factor is applied because BVID has been taken into account by introducing the hole in the panel.

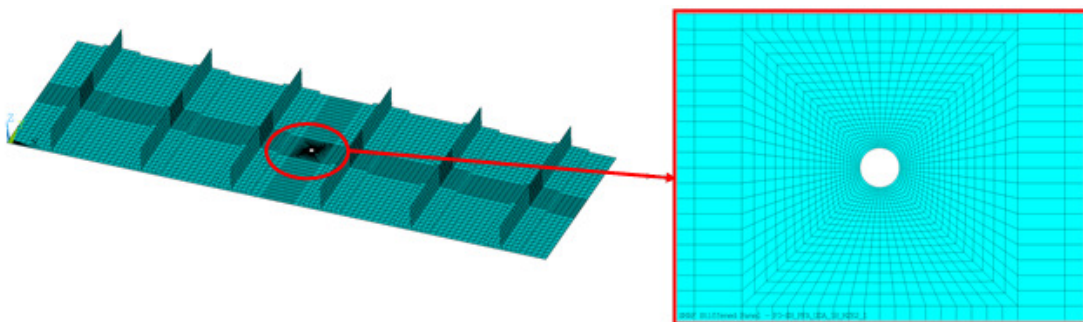
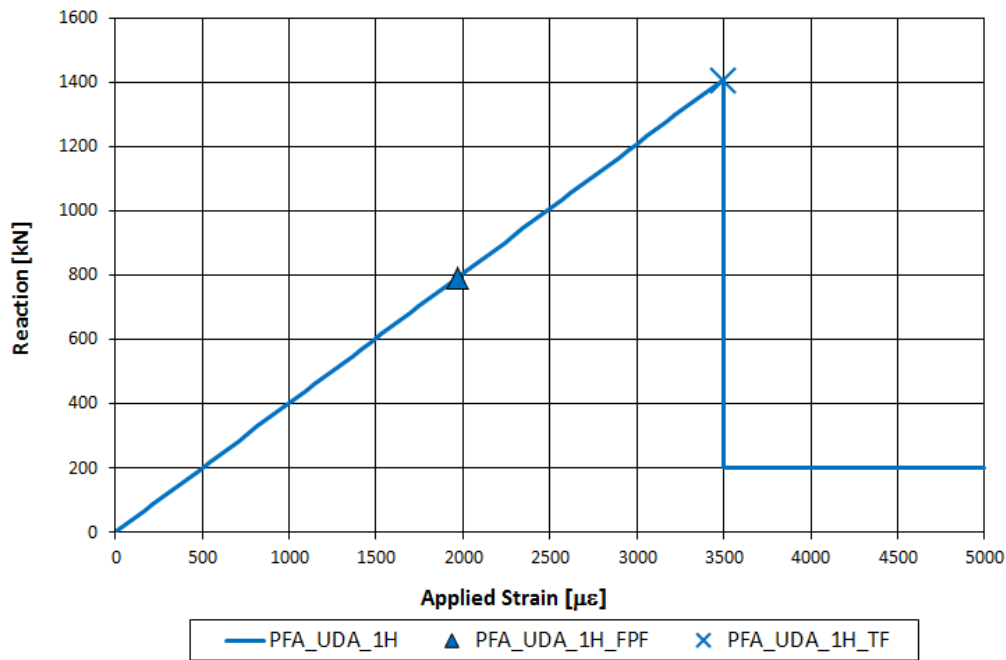


Figure 36: FE model of the panel with one hole in the middle of the central stringer bay

Figure 37 illustrates the Reaction Force vs the Applied Strain for the above panel (UDA\_1H). The presence of *the hole* (i.e. defect/damage) *triggers off the degradation of the material* inducing a propagation of the damage from the initiation of the failure in a lamina, FPF load, up to the total failure of the panel, TF load: FPF load and TF load are not coincident.

This result is in contrast respect to that one obtained for the UDA and DA panels (i.e. without hole, § 5.1.1).



**Figure 37: Reaction vs Applied Strain – panel with hole in the middle of the central stringer bay**

Figure 38 illustrates the damaged elements (elements in red) at different load substeps: from the FPF up to the total failure. As expected, the failure of the panel starts close to the hole and it propagates along a line perpendicular to the load direction. The damaged ply is the fifth one of the skin laminate, oriented at  $0^\circ$  (Figure 32), and characterized by compressive fiber failure.

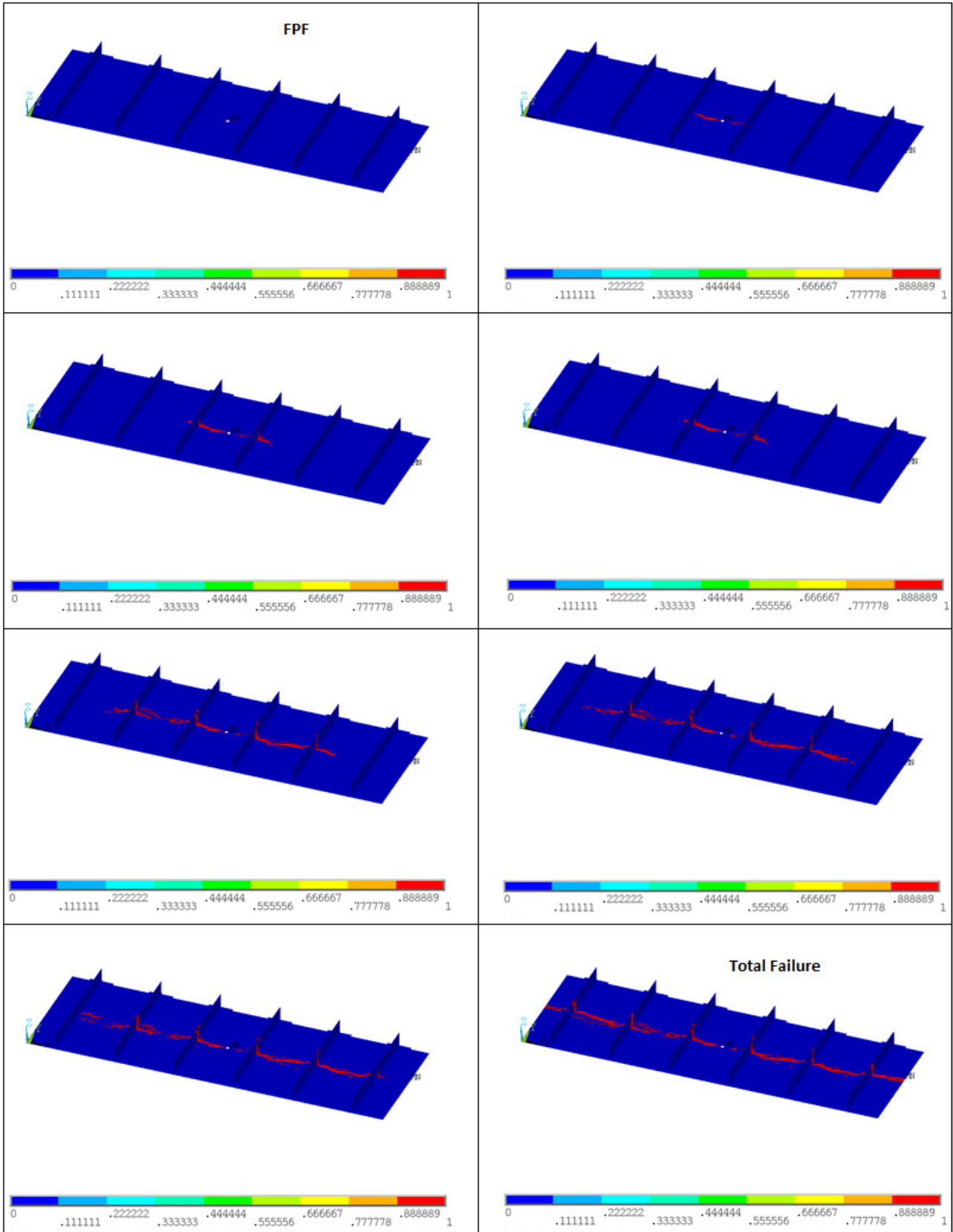


Figure 38: progressive failure of the panel UDA\_1H

Figure 39 compares the Reaction Force vs the Applied Strain of the PFA for the panel with the hole (PFA\_UDA\_1H, Figure 37) and of the PFA for the DA panel (uniformly damaged panel by the application of  $K_{BVID}$ , Figure 35).

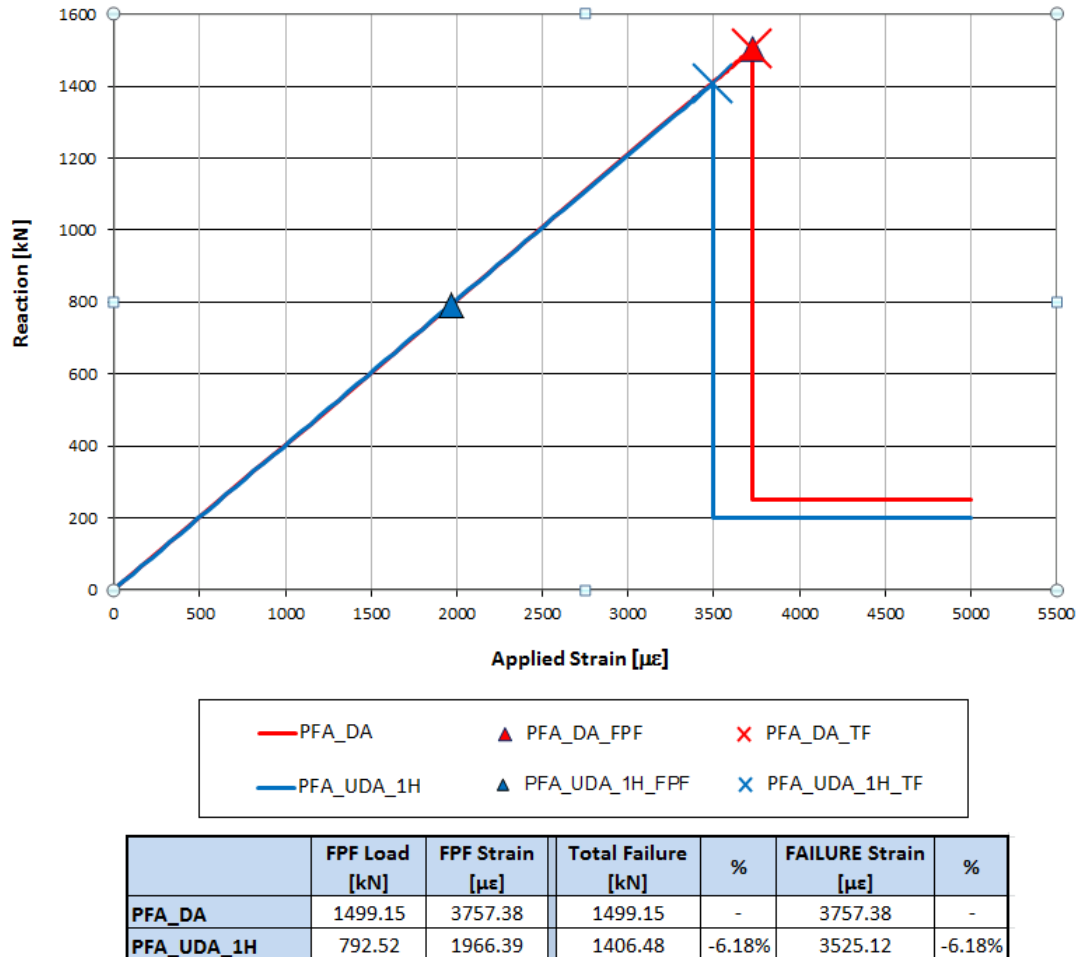


Figure 39: Reaction vs Applied Strain – PFA – panel with hole and DA panel

The difference of the total failure is only of about 6% between the two models, Figure 40.

The presence in the skin of only one hole 6.35 mm in diameter, the same hole diameter on which is based the OHC test [25], returns practically the same residual strength of the DA panel. In particular the slight lower value of residual strength of the *panel 1* with one hole respect to the DA panel should be due to the fact that the factor  $K_{OHC}$ , applied to the material compressive allowable as BVID, is based on the test executed on the QI laminate (25% 0°, 50% ± 45°, 25% 90°) as demanded by OHC test, while the layup of the skin of the panel is characterized by a different layup: 42.86% 0°, 42.86% ± 45°, 14.28 % 90° (Figure 18).

The increment of the plies along 0° direction respect to the QI laminate should reduce the residual strength of the laminate.

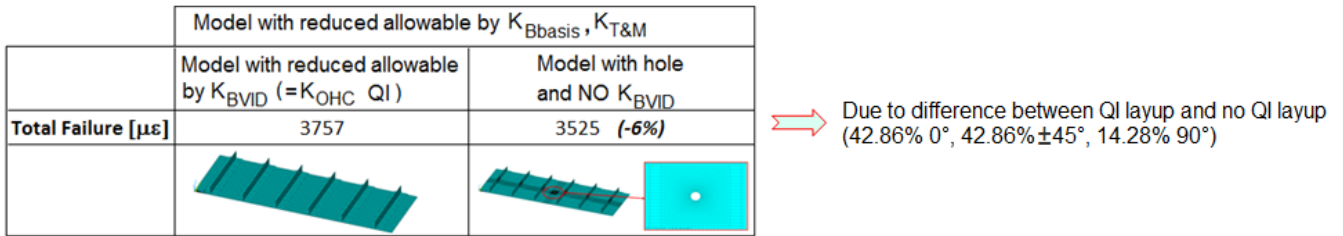


Figure 40: panel 1H vs DA panel

In support of this result a campaign of numerical validation of the OHC test has been executed and also a sensitivity analysis of the residual strength with the ratio W/D (ratio between the width of the coupon and the hole diameter).

In particular on the base of the result of the OHC test available from the material datasheet, PFA analysis has been performed in order to reproduce numerically this test and to confirm the capability of the PFA to give realistic results, therefore also for the above stiffened panel even if it is characterized by a more complexity of the FE model.

The results of the residual strength for different layups and W/D values are shown in Figure 41.

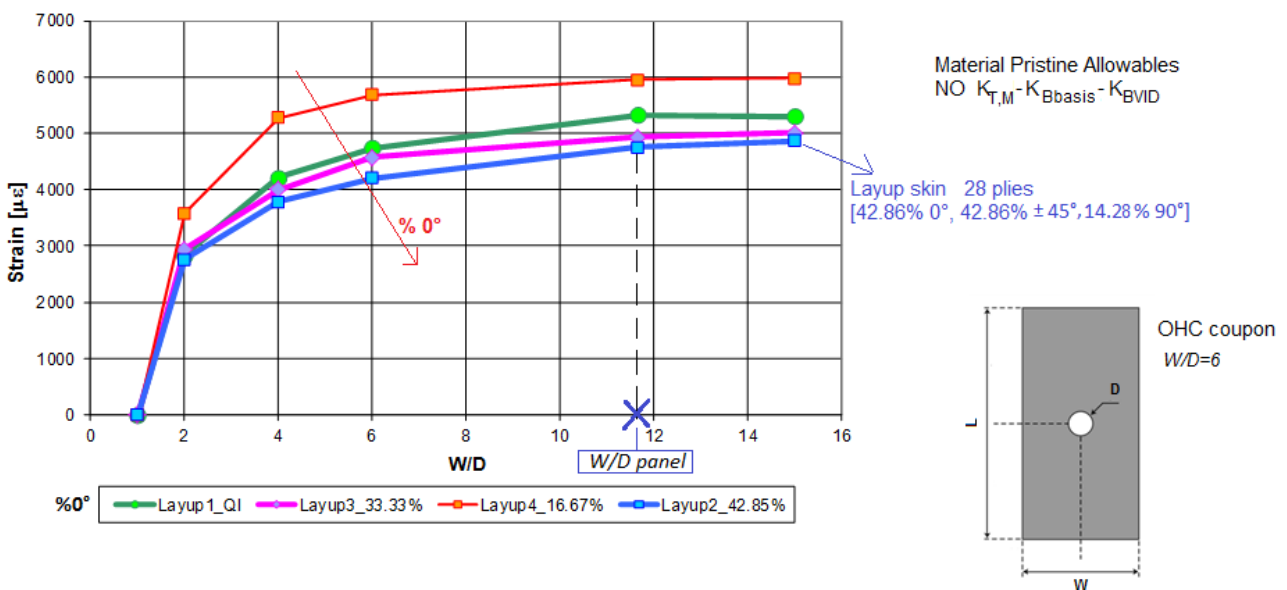


Figure 41: OHC test simulation – failure strain vs W/D for different layups

$W/D = 6$  is the value specified in the ASTM standard regulation for the OHC test [25].

For all the layups the ultimate strain (i.e. total failure) reaches a plateau for  $W/D = 15$ .

The ultimate strain decreases with the increment of the percentage of the plies oriented along  $0^\circ$  direction; in particular the lowest value is that one relative to the layup of the skin of the stiffened panel under investigation (layup 2, Figure 41), and therefore lower than the value obtained for the QI laminate.

The open span  $W$  of the panel is equal to 75 mm, Figure 42; the ratio  $W/D$  is 11.81.

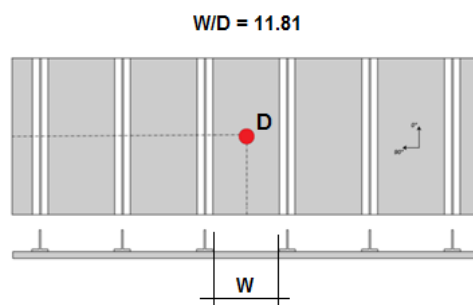


**Figure 42: reference panel –  $W/D$  ratio**

According to the results illustrated in Figure 41, the knock-down factor  $K_{OHC}$  for the same layup of the skin of the panel and for  $W/D = 11.81$  is equal to 0.65:

$$K_{OHC} = \epsilon_{OHC} (W/D=11.81) / \epsilon_{cu\_unnotched} = 4750/7333 = 0.65.$$

This factor, if applied to the total failure value of the UDA panel (PFA\_UDA), that is  $5430 \mu\epsilon$  (Figure 35), would give an ultimate strain of the same panel but with one hole of about  $3530 \mu\epsilon$ , that is practically coincident with the value of total failure obtained by the PFA executed on the FE model of the panel with one hole and without  $K_{BVID}$ , PFA\_UDA\_1H (Figure 39), as it is summarised in the next Figure 43.

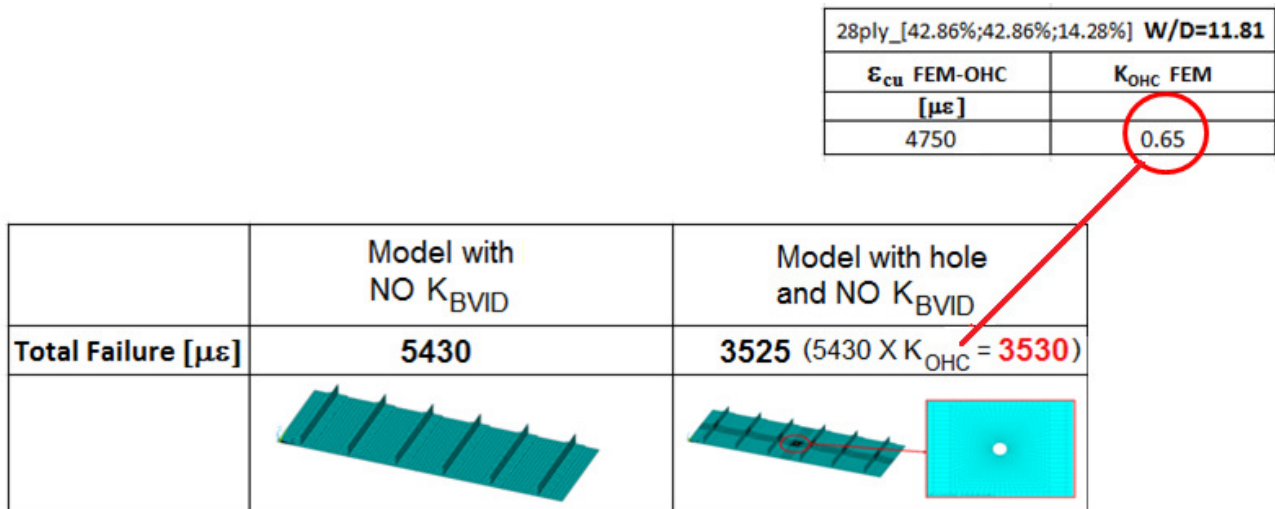


Figure 43: total failure of the stiffened panel on the base of OHC test

This result establishes that in the evaluation of the total failure of the stiffened panel it is dominant the effect of the ratio W/D:

- the total failure of the stiffened panel is obtained from the OHC curve (ultimate strain vs W/D, Figure 41) for the same skin layup and W/D value of the panel.

In confirmation of this consideration, the PFA has been performed also for the two stringers subpart of the reference panel (same W/D ratio), as illustrated in Figure 44; the value of the total failure of the panel with two-stringers is practically equal to that one of the whole panel with six stringers, confirming that the dominant parameter is the ratio W/D.

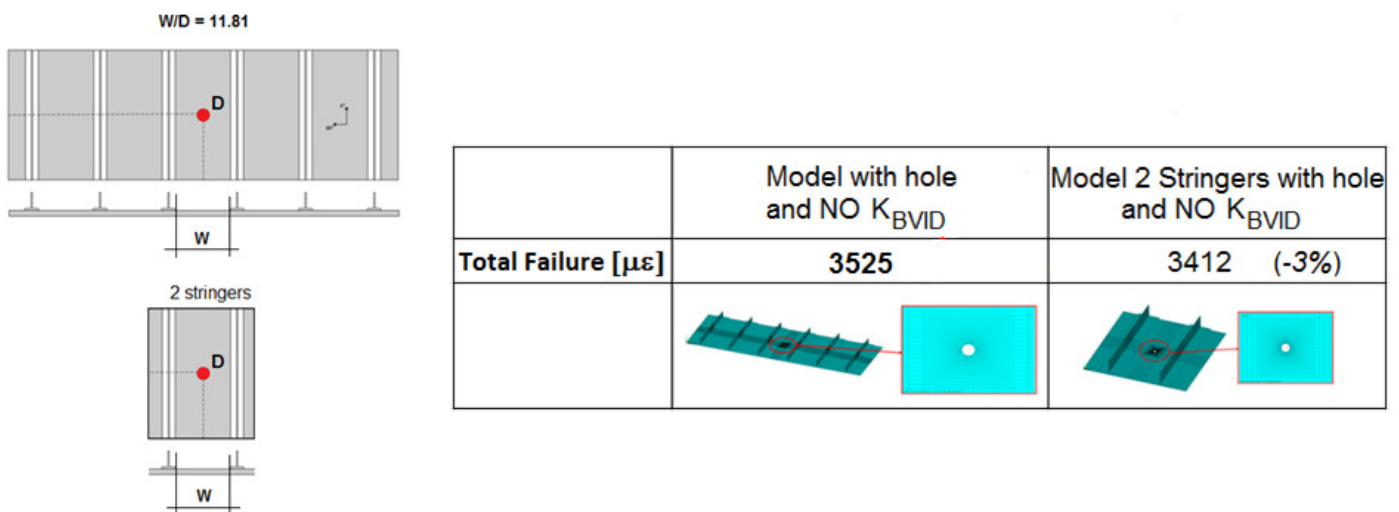


Figure 44: total failure – reference panel (6 stringers) vs panel with 2 stringers

## 5.2 Sensitivity of the total failure to damage density for the panel critical at strength

Discrete damages, holes 6.35 mm in diameter, have been considered in different locations in the skin of the panel critical at strength, *panel 1* (Figure 18), and without the application of the knock-down factor  $K_{BVID}$ . The scope has been the evaluation of the sensitivity of the collapse load of the panel with respect to the different locations of a single damage and also in presence of multi-damage maps (damage density). In the latter case maps with three, five, and seven holes have been considered.

Figure 45 illustrates a scheme of the different locations of the holes in the skin and the relative identification code.

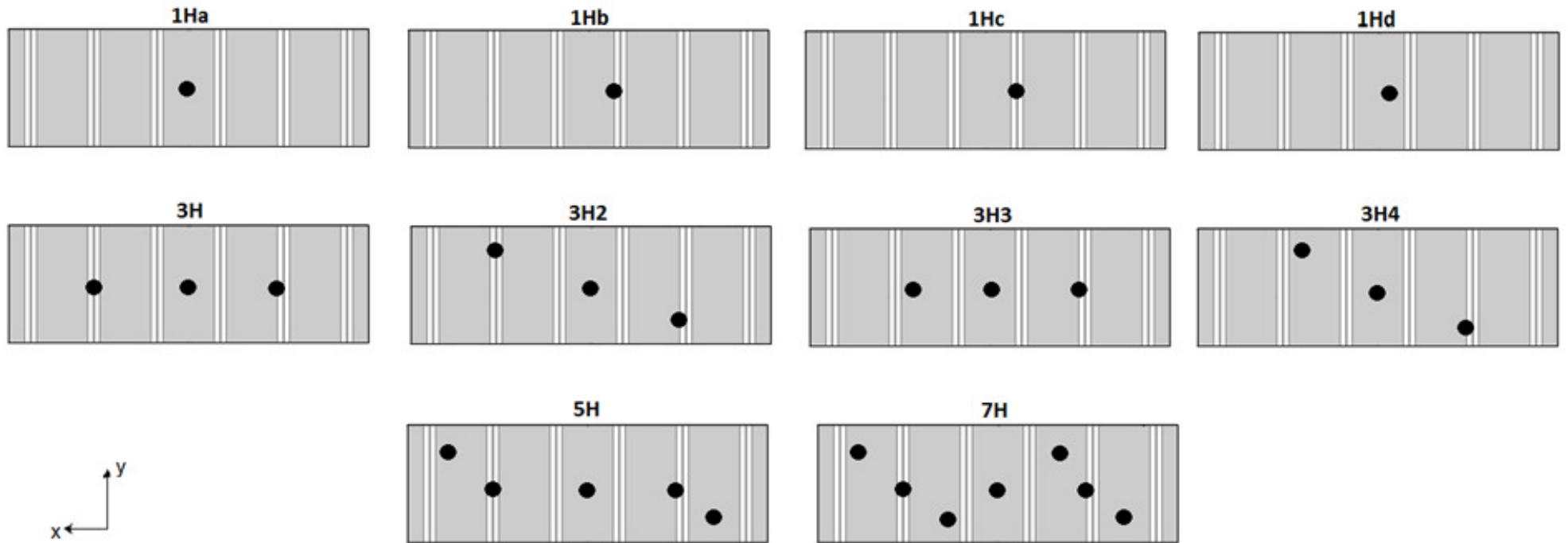


Figure 45: schemes of the hole locations

In particular the main locations of the single hole in the skin are:

- in the middle of a stringer bay (1Ha),
- at the edge of the cap of the stringer (1Hb),
- under the cap of the stringer (1Hc),
- very close to the cap of the stringer (1Hd).

The multi-hole maps, with 3, 5 and 7 holes are a combination of the above mentioned cases with a single hole.

### ***5.2.1 PFA results for the panels with one hole***

Figure 46 summarizes the PFA results obtained for the four different hole locations, 1Ha, 1Hb, 1Hc, 1Hd, reported in Figure 45. The results show that:

- all the hole locations anticipates the TF load respect to the UDA panel (2166.42 kN, Figure 35) of at least 33%, for the least critical case 1Hc, up to 38% for the most critical case 1Hb;
- in terms of FPF and TF load, the hole under the cap of the stringer (1Hc) is the least critical location;
- the most critical location in terms of FPF is obtained with the hole 1Ha (in the middle of the stringer bay);
- the total failure reaches its lowest value with the hole at the edge of the cap of the stringer (1Hb), in particular it is lower of about 8% than the least critical case 1Hc.

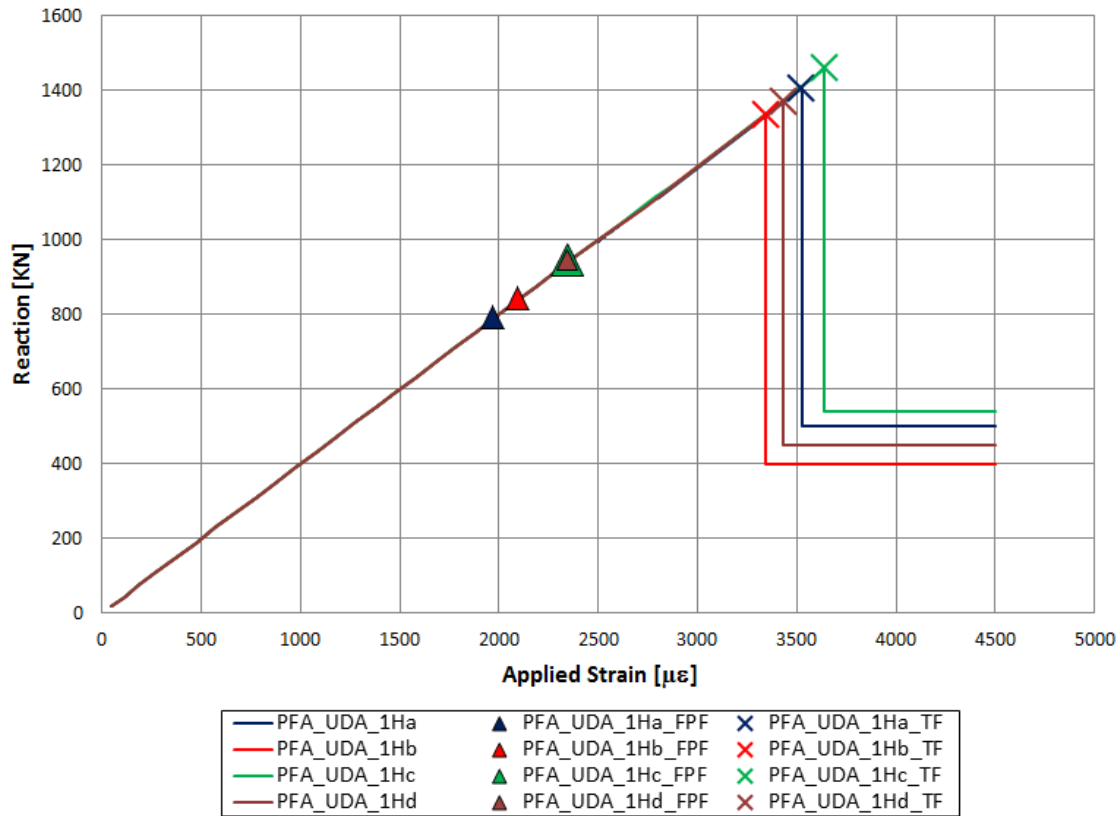


Figure 46: Reaction vs Applied Strain – panels with all the hole locations 1H

The panel 1Hc is the least critical panel thanks to the stringer; in fact the cap of the stringer performs the function of a sort of bridge for the load.

### 5.2.2 PFA results for the panels with multi-hole maps

Four different maps characterized by the simultaneous presence of three holes have been analysed: 3H, 3H2, 3H3, 3H4 (Figure 45); in particular:

- maps 3H and 3H2 are a combination of 1Ha (hole in the middle of a stringer bay), 1Hb (hole at the edge of the cap of the stringer), 1Hc (hole under the cap of the stringer);
- map 3H3 and 3H4 are a combination of 1Ha, 1Hb, and 1Hd (hole very close to the cap of the stringer).

Figure 47 summarizes the PFA results obtained for these maps:

- all the four maps, 3H, 3H2, 3H3, 3H4, anticipate the TF load respect to the panels with one hole (Figure 46), also up to a reduction of about 11%;
- in terms of FPF load, the results are coincident for the maps 3H2 and 3H4;
- in terms of total failure, the results are very close to each other; the results of the maps 3H2 and 3H4 are the same. The total failure reaches its lowest numerical value with the map 3H.

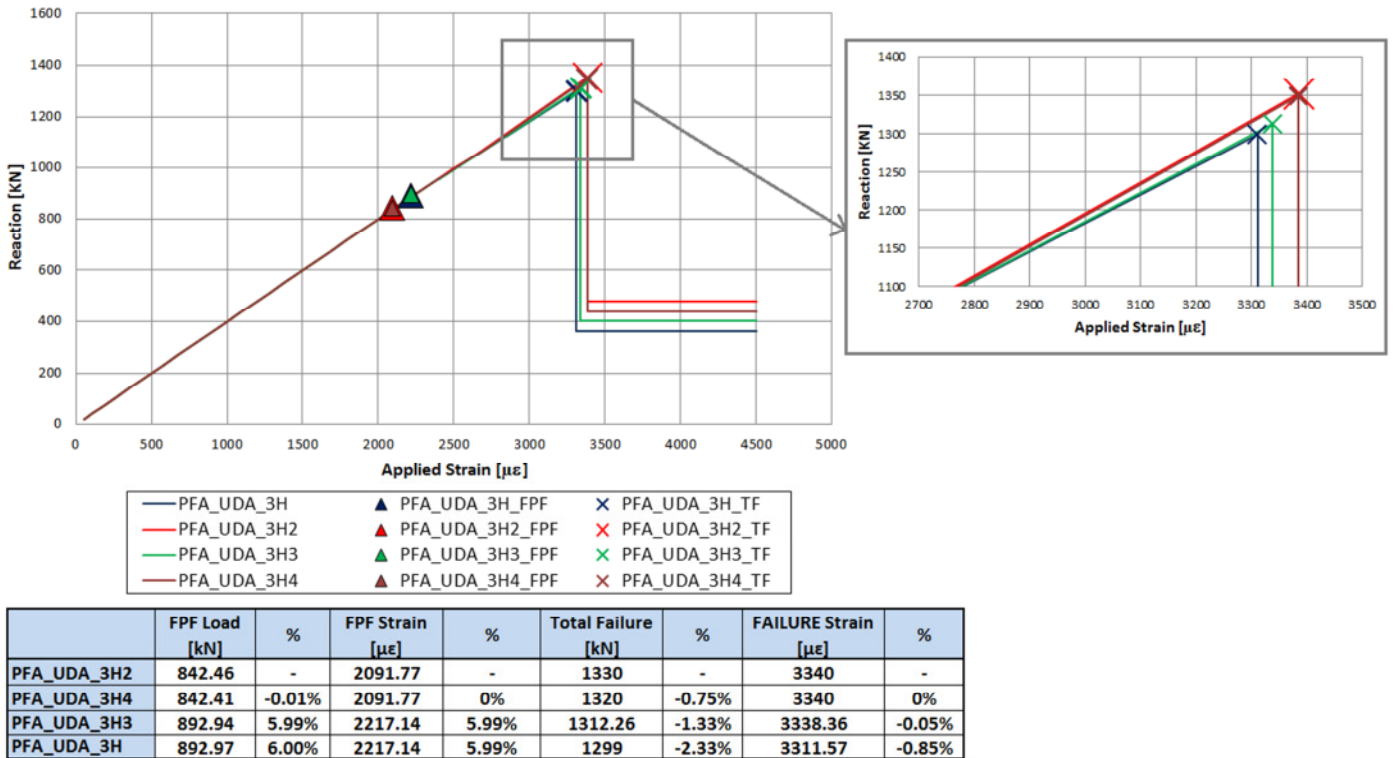


Figure 47: Reaction vs Applied Strain – panels with 3 holes

In order to evaluate if further holes in the skin of the panel, in addition to the ones just considered, could reduce the total failure of the panel further, the PFA has been performed considering maps of five holes, 5H, and 7 holes, 7H (Figure 45). In Figure 48 the PFA results for the panel with five holes and seven holes have been compared with those ones of the panels with three holes of Figure 47.

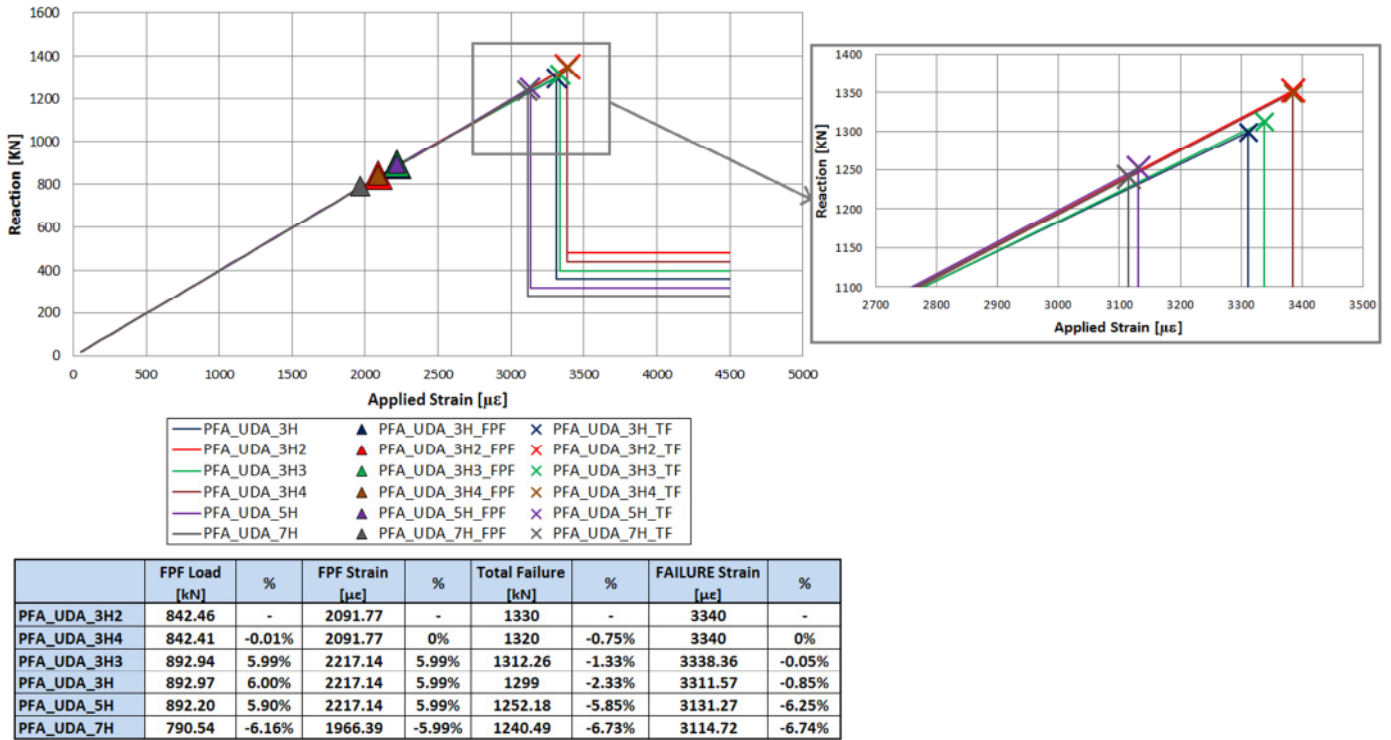


Figure 48: Reaction vs Applied Strain – panels with 3 holes, 5 holes, and 7 holes

As expected, the panel 5H and 7H have a lower collapse load respect to the panels with 3 holes. The residual strength of the panel with seven holes, 7H, is practically coincident with that one of the panel with five holes, 5H:

1240.49 kN of the panel 7H against 1252.18 kN of the panel 5H, with a difference of only about 1%.

Figure 49 shows the damaged elements at the collapse point of the panel 5H.

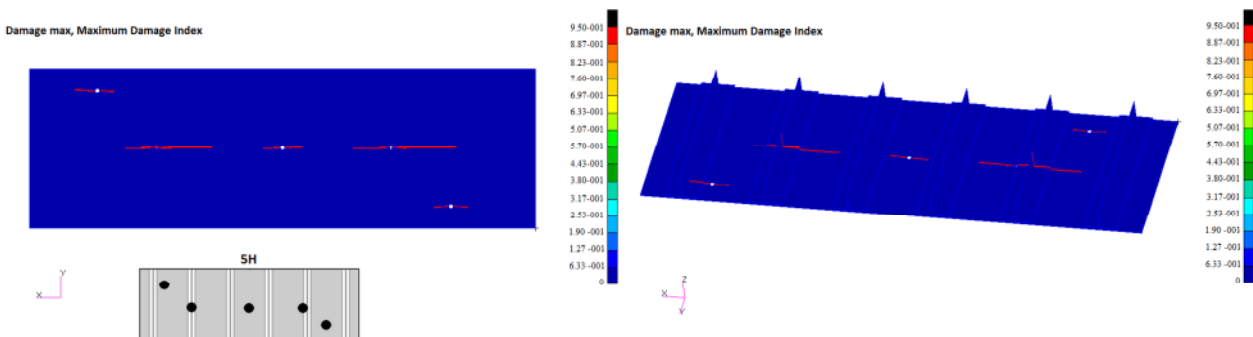


Figure 49: collapse of the panel 5H – without deformed shape

### 5.2.3 Resume of the PFA results

Table 1 summarizes the most critical values of the total failure load obtained for the UDA panel and for each of the four panel configurations (with one hole, three holes, five holes, and seven holes), and Table 2 summarizes their relative comparison.

	UDA	1 hole	3 holes	5 holes	7 holes
<b>Total Failure (kN)</b>	2166.42	1334.78	1299	1252.18	1240.49
<b>FAILURE Strain [<math>\mu\epsilon</math>]</b>	5430	3346	3312	3131	3115

**Table 1: summary of the most critical values of the Total Failure load for the different damage scenarios**

<b>1 hole</b>	-38.39% vs UDA			
<b>3 holes</b>	-40% vs UDA	-2.68% vs 1 hole		
<b>5 holes</b>	-42.20% vs UDA	-6.19% vs 1 hole	-3.60% vs 3 hole	
<b>7 holes</b>	-42.74% vs UDA	-7% vs 1 hole	-4.50% vs 3 hole	-0.93% vs 5 hole

**Table 2: comparison between the most critical values of the Total Failure load for the different damage scenarios**

The progressive failure analysis performed has shown the sensitivity of the total failure load of the panel to different damage scenarios.

Both a single hole, but positioned in different locations, and maps of three, five and seven holes, have been considered. The results are the following ones:

- the total failure load of the damaged panels is rather lower than that one related to the undamaged panel;
- the results of the PFA have shown the sensitivity of the collapse load to the hole location;
- the presence of three holes, five holes and seven holes in the skin reduces further the total failure with respect to the panel with only one hole;
- the results obtained for the maps with 3 holes are very close to each other;
- the total failure of the panel with seven holes is practically the same of that one of the panel with five holes;
- a damage scenario with five holes is sufficient to completely exhaust the residual strength of the stiffened panel, as illustrated in Figure 50.

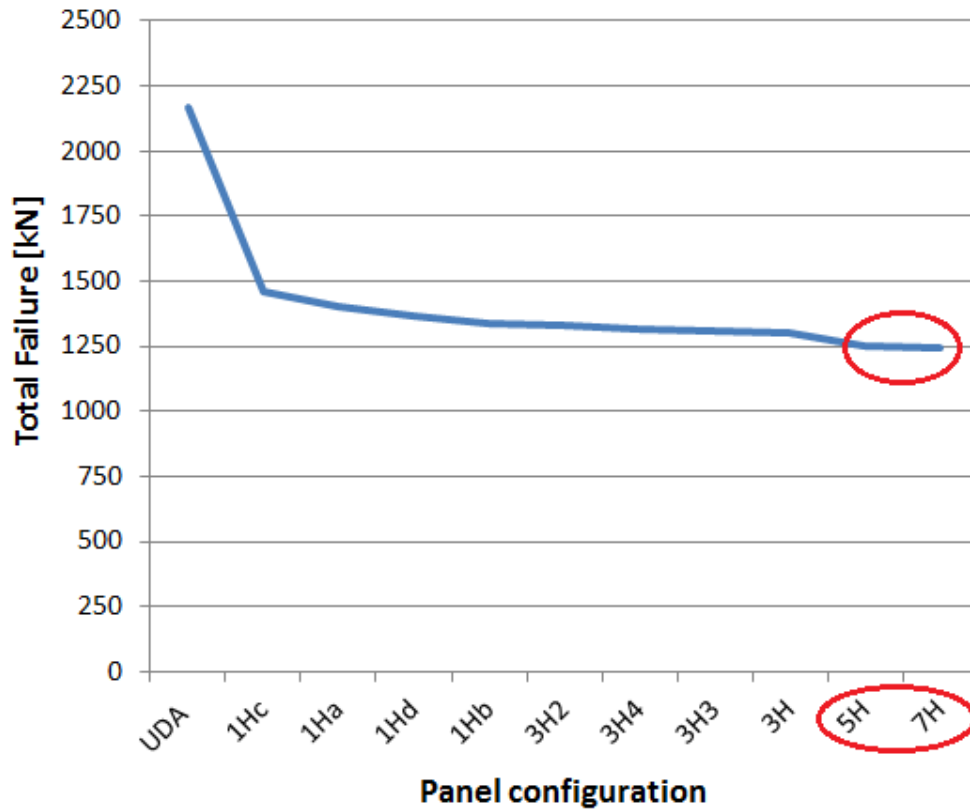


Figure 50: total failure of all the panel configurations

The above results provide useful guidelines in terms of **real design value in compression** to be considered in the design of the stiffened panel respect to the traditional one.

In particular, even if a limited number of holes completely exhausts the residual strength of the panel, on the other hand the compressive failure strain (**3115  $\mu\epsilon$** , seven holes, Table 1) is higher than the design allowable obtained at coupon level by CAI tests, **2120  $\mu\epsilon$** , and used in the traditional design approach (§ 3.2.2). The compressive failure strain of 3115  $\mu\epsilon$  could allow to design a lighter panel and/or a panel with higher load carrying capability with respect to the panel obtained by the traditional design. Figure 51 and Figure 52 summarize the latter considerations.

A measure of the low weight reduction achievable can be appreciated considering that according to Figure 27 (weight vs compressive design value, § 3.2.2), the above panel designed by using as design value 3115  $\mu\epsilon$ , should have a weight lower of at least **30%** than that one obtained by going to resize the panel but using the traditional compressive allowable based on BVID degradation factor, 2120  $\mu\epsilon$ .

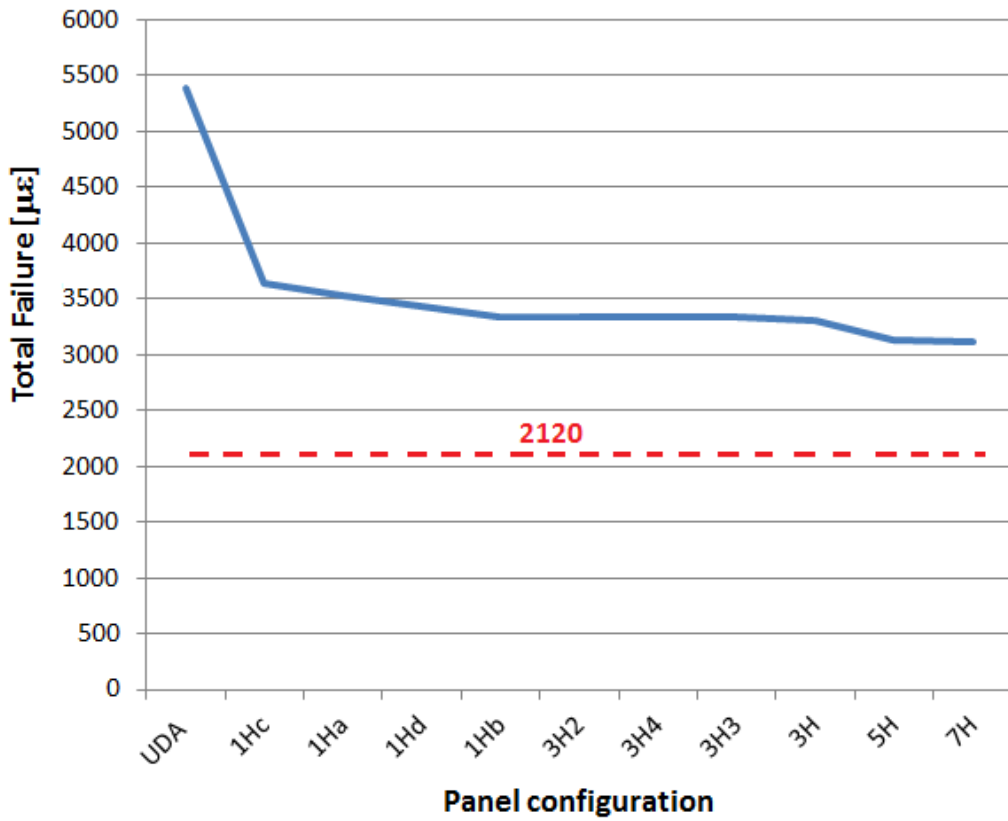


Figure 51: total failure of all the panels vs design allowable obtained at coupon level

$\epsilon_{cu}$ ( $\mu\epsilon$ )		
UDA panel	7H panel	Traditional design approach ( $K_{BVID}$ ) by CAI
5383	3115	2120

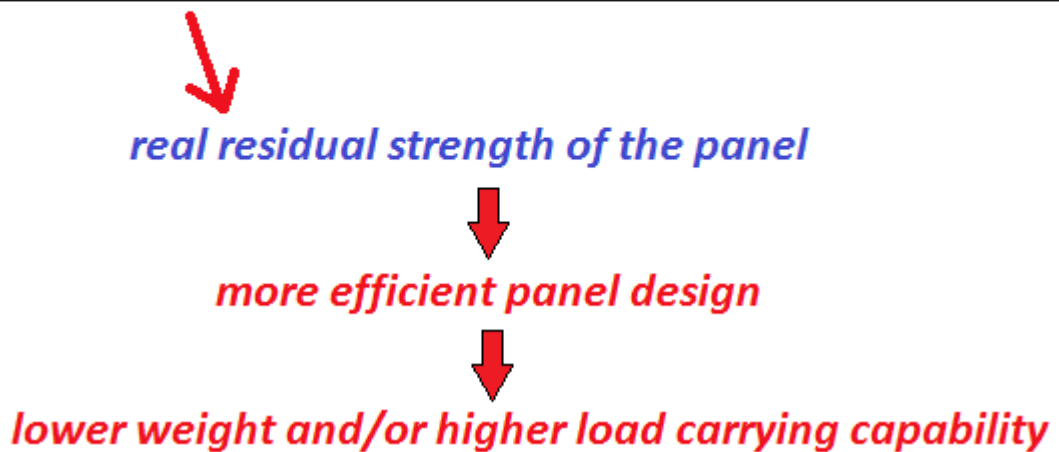


Figure 52: design considerations

### 5.3 Influence of post-buckling on the total failure of the panel with discrete damages

The sensitivity of the residual strength of a stiffened panel respect to different damage locations and damage density has been performed also on a panel under compressive load but in post-buckling regime.

In particular, the combined effects of the reduction of the panel stiffness and of the damage propagation, and the sensitivity of the buckling onset and of the residual strength of the panel to different damage scenarios, have been evaluated.

In this case it has been selected a stiffened panel with the buckling load lower than the failure load ( $5383 \mu\epsilon$ , no  $K_{BVID}$ , Figure 17-a). This panel can be considered as an equivalent upper skin panel located toward the wing tip of the reference regional aircraft wing box. It is a flat panel, characterized by T shaped stringers, and by a layup of 14 plies for the skin and 10 plies for the cap of the stringer; Figure 53 illustrates the panel geometry and its boundary conditions.

The panel is loaded in axial compression: a uniform displacement along the y-axis is applied to the edge AB.

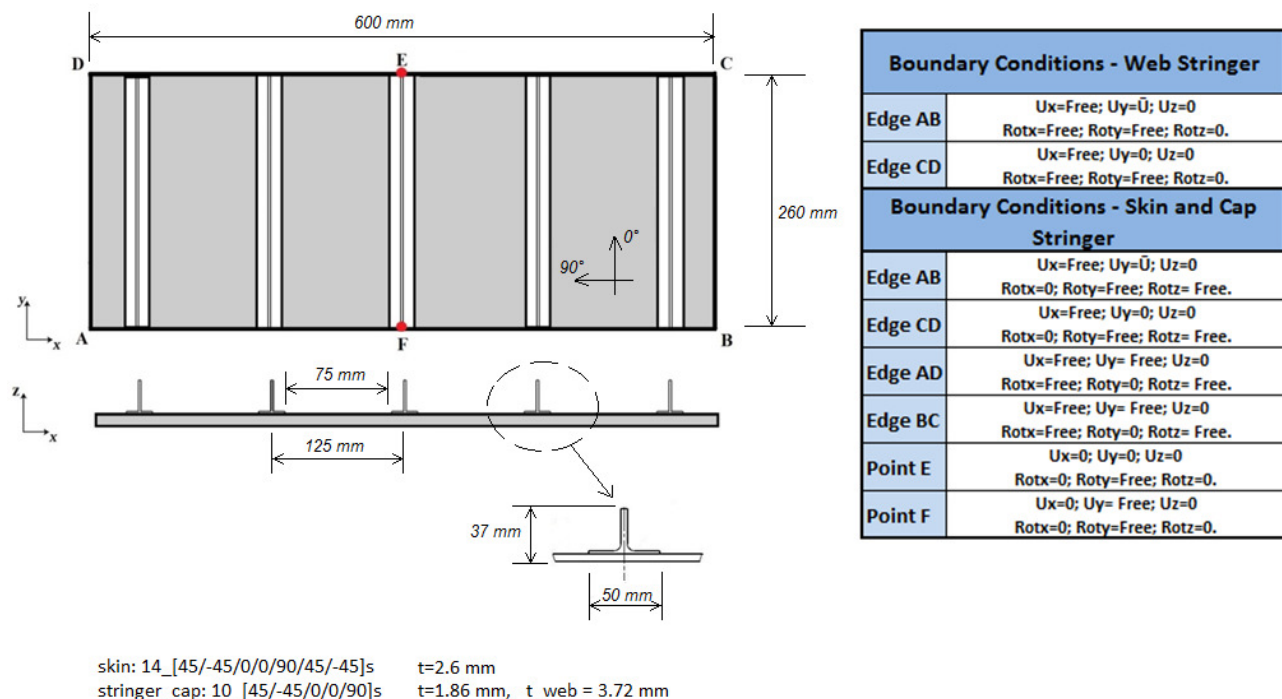
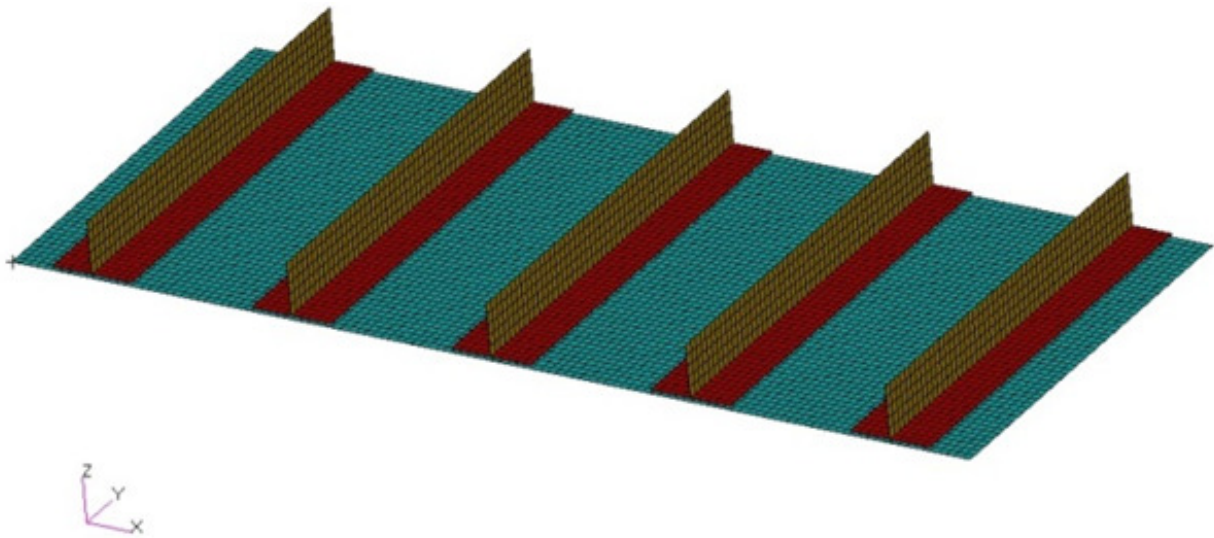


Figure 53: panel geometry and boundary conditions

The above panel is the UDA panel: it is characterized by lamina material properties degraded only for temperature and moisture effects, and B-basis statistical reduction, and without degradation due to BVID, Figure 17-a.

As for the panel critical at strength illustrated in § 5.1, the damage degradation has been simulated by introducing discrete holes in the skin of the panel.

The finite element model of the UDA panel is shown in Figure 54.



**Figure 54: FE model of the UDA panel**

The FE analysis of the UDA panel, performed according to the traditional design approach which is essentially based on linear analysis and on the first-ply-failure design criteria, has given the critical values shown in Table 3 for buckling and failure, where  $U_{y-cr}$  is the critical displacement,  $P_{y-cr}$  is the critical load, and  $\epsilon_{y-cr}$  the critical compressive strain. Hashin criteria ([45], § 4.2) has been used to predict the lamina failure load.

	$U_{y-cr}$ (mm)	$P_{y-cr}$ (kN)	$\epsilon_{y-cr}$ ( $\mu\epsilon$ )
Linear Buckling Analysis	0.85	516.60	3280
Linear Failure Analysis	1.40	864.98	5385

**Table 3: UDA panel – linear buckling and failure analysis results**

The panel buckles at an imposed displacement of 0.85 mm and would fail at 1.40 mm in absence of buckling. Figure 55 shows the first buckling mode.

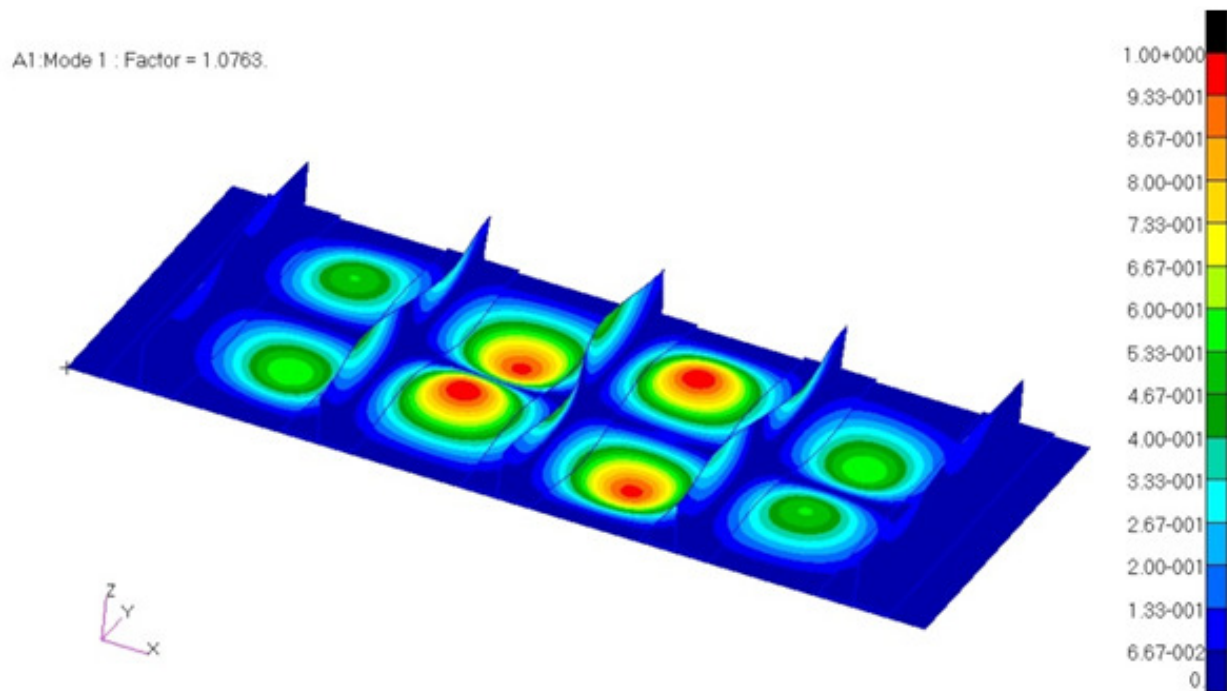


**Figure 55: UDA panel – linear buckling analysis: first mode.**

Before performing the PFA on the panel with discrete damages, preliminary nonlinear analysis and also PFA have been performed on the UDA panel in order to compare these results with those ones obtained by linear FE analysis.

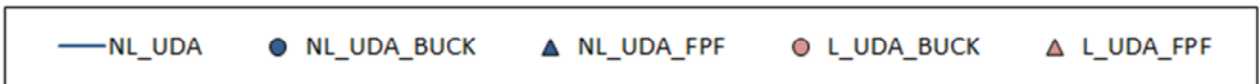
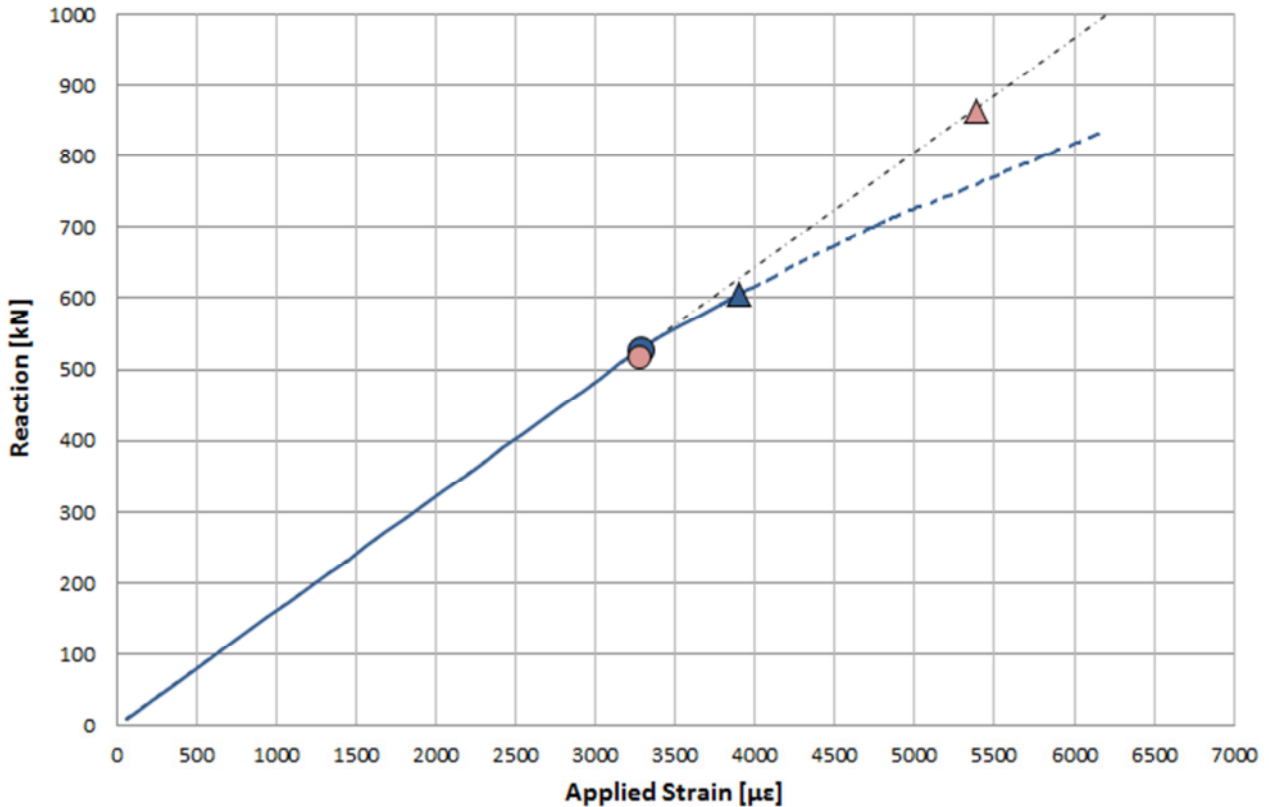
### **5.3.1 Nonlinear and PFA results for the UDA panel**

Figure 56 illustrates the Reaction Force vs the Applied Strain obtained by linear analysis (L) and nonlinear analysis (NL) for the UDA panel. According to the results of nonlinear analysis illustrated in Figure 56, it has been not necessary the introduction of a buckling trigger (perturbed mesh) to predict the buckling load of the panel.

The comparison of the results highlights that the buckling loads ( $L\_UDA\_BUCK$ ,  $NL\_UDA\_BUCK$ ) are practically the same for linear and nonlinear analyses as expected. With regard to the failure analysis, in the nonlinear case the failure occurs before. As expected, this result is due to buckling event:

when the structure reaches the onset of buckling, it assumes a deformed shape that leads to FPF anticipation; additional analyses performed constraining the out-of-plane displacements of the panel

(to prevent buckling phenomena) have confirmed the previous result. In the nonlinear analysis shown in Figure 56 the *PFA is not activated*, so *the damage of the panel does not trigger the degradation of material* causing a stiffness reduction of the structure; the slope changing is only due to the buckling phenomena.

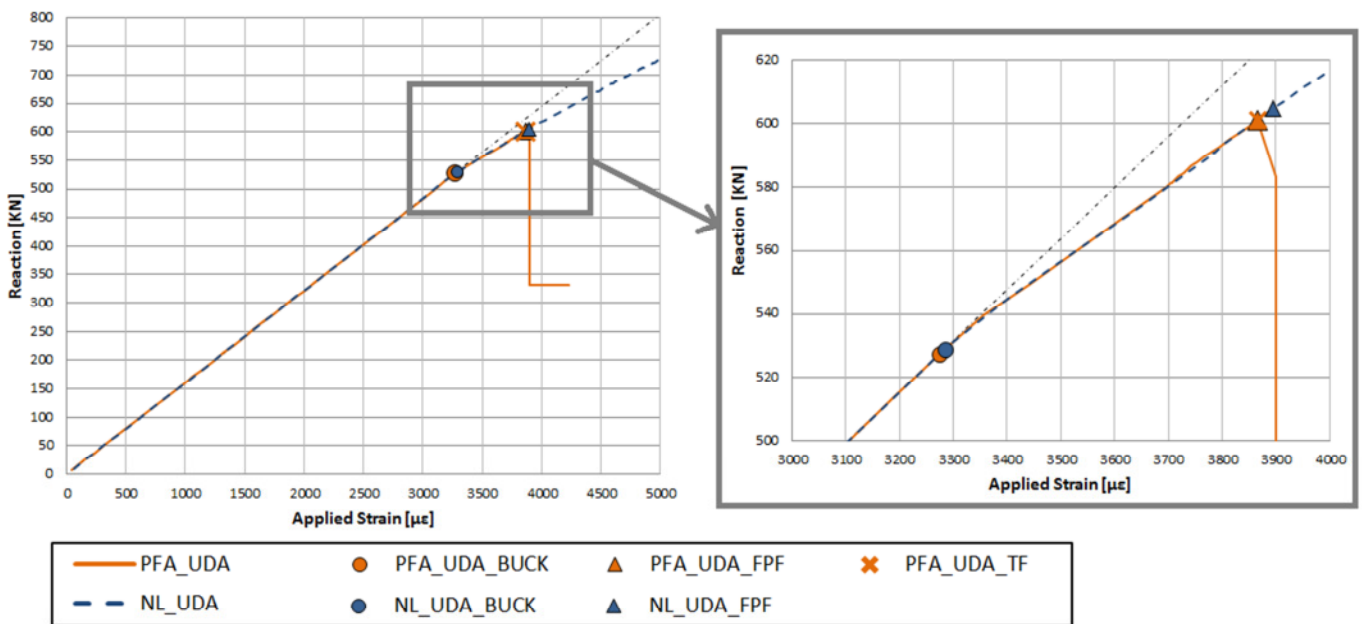


Summary Table						
	Buckling Load [kN]	Diff %	FPF Load [kN]	Diff %	FPF Strain [µε]	Diff %
L_UDA	516.60	-	864.98	-	5385	-
NL_UDA	529.02	+ 2.40%	604.89	-30.07%	3895.35	-27.66%

Figure 56: Reaction vs Applied Strain – UDA panel – Linear and Nonlinear analysis

Figure 57 compares the Reaction Force vs the Applied Strain of the nonlinear analysis (NL) and of the PFA for the UDA panel. The PFA has been performed to evaluate the structural behaviour after the FPF point, therefore the total failure TF, i.e. the collapse load. Applying the PFA, the values of the FPF load and of the TF load are coincident, so *no damage evolution occurs*. After the buckling onset, the stress distribution is such that at each buckle crest there are the maximum stress values

(due to the local bending), therefore the failure starts in that points. Because of the type of load and boundary condition and the panel configuration, at each buckle crest the stress assumes the same value and there are several failed plies. So, the trigger failure points are more than one and they are positioned in the panel in such way that, immediately after the failure onset, the panel collapses. This explains that the FPF load and the TF load are the same. Figure 58 illustrates the deformed stiffened panel at the total failure point with the displacements (left side) and damaged elements (right side) contour plot.



	Buckling Load [kN]	%	FPF Load [kN]	%	FPF Strain [μϵ]	%	Total Failure [kN]	%	FAILURE Strain [μϵ]	%
NL_UDA	529.02	-	604.89	-	3895.35	-	-	-	-	-
PFA_UDA	527.27	-0.33%	601.09	-0.63%	3865.78	-0.76%	601.09	-	3865.78	-

Figure 57: Reaction vs Applied Strain – UDA panel – Nonlinear analysis and PFA

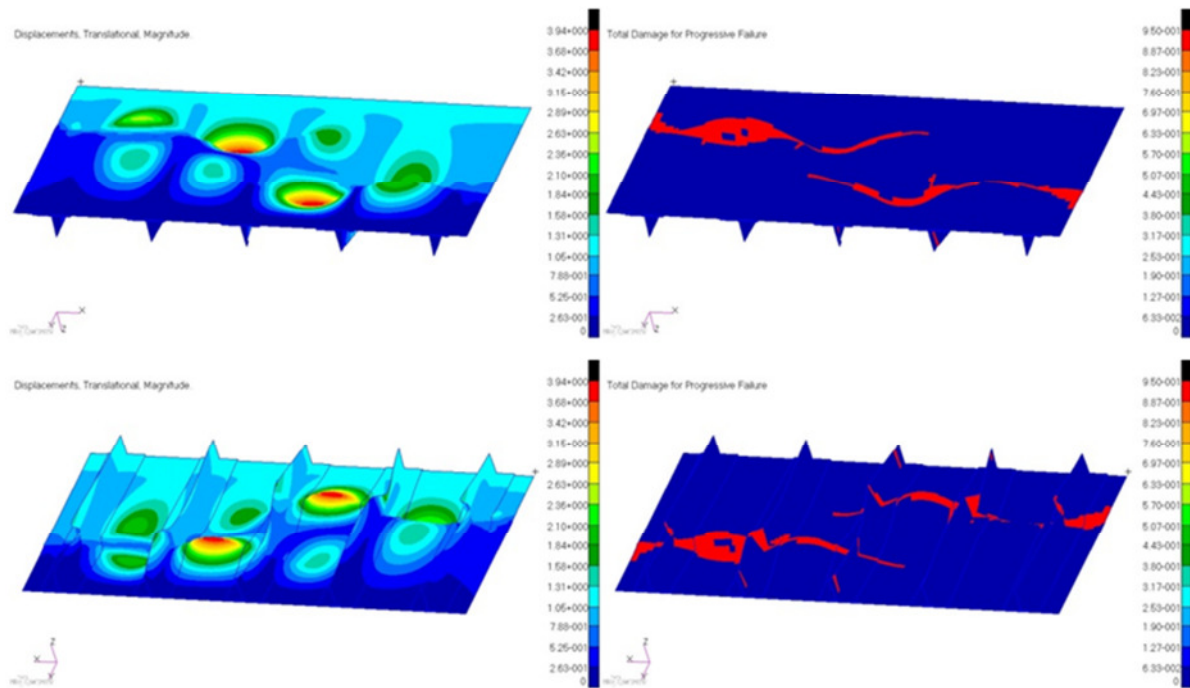


**Figure 58: deformed panel at the collapse point. Displacements (left side) and damaged elements (right side) contour plot**

The above results have confirmed that the UDA panel buckles prior to failure; it enters the post-buckling regime before its collapse.

### 5.3.2 PFA results for the discrete damage model

Discrete damages, simulated by 6.35 inch diameter holes, have been introduced in the skin of the UDA panel. At first, the sensitivity of the residual strength of the panel to the different locations of a single hole has been evaluated. Then also multi-hole (multi-damage) scenarios have been considered. Maps with three and five holes have been applied to evaluate the sensitivity of the total failure of the panel with respect to the damage density.

Figure 59 illustrates a scheme of the different locations of the holes in the skin and the relative identification code.

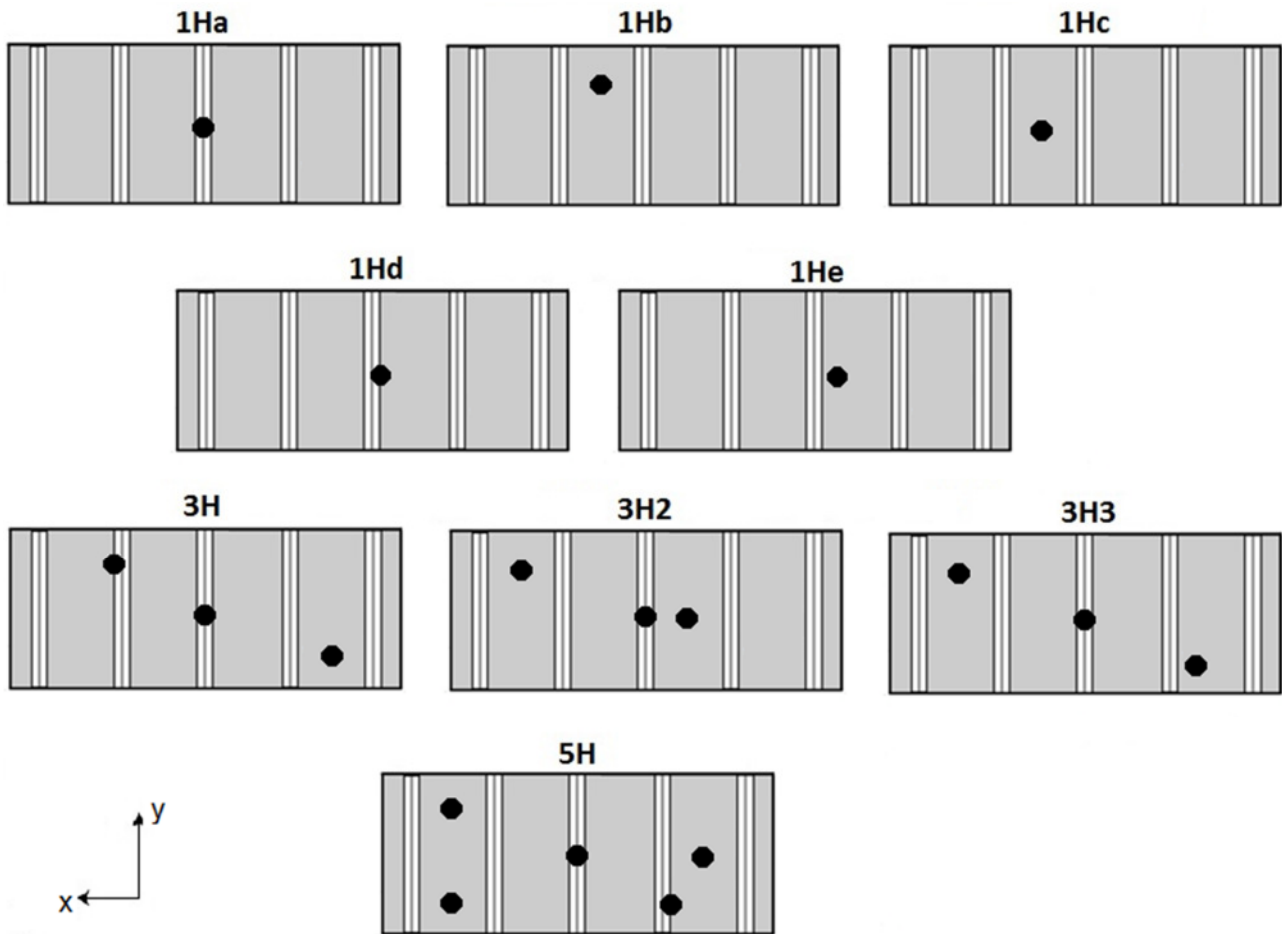


**Figure 59: schemes of the hole locations**

In particular the main locations of the single hole in the skin are:

- under the cap of the stringer (1Ha),
- at a buckle crest (1Hb),
- in the middle of a stringer bay (1Hc),
- at the edge of the cap of the stringer (1Hd),
- very close to the cap of the stringer (1He).

For sake of clarity, Figure 60 shows the images of the FE models of the panels with a single hole. The multi-hole maps are a combination of the above mentioned cases with a single hole.

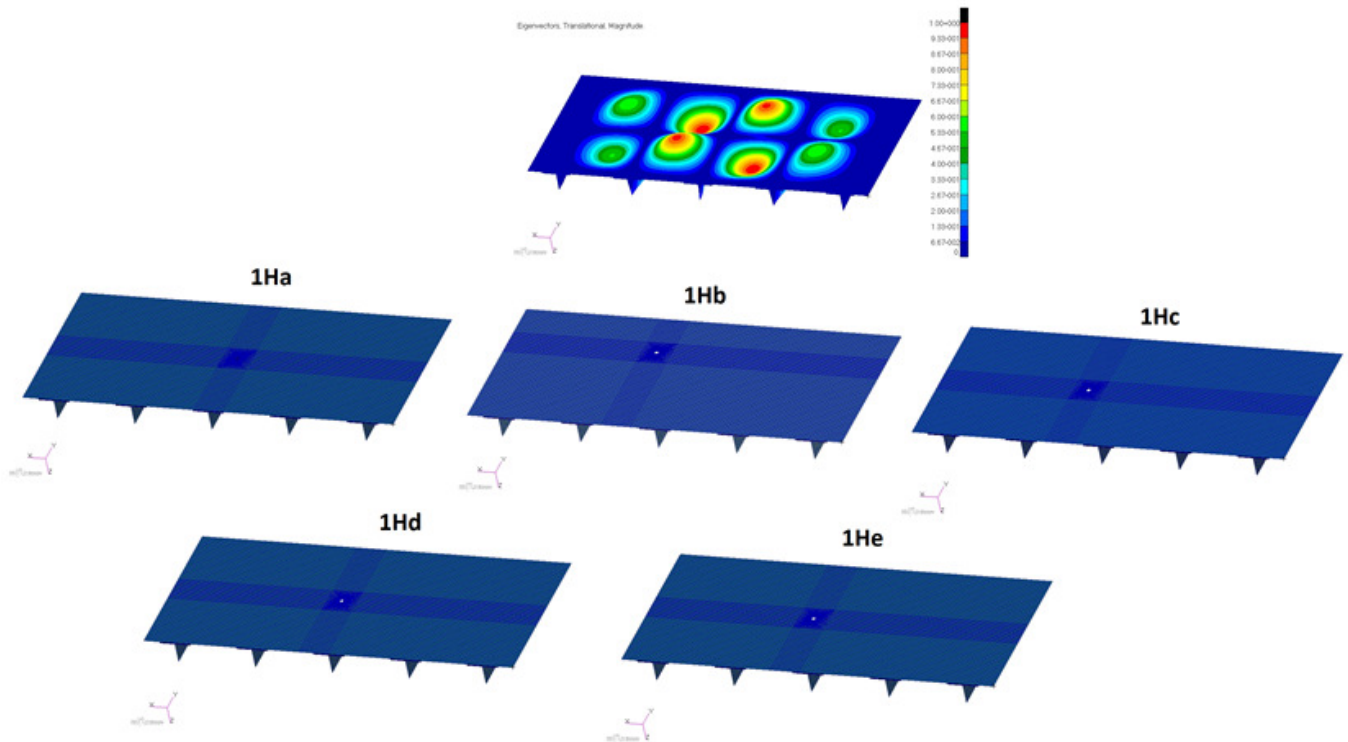
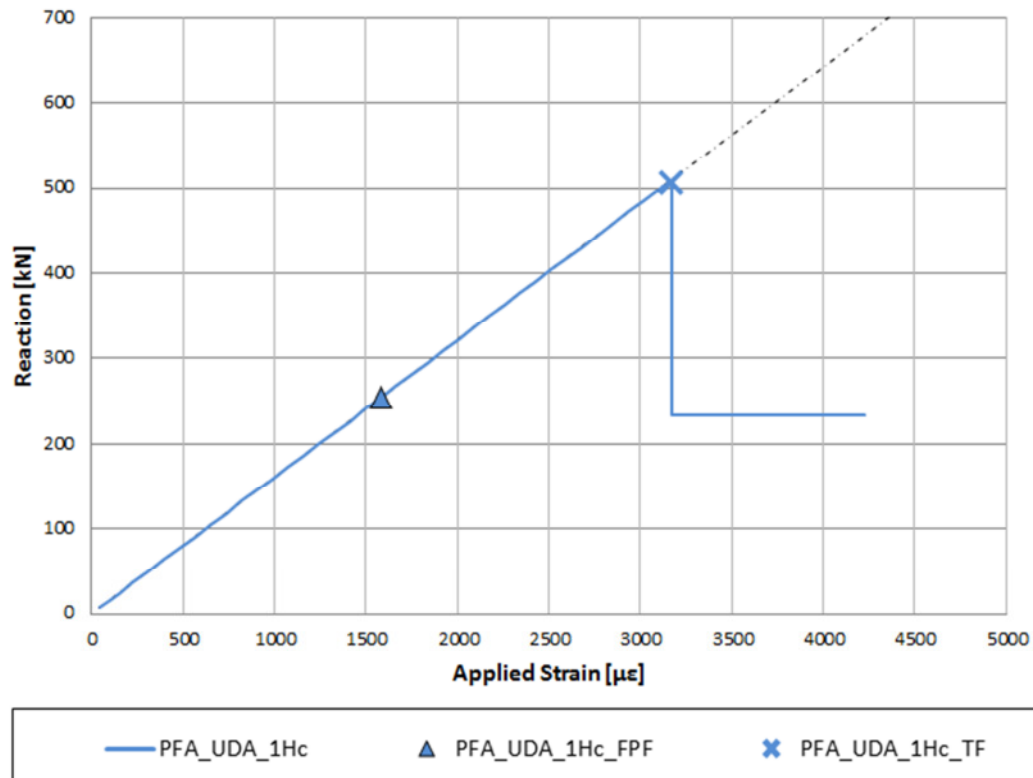


Figure 60: FE models of the UDA panel with a single hole

➤ *PFA results for the panel with one hole*

The results of the PFA performed on the UDA panel with a single hole in the skin (Figure 60), have shown that the presence of the hole triggers off the degradation of the material inducing a propagation of the damage from the initiation of the failure in a lamina, FPF load, up to the total failure of the panel, TF load: ***FPF load and TF load are not coincident***. This result is in contrast respect to that one obtained for the UDA panel (i.e. without hole, § 5.3.1).

For example, in Figure 61 the Reaction Force vs the Applied Strain for the panel 1Hc (hole in the middle of the stringer bay) is shown. Respect to the UDA panel (PFA\_UDA results, Figure 57), the presence of the hole 1Hc induces no-buckling onset and anticipates both the FPF load and the TF load. The TF load reduction is about 16%: 507.50 kN against 601.09 kN of Figure 57.



	Buckling Load [kN]	FPF Load [kN]	FPF Strain [μϵ]	Total Failure [kN]	FAILURE Strain [μϵ]
PFA_UDA_1Hc	-	254.22	1580.95	507.50	3169.35

Figure 61: Reaction vs Applied Strain – panel with hole 1Hc

Figure 62 shows the damaged elements at different time substeps. As expected, the failure of the panel starts close to the hole (Figure 63) and it propagates along a line perpendicular to the load direction. The damaged ply is the third one of the skin laminate, oriented at  $0^\circ$  (Figure 53), and characterized by compressive fiber failure. Figure 64 shows the displacements and the damaged elements contour plot on the deformed panel at the collapse point.

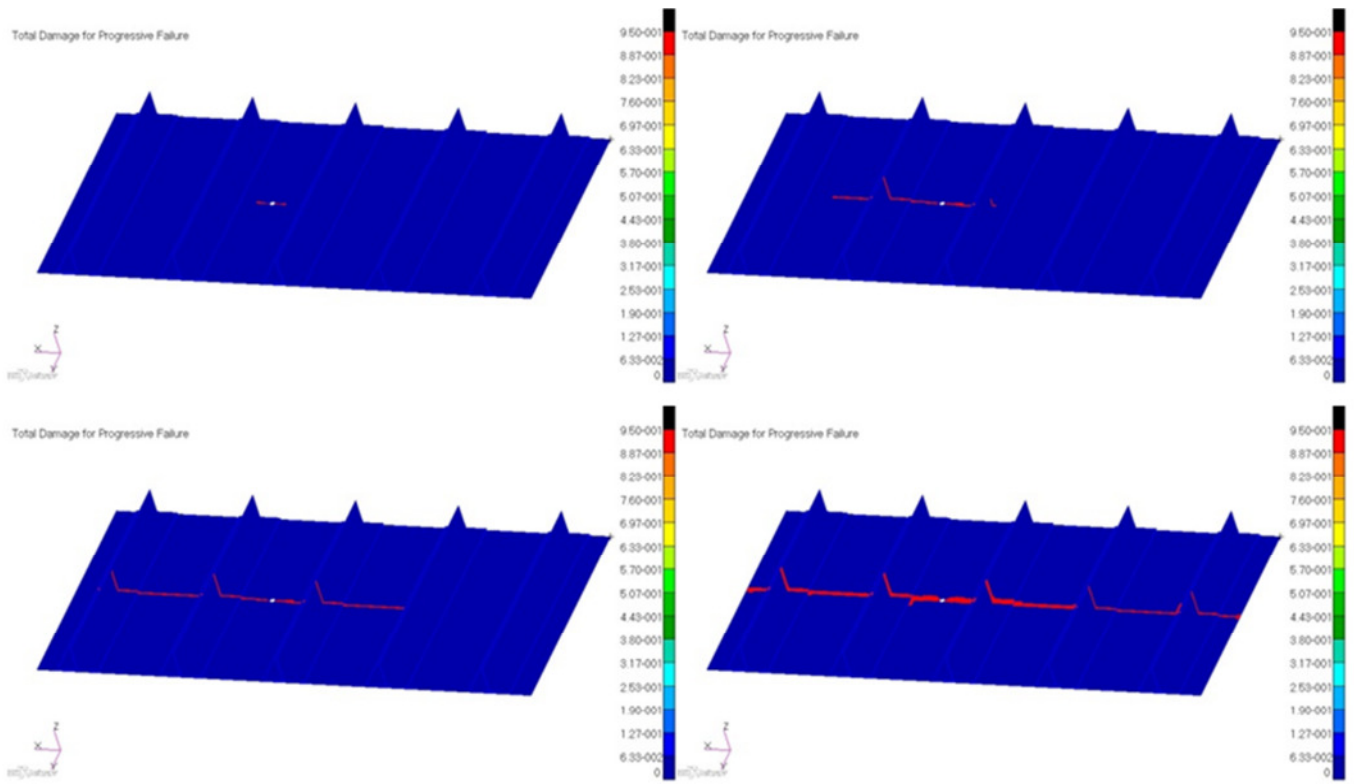


Figure 62: progressive failure of the panel with hole 1Hc (without deformed shape)

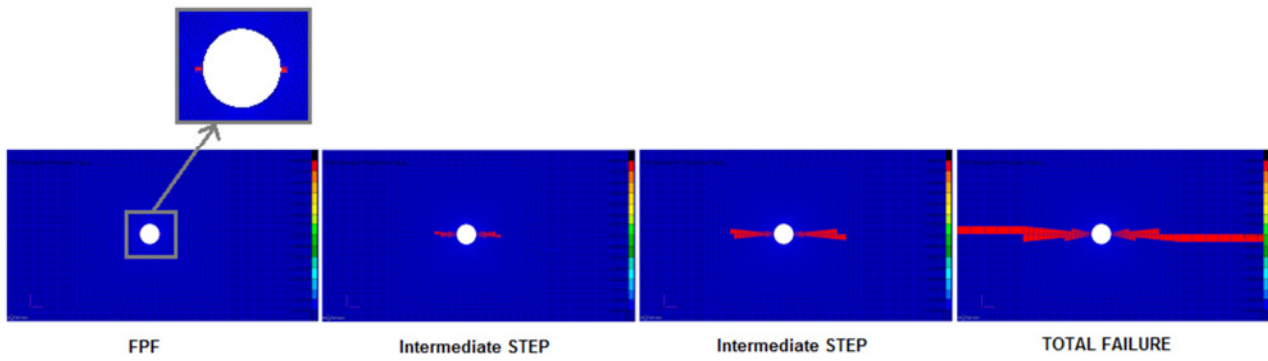
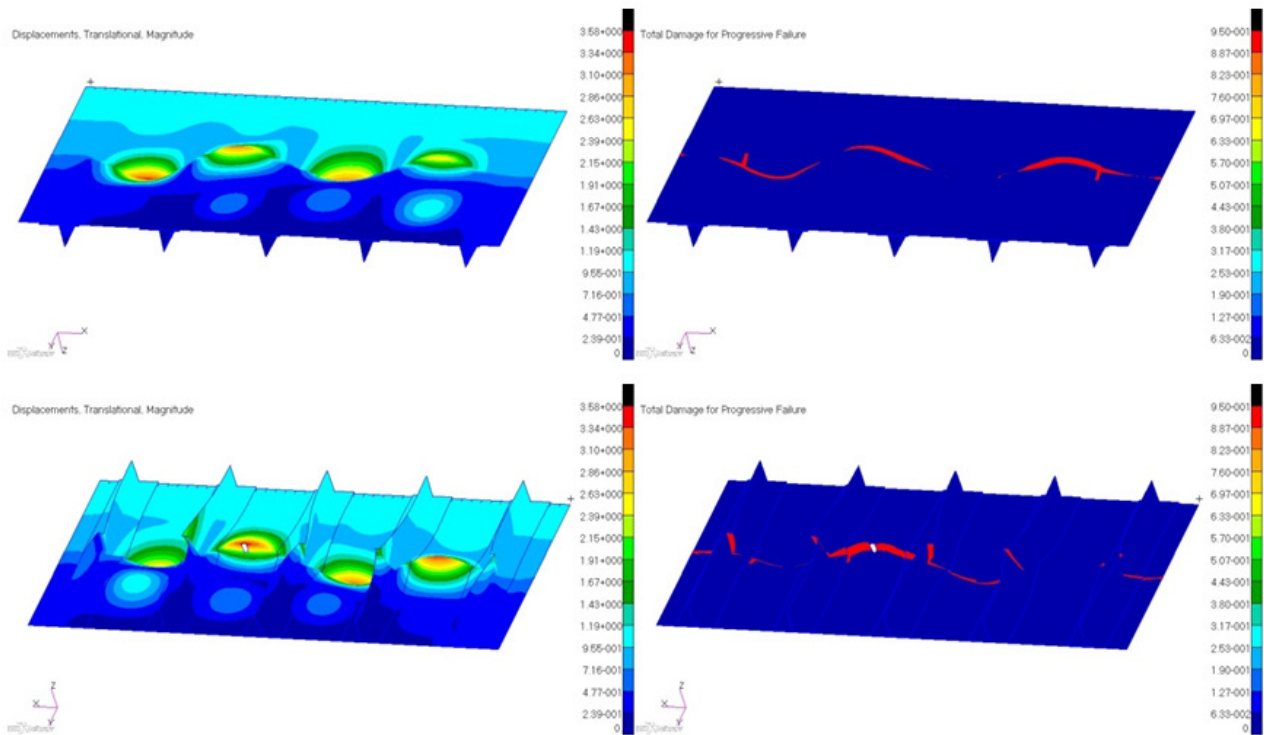


Figure 63: progressive damage around the hole – panel with hole 1Hc



**Figure 64: deformed panel at the collapse point. Displacements (left side) and damaged elements (right side) contour plot**

Figure 65 summarizes the PFA results obtained for the five different hole locations, 1Ha, 1Hb, 1Hc, 1Hd, 1He (Figure 59). The results show that:

- all the hole locations anticipates the TF load respect to the UDA panel (601.09 kN, Figure 57) of at least 6%, for the least critical case 1Ha, up to about 19% for the most critical case 1He;
- the onset of buckling is sensitive to the hole location;
- only for the panels 1Ha (hole under the cap of the stringer) and 1Hb (hole at the buckle crest), there is the onset of the buckling and therefore these panels enter the post-buckling regime before the total failure occurs; the buckling loads of these panels are practically coincident and they are also the same of that one of the UDA panel (527.27 kN, Figure 57);
- in terms of FPF and TF load, the hole 1Ha is the least critical location;
- the most critical location in terms of FPF is obtained with the hole 1Hc (hole in the middle of a stringer bay);
- in terms of TF load, the results of the panels 1Hc, 1Hd and 1He, are very close to each other; with the panel 1He, hole very close to the cap of the stringer, the total failure reaches the lowest value, that is lower of about 14% than the least critical case 1Ha.

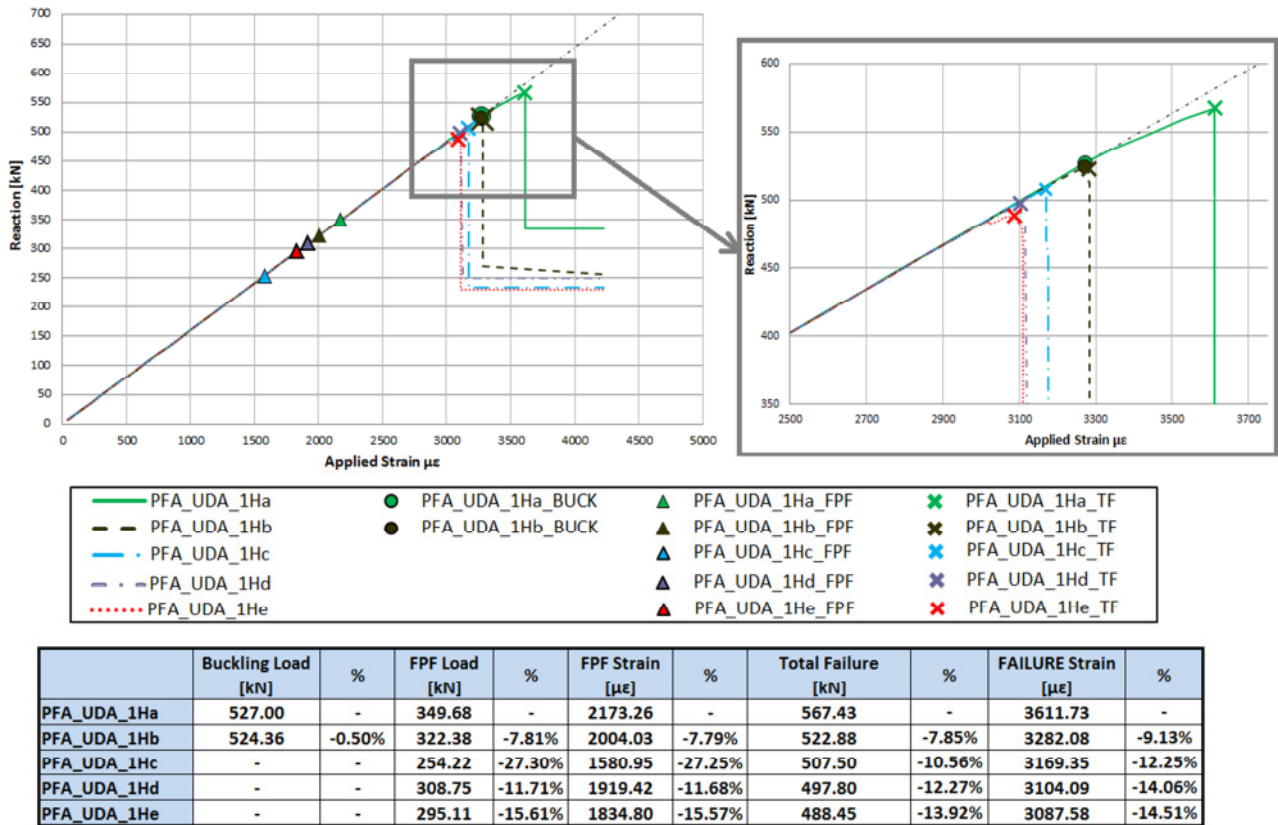


Figure 65: Reaction vs Applied Strain – panels with all the hole locations 1H

The panel 1Ha is the least critical panel thanks to the stringer; in fact the cap of the stringer performs the function of a sort of bridge for the load.

About the hole at the buckle crest, as it is known, generally at the buckle crest the stress reaches the maximum value due to bending state induced by the buckling event. The presence of the hole at a buckle crest, 1Hb, implies that the zone undergoes a stress reduction since the region with the maximum bending has been eliminated. At the same time the hole generates a stress concentration which depends by several geometrical parameters, so the maximum stress value could be so close to the hole or to the buckle crest or so far from them. As it is illustrated in Figure 65, the higher total failure load of the panel 1Hb respect to the cases 1Hc, 1Hd and 1He (holes no located at the buckle crest), confirms that the hole 1Hb does not increase the stress distribution at the buckle crest.

➤ **PFA results for the panels with multi-hole maps**

Three different maps characterized by the simultaneous presence of three holes have been analysed: 3H, 3H2, 3H3 (Figure 59); in particular:

- map 3H is a combination of 1Ha (hole under the stringer cap), 1Hb (hole at a buckle crest), 1Hd (hole at the edge of the cap of the stringer).
- map 3H2 is a combination of 1Ha, 1Hb, and 1Hc (hole in the middle of the stringer bay).
- map 3H3 is a combination of 1Ha, 1Hb, and 1He (hole very close to the cap of the stringer).

Figure 66 summarizes the PFA results obtained for these maps:

- all the three maps, 3H, 3H2, 3H3, anticipate the TF load respect to the panels with one hole (Figure 65), up to a reduction of about 15%;
- only for the first map, 3H, there is the onset of the panel buckling, and therefore the panel enters the post-buckling regime before the total failure occurs; the buckling load is lower of about 10.5% than the one obtained with the panels with a single hole 1Ha and 1Hb (Figure 65);
- in terms of FPF load, the results are coincident for the maps 3H2 and 3H3; these values are lower of 4.42% than the FPF load of the map 3H;
- in terms of total failure, the results are very close to each other and practically they are the same for the cases 3H and 3H3. Figure 67 shows the damaged elements at the collapse point of the panel 3H3.

In order to evaluate if further holes in the skin of the panel, in addition to the ones just considered, could reduce the total failure of the panel further, PFA has been performed considering a damage map of five holes, 5H (Figure 59). In Figure 68 the PFA results for the panel with five holes have been compared with those ones of the panels with three holes of Figure 66.

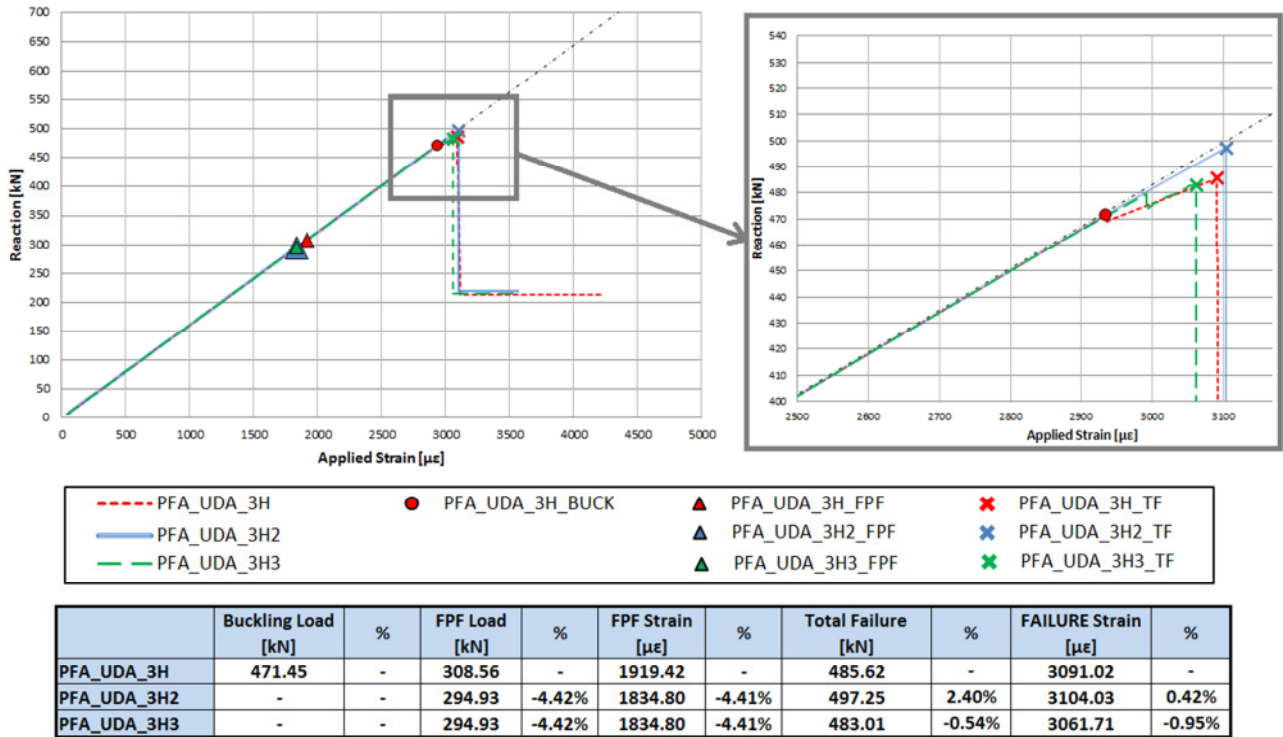


Figure 66: Reaction vs Applied Strain – panels with 3 holes

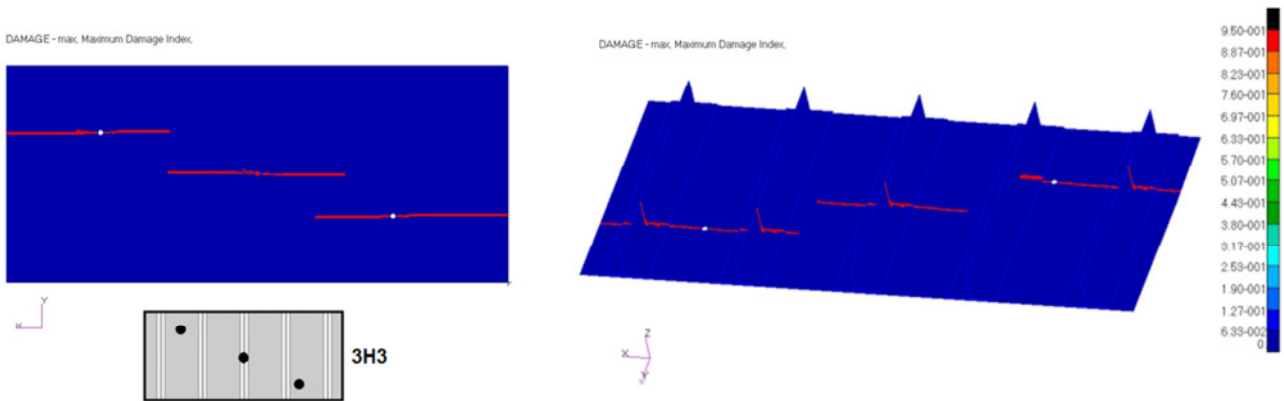


Figure 67: collapse of the panel 3H3 – without deformed shape

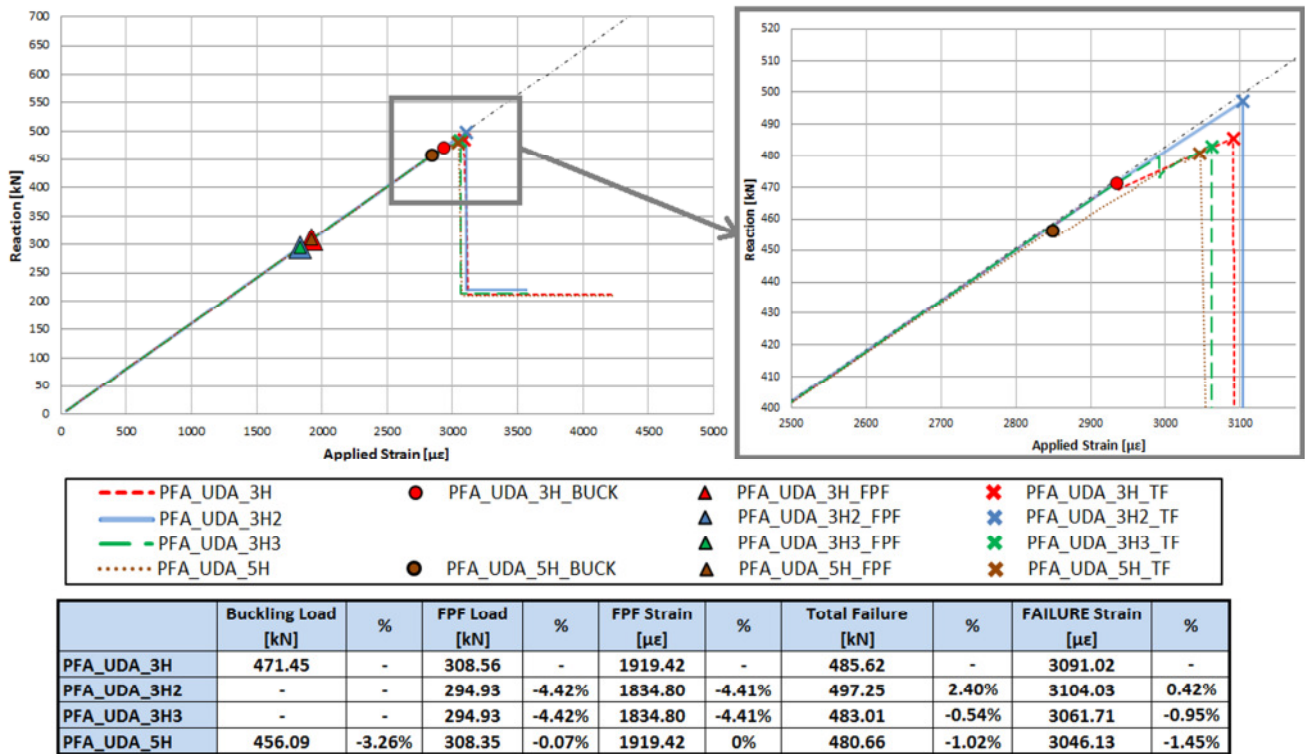


Figure 68: Reaction vs Applied Strain – panels with 3 holes and 5 holes

The particular distribution of the five holes in the skin of the panel is such to promote a little anticipation of the buckling onset respect to the panel 3H. As expected, the panel 5H has a lower collapse load respect to the panels with three holes, but however this value is practically coincident with the lowest value of the TF load of the panels with three holes: 480.66 kN against 483.01 kN of the panel 3H3, with a difference of only 0.5%.

### 5.3.3 Resume of the PFA results

Table 4 summarizes the most critical values of the total failure load obtained for the UDA panel and for each of the three panel configurations (with one hole, three holes, and five holes), and Table 5 summarizes their relative comparison.

	UDA	1 hole	3 holes	5 holes
<b>Total Failure (kN)</b>	601.09	488.45	483.01	480.66
<b>FAILURE Strain [μϵ]</b>	3866	3088	3062	3046

Table 4: summary of the most critical values of the Total Failure load for the different damage scenarios

<b>1 hole</b>	-18.74% vs UDA		
<b>3 holes</b>	-19.64% vs UDA	-1.11% vs 1 hole	
<b>5 holes</b>	-20.04% vs UDA	-1.59% vs 1 hole	-0.49% vs 3 hole

**Table 5: comparison between the most critical values of the Total Failure load for the different damage scenarios**

The progressive failure analysis performed has shown the sensitivity of the final failure load and of the buckling onset of the panel to different damage scenarios.

Both a single hole, but positioned in different locations, and maps of three and five holes have been considered. The results are the following ones:

- the total failure load of the damaged panels is rather lower than that one related to the undamaged panel;
- the results of the PFA have shown the sensitivity of the buckling onset to the hole location;
- in some cases the panel doesn't buckle and it fails without enter the post-buckling regime, as it happens instead for the undamaged panel;
- the presence of three holes in the skin reduces further the total failure with respect to the panel with only one hole;
- the results obtained for the maps with 3 holes are very close to each other;
- the total failure of the panel with five holes is practically the same of the most critical value obtained for the panels with three holes;
- a damage scenario with three holes in the skin, is sufficient to completely exhaust the residual strength of the stiffened panel, as illustrated in Figure 69.

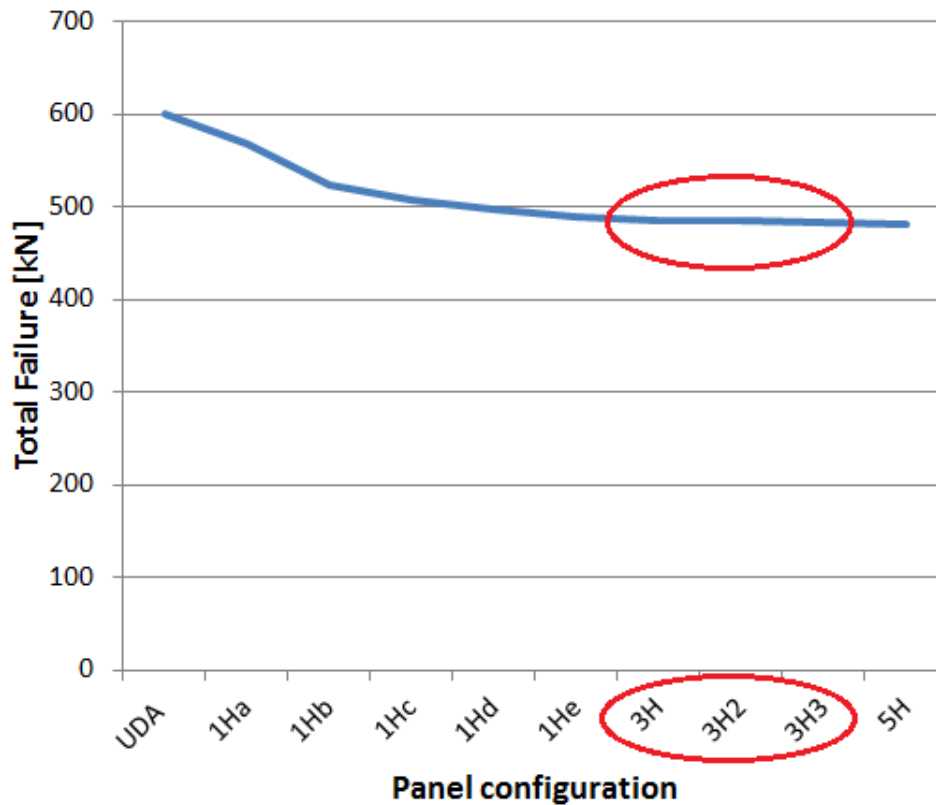


Figure 69: total failure of all the panel configurations

The above results provide useful guidelines in terms of **real design value in compression** to be considered in the design of the stiffened panel respect to the traditional one.

In particular, even if a limited number of holes completely exhausts the residual strength of the panel, on the other hand the compressive failure strain (**3046  $\mu\epsilon$** , panel with five holes, 5H, Table 4) is higher than the design allowable obtained at coupon level by CAI test, **2120  $\mu\epsilon$** , and used in the traditional design approach (§ 3.2.2). The compressive failure strain of 3046  $\mu\epsilon$  could allow to design a lighter panel and/or a panel with higher load carrying capability with respect to the panel obtained by the traditional design. Figure 70 and Figure 71 summarize the latter considerations.

A measure of the low weight reduction achievable can be appreciated considering that the above panel designed by using as design value 3046  $\mu\epsilon$ , should have a weight lower of about **30%** than that one obtained by going to resize the panel but using the traditional compressive allowable based on BVID degradation factor, 2120  $\mu\epsilon$ , and with equal load carrying capability.

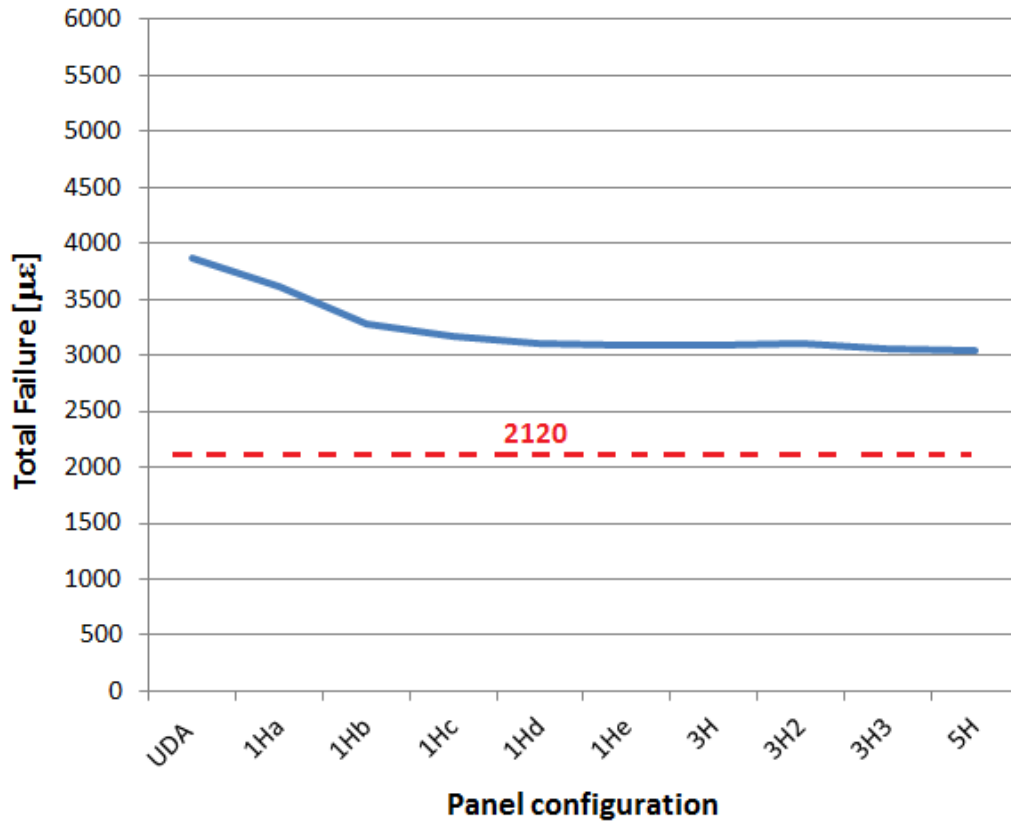


Figure 70: total failure of all the panels vs design allowable obtained at coupon level

$\epsilon_{cu}$ ( $\mu\epsilon$ )		
UDA panel	<b>5H panel</b>	Traditional design approach ( $K_{BVID}$ ) by CAI
3866	<b>3046</b>	<b>2120</b>

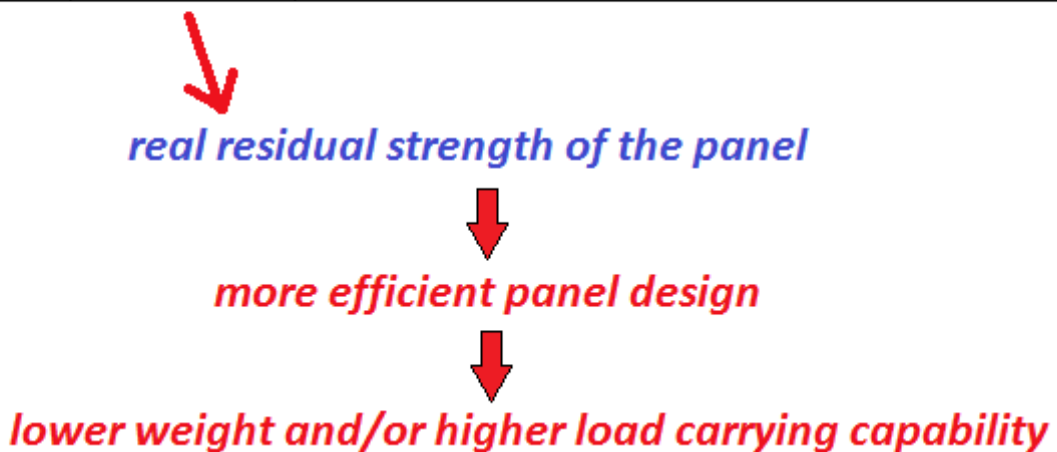


Figure 71: design considerations

## 6 CAI TESTS AND EQUIVALENCE HOLE-BVID

CAI tests have been executed on coupons of the same layup of the skin of the panel critical at strength characterised by 28 plies (42.86% 0°, 42.86% ±45°, 14.28% 90°), § 5.1, and also on coupons characterised by the basic laminate 24 plies QI. According to the design approach illustrated in § 2.2.3, also compression tests on coupons of the same geometry of CAI ones but with a central hole of 6.35 mm in diameter have been executed, in order to verify the equivalence between the residual strength of the impacted laminate and that one of the open hole laminate. The tests have been executed at different impact energy levels.

50 joule, according to the possible threats to the composite wing, is commonly accepted as cut-off energy level for the definition of BVID.

PFA analyses have been performed to simulate the compression tests on the impacted and open-hole coupons, and also the hole size equivalent, in terms of residual strength, to the experimental impact damage has been numerically determined.

### 6.1 Test description and results

The impact tests on the coupons and the subsequent compressive residual strength tests have been executed according respectively to the standard regulations ASTM D 7136/D 7136M – 07 [51], and ASTM D 7137/D 7137M – 07 [6]; this test method is called CAI.

The method allows to measure the residual strength of a laminate through two separate steps:

1. a flat, rectangular composite plate is subjected to an out-of-plane, concentrated impact using a drop-weight device with a hemispherical impactor [51];
2. the composite plate, previously subjected to a damaging event, is tested under compressive loading using a stabilization fixture [6].

A sketch of the coupon (i.e. plate) and of the impact test configuration is shown in Figure 72.

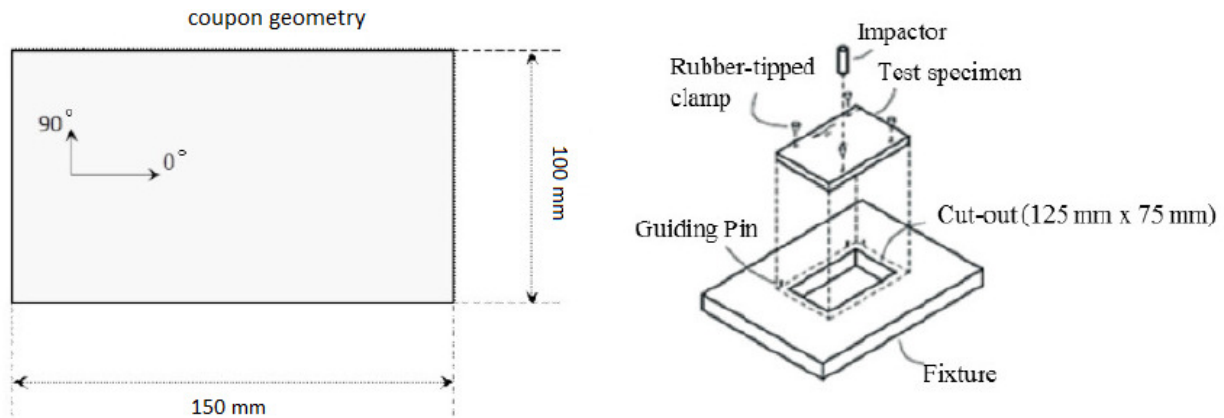


Figure 72: coupon dimensions (mm) and sketch of the impact test

Four rubber tipped clamps restrain the specimen over a rigid fixture base and an hemispherical impactor drops vertically with a certain impact energy.

The laminates tested are that ones of the skin of the stiffened panel critical at strength, § 5.1, and the 24-ply QI; according to the material reference system shown in Figure 72, the laminates have respectively the following stacking sequence:

- 28 plies, [45/-45/45/-45/0/0/90/0/0/45/-45/0/90/0]<sub>s</sub>,  
42.86% 0°, 42.86% ±45°, 14.28% 90°; t = 5.208 mm;
- 24 plies, [45/-45/0/90]<sub>3s</sub>,  
QI laminate, 25% 0°, 50% ±45°, 25% 90°; t = 4.464 mm;

The following energy levels have been applied for the two laminates:

- 30 J and 50 J for the laminate 28 plies;
- 50 J and 100 J for the QI laminate 24 plies;

in particular, for a wider investigation, also an energy level of 100 joule and therefore higher than the cut-off energy has been considered for the QI laminate.

The impact tests have been performed by using the Ceast Fractovis 6789 machine with an hemispherical impactor of mass equal to 8.64 kg and diameter equal to 20 mm. Figure 73 shows the Ceast machine, the impactor and the fixture.



**Figure 73: impact machine and fixture**

The compression after impact tests have been performed at room temperature and under displacement control by using the MTS 810 servo hydraulic testing machine, Figure 74. As prescribed by the standard regulation [6], an anti-buckling device has been used to avoid the onset of instability in order to guarantee a pure compression failure, Figure 75-a. The compression load has been applied along the largest dimension of the coupon which is the  $0^\circ$  laminate direction, and strain gage sensors have been applied, as recommended by the standard regulation [6], Figure 75-b, to monitor the deformation and the reaction.

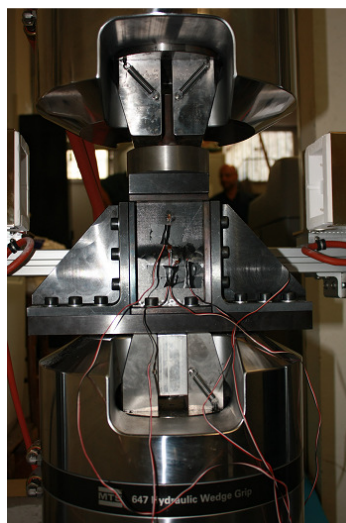


**Figure 74: MTS 810 servo hydraulic testing machine**

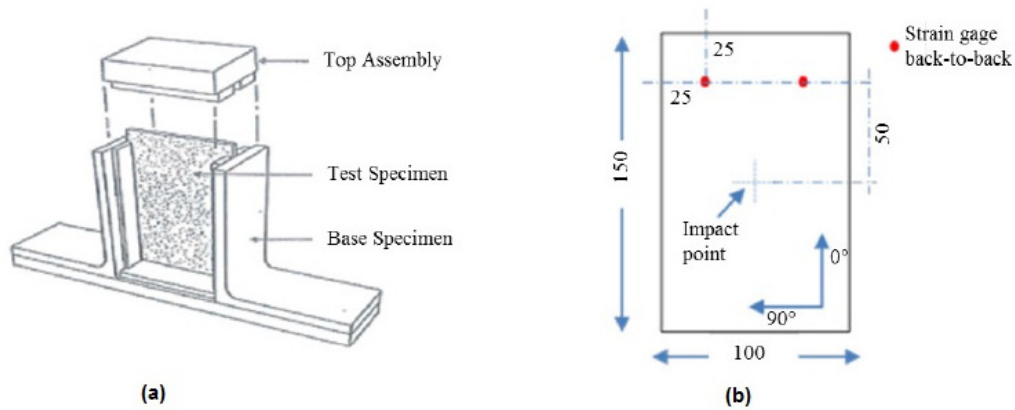


**Figure 75: sketch of the CAI test (dimensions in mm)**

The coupons with the central hole of 6.35 mm in diameter have the same dimensions of the CAI specimens; they have been tested in compression according to the same standard, ASTM D 7137/D 7137M – 07 [6].

Figure 76 shows a CAI coupon of 28 plies before impact and another one characterized by the same laminate and with the central hole 6.35 mm in diameter.

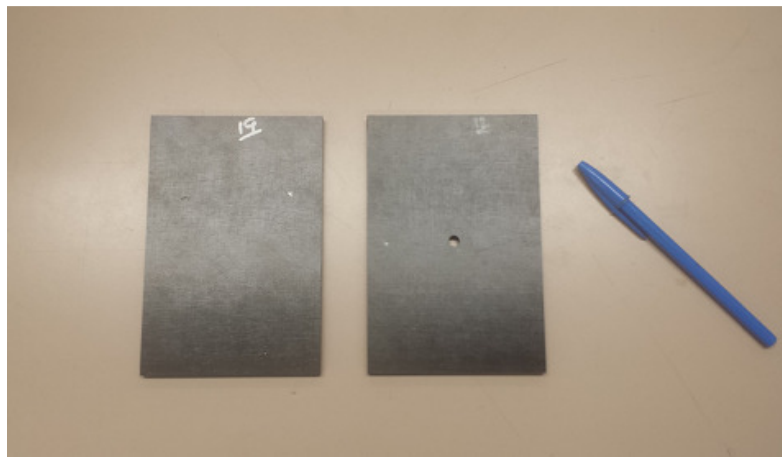


**Figure 76: CAI coupon before impact and with the hole**

For each energy level five coupons have been tested and a high repeatability has been found. In order to evaluate the compression strength of the pristine coupons, compression tests has been also performed on non-impacted coupons (Compression Before Impact - CBI tests). Table 6 shows the results of the compression tests in terms of main total failure and indentation.

		P [kN]	$\epsilon_{cu}$ ( $\mu\epsilon$ )	% $\epsilon_{cu}$ vs pristine	Dent Depth (mm)
<i>28-ply laminate</i>	Pristine	255.764	6870	-	
	30 joule	156.706	4210	-38.72%	0.18
	<b>50 joule</b>	138.206	<b>3710</b>	-46%	<b>0.24</b>
	<b>Hole</b>	183.714	<b>4930</b>	-28.24%	NA
<i>24-ply laminate</i>	Pristine	177.544	7579	-	
	<b>50 joule</b>	102.643	<b>4382</b>	-42.18%	<b>0.18</b>
	<i>QI</i> 100 joule	89.413	3817	-49.64%	0.83
	<b>Hole</b>	114.922	<b>4906</b>	-35.27%	NA

Table 6: compression test results at RTD

The failure strains are evaluated according to the standard regulation ASTM D 7137/D 7137M – 07 [6].

For both the laminates

- the compressive failure strain with the hole is practically equal to the asymptotic value of the corresponding numerical curves illustrated in Figure 41 being the W/D value of this coupons equal to 15.75: this result confirms the rightness of the PFA;
- the compressive failure strain with the hole is higher than that one of the impacted laminates for all the impact energies tested.

According to the test results, *the hole 6.35 mm in diameter is representative of a less critical damage respect to the BVID* (indentation 0.8-1 mm, § 2.1.1) *and/or the damage associated to the cut-off energy level, 50 joule.*

At least 100 joule are necessary to induce in the laminates an indentation of 0.8-1 mm, but this energy level is anyway higher than the cut-off energy. For both the tested laminates the BVID is that one associated to the cut-off energy level.

Figure 77 shows a coupon of 28 plies after the impact test at 50 joule, and Figure 78 shows the corresponding ultrasonic C-SCAN image in amplitude and the associated damaged area: this value is very close to the experimental values obtained by the test campaign on the 28-ply coupons.

Figure 79 shows, for the same laminate of 28 plies, an open hole coupon after the compression test.



Figure 77: 28-ply laminate – impact test at 50 joule

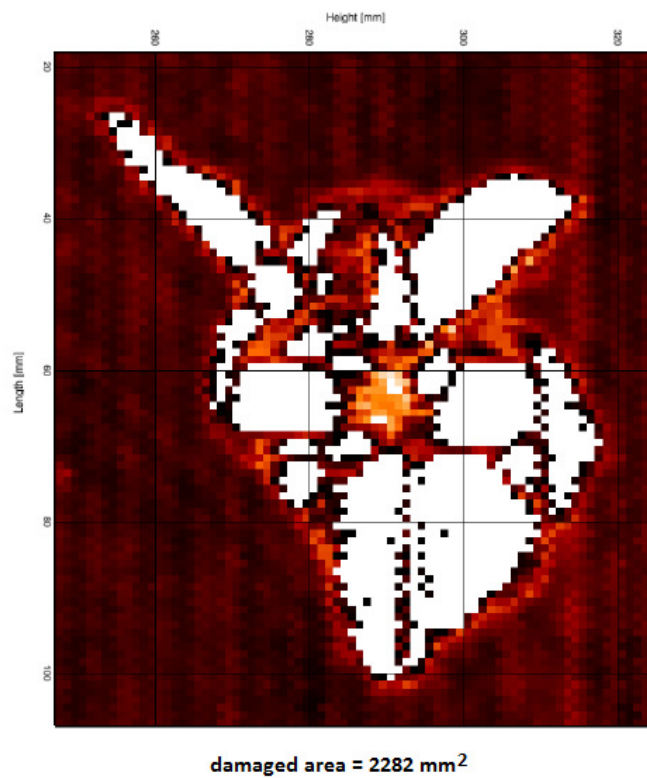


Figure 78: 28-ply laminate – C-SCAN image, impact at 50 joule



Figure 79: 28-ply laminate – open hole CAI coupon after compression test

## 6.2 Numerical simulation by PFA

FE models and PFA analyses have been performed to simulate the compression tests on the impacted and open-hole coupons. In particular these numerical simulations have been focused on the laminate *28-ply*, and considering the impact at the cut-off energy level of *50 joule*, BVID (Table 6, § 6.1).

Also the hole size equivalent, in terms of residual strength, to the experimental impact damage has been numerically determined.

The PFA has been performed by using the progressive failure analysis MSC Nastran<sup>®</sup> capability (§ 4.5).

### 6.2.1 Residual strength of the impacted coupons

The FE model of the impacted 50 joule coupon was developed at CIRA in LS-DYNA<sup>®</sup> software for the simulation of the impact test, and it was a result of an investigation presented in [52] aimed at tuning a FE model reproducing the impact response of the composite laminate. Then the LS-DYNA<sup>®</sup> model, with the damage distribution induced by the impact analysis, has been transferred

to the MSC Nastran<sup>®</sup> model for the subsequent compression after impact analysis: shell layered model, Figure 80.

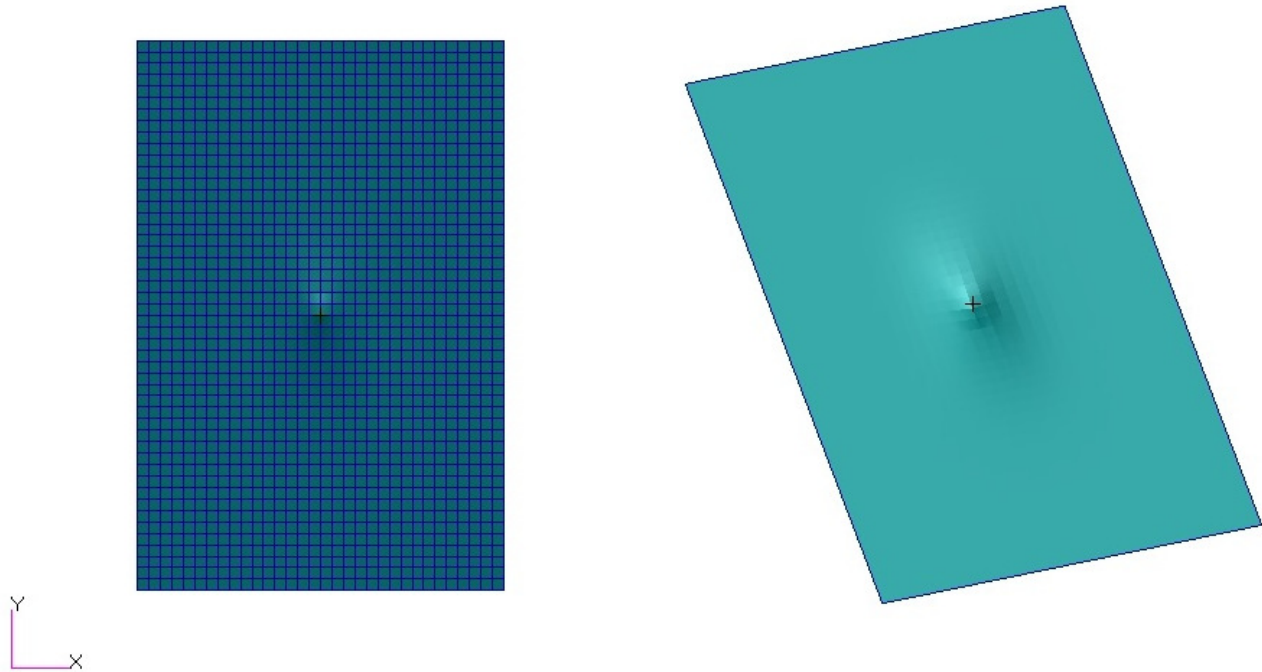


**Figure 80: laminate 28-ply – FE model of the impacted coupon at 50 joule.**

Figure 81 shows the numerical damage envelope for the 50 J impact test (elements plotted in red/orange); this envelope is the projection on the plane of the coupon of all the shell elements wherein at least one ply is failed according to the four failure modes: tensile fiber, compression fiber, tensile matrix and compression matrix.

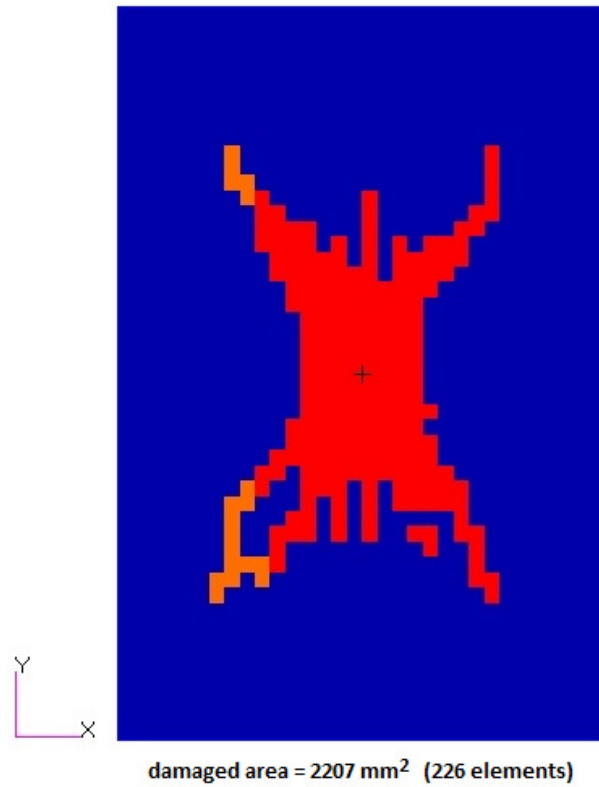


**Figure 81: laminate 28-ply – numerical damage envelop at 50 joule**

The measured numerical damaged area correlated quite well with that one measured from NDI evaluation, Figure 78; in particular, the numerical value was 2207 mm<sup>2</sup>, estimated with a deviation of only -3% with respect to the experimental data.

Figure 82 shows the numerical damage envelops for the four different failure modes.

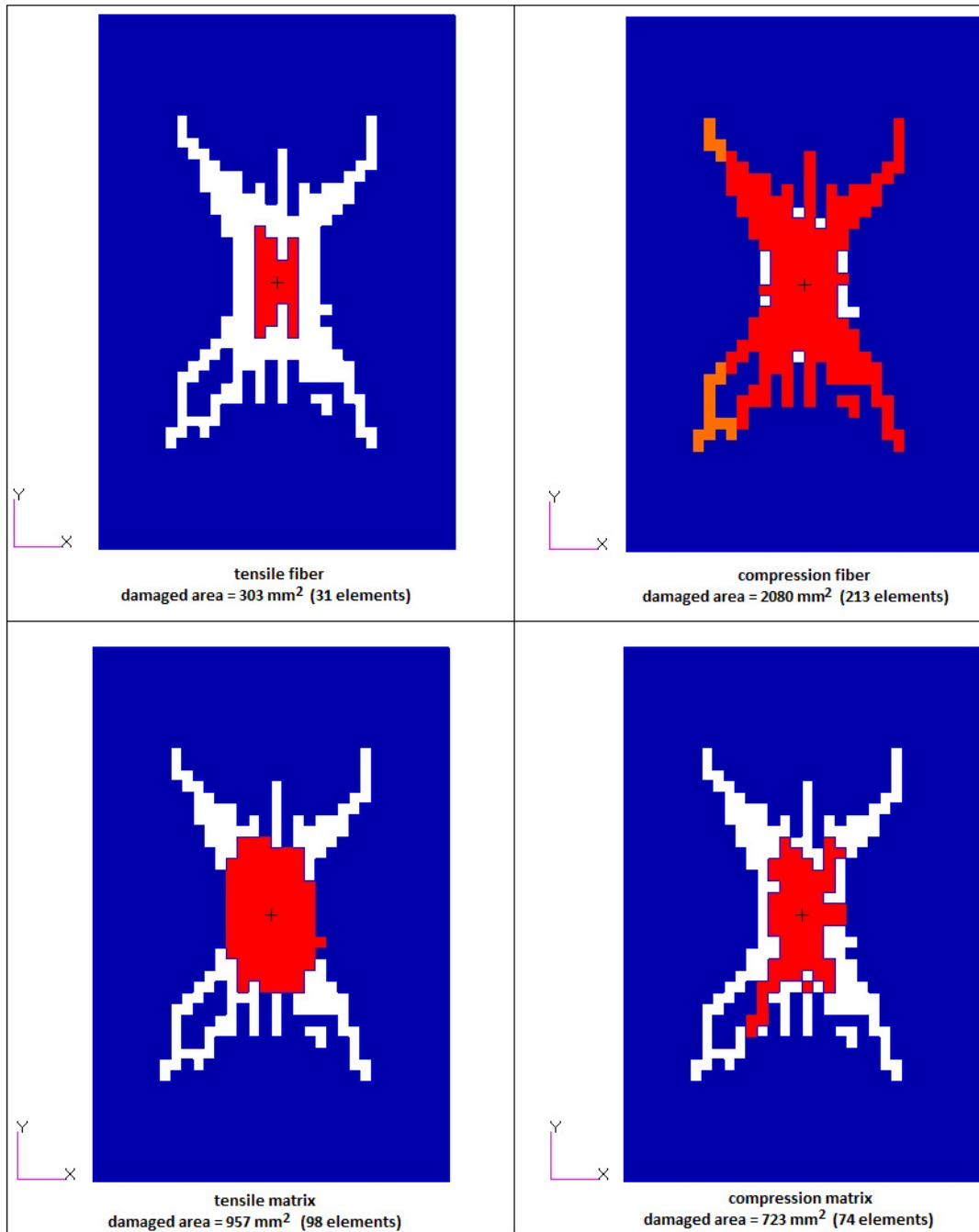


**Figure 82: laminate 28-ply – numerical damage envelopes at 50 joule for the different failure modes**

For the subsequent compression after impact analysis by MSC Nastran<sup>®</sup>, for each element of the FE model, the elastic material properties of each damaged lamina have been degraded, with respect to the pristine material properties, by applying the degradation rules illustrated in § 4.5. Hence, the damage status generated by the impact event in a certain area of the coupon is taken into account by using degraded material properties in that zone.

Once transferred the impact damage status to the MSC Nastran<sup>®</sup> FE model, the CAI analysis has been performed by using the PFA; the boundary conditions applied to the FE model are defined by the standard regulation of the CAI test, § 6.1 ([6]), and they are illustrated in Figure 83.

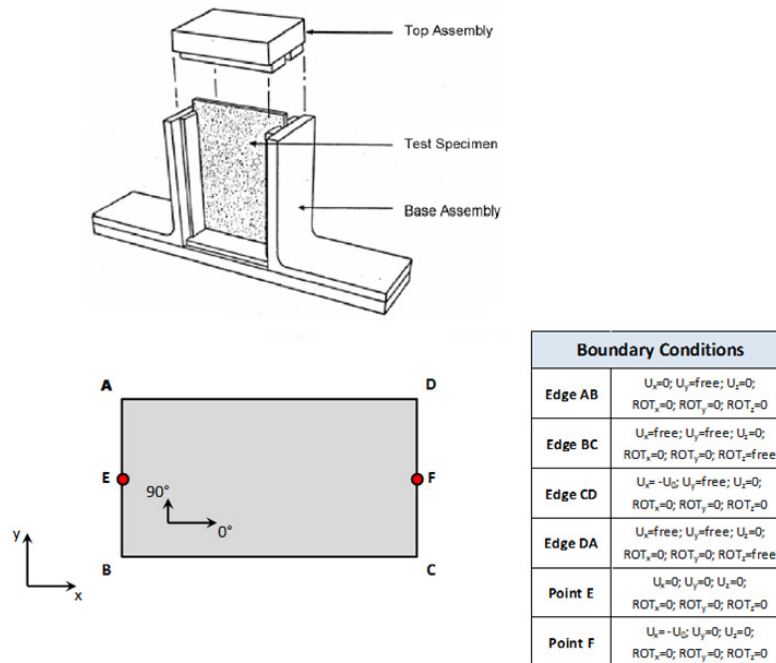
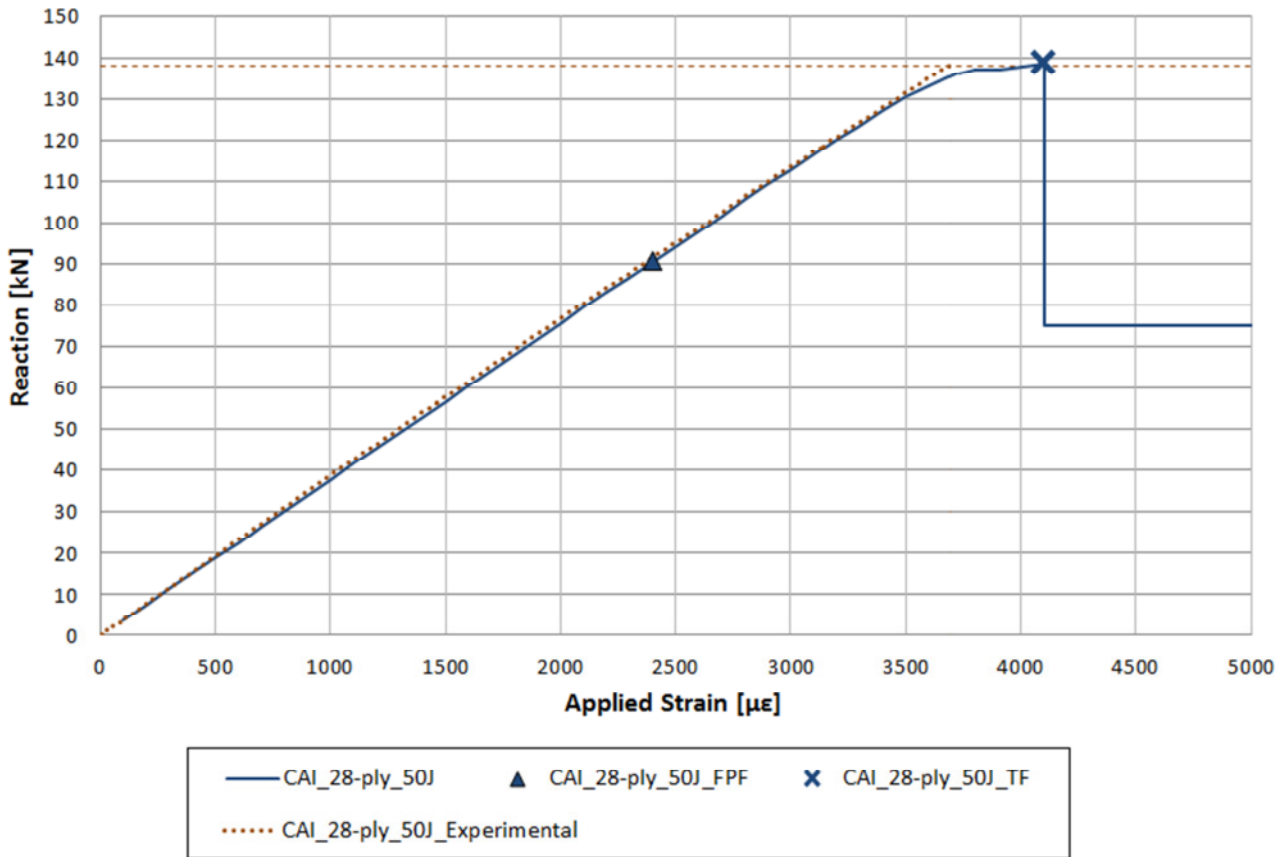


**Figure 83: boundary conditions for the numerical simulation of the CAI test**

Figure 84 compares the numerical and the experimental results in terms of Reaction Force vs Applied Strain; as far as the experimental curve is concerned, the average curve obtained from five compression tests is reported. The mean failure load (138.21 kN, Table 6) and the stiffness of the 50 J impacted coupon have been well reproduced by the numerical CAI; Table 7 shows the comparison between the total failure load, TF, evaluated numerically and that one experimental: the values are practically coincident.



	FPF Load [kN]	FPF Strain [µε]	Total Failure [kN]	FAILURE Strain [µε]
CAI_28-ply_50J - numerical	90.62	2400	138.70	4100

Figure 84: Reaction vs Applied Strain – laminate 28-ply impacted at 50 joule

		Total Failure [kN]	
28-ply laminate 50 joule	Experimental	138.21	-
	Numerical	138.70	+ 0.36%

Table 7: laminate 28-ply impacted at 50 joule – numerical TF vs experimental TF

### 6.2.2 Residual strength of the open hole coupons

The FE model of the coupon with the hole 6.35 mm in diameter is shown in Figure 85. The boundary conditions are the same illustrated in Figure 83.

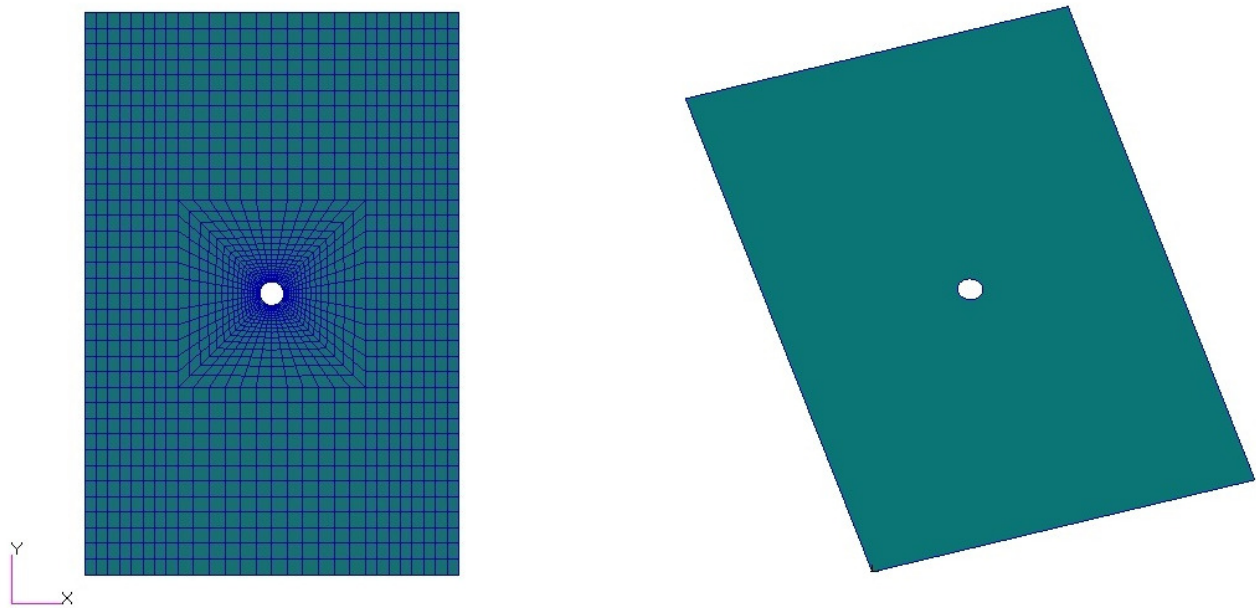
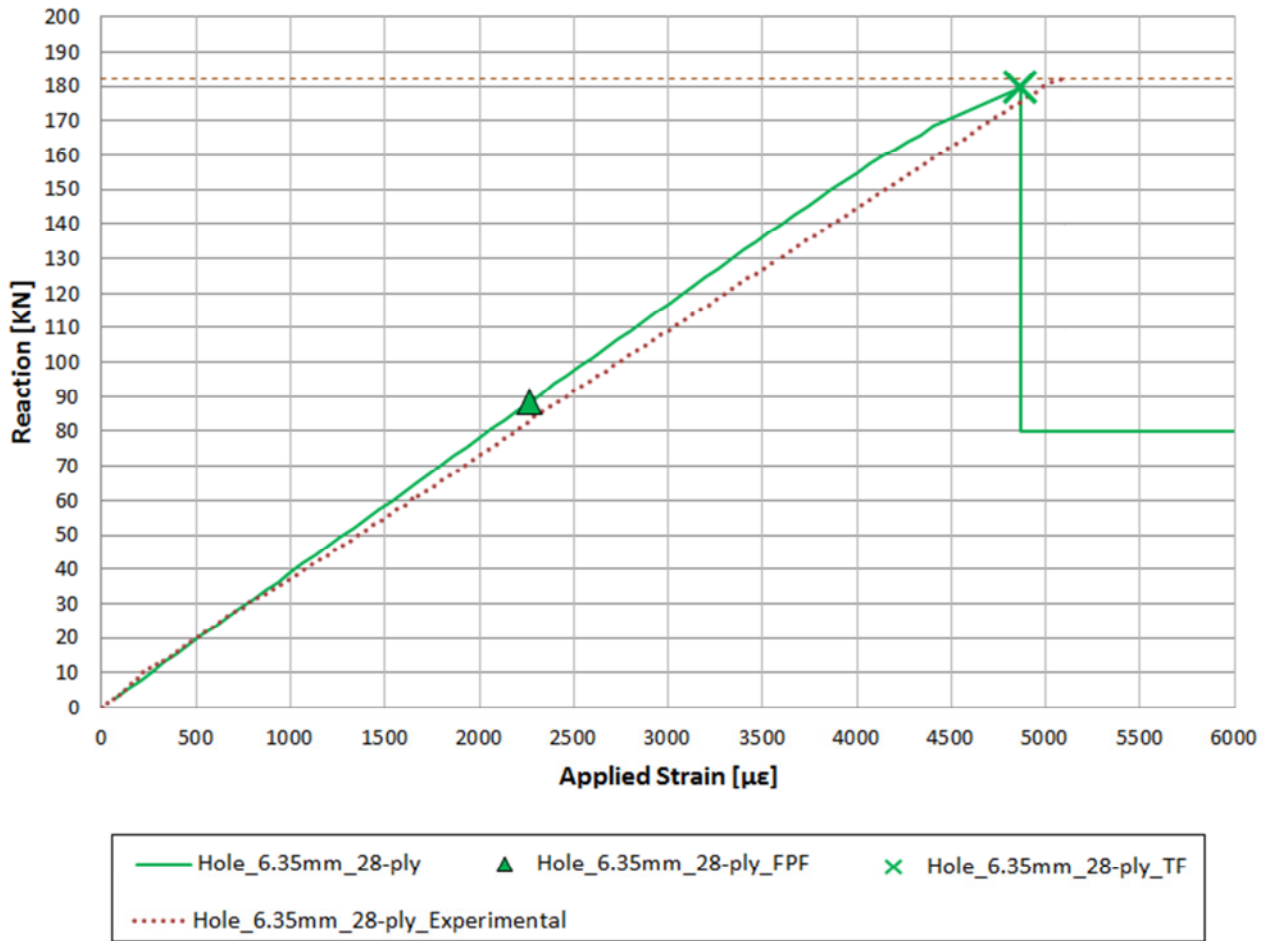


**Figure 85: laminate 28-ply – FE model of the coupon with hole 6.35 mm in diameter**

Figure 86 compares the numerical and the experimental results in terms of Reaction Force vs Applied Strain; as far as the experimental curve is concerned, the average curve obtained from five compression tests is reported. The mean failure load (183.71 kN, Table 6 ) is very close to that one reproduced by the numerical compression test: Table 8 shows the comparison between the total failure load evaluated numerically and that one experimental.

Figure 87 shows the damaged elements at different load substeps between the FPF load and the collapse load TF; as expected, the failure of the panel starts close to the hole and propagates along a line perpendicular to the load direction



	FPF Load [kN]	FPF Strain [µε]	Total Failure [kN]	FAILURE Strain [µε]
Hole_6.35mm_28-ply_numerical	88.48	2267	179.65	4866.67

Figure 86: Reaction vs Applied Strain – laminate 28-ply with hole 6.35 mm

		Total Failure [kN]	
<i>28-ply laminate Hole 6.35 mm</i>	<b>Experimental</b>	183.71	-
	<b>Numerical</b>	179.65	- 2.21%

Table 8: laminate 28-ply with hole 6.35 mm – numerical TF vs experimental TF

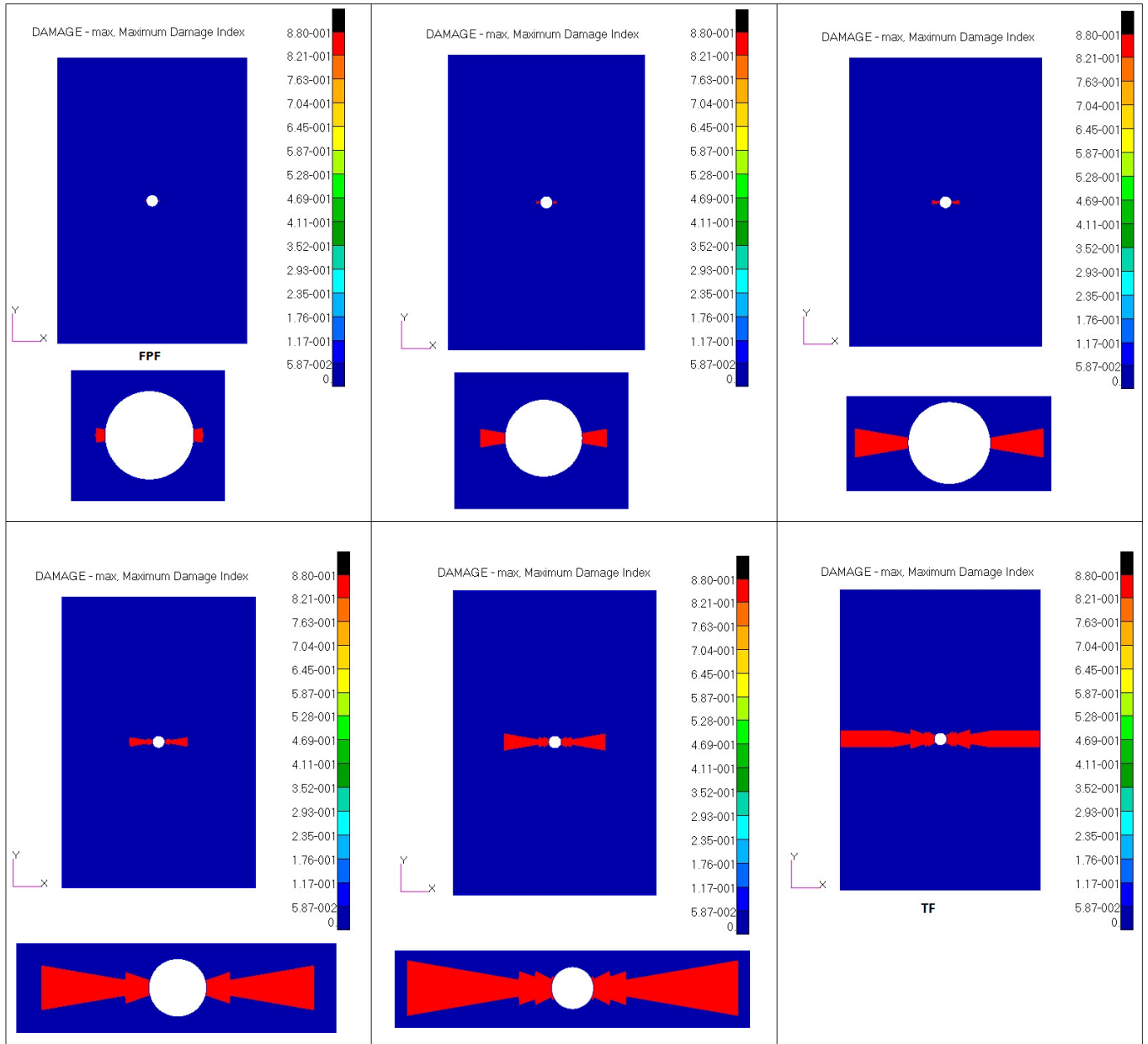


Figure 87: laminate 28-ply with hole 6.35 mm – progressive damage

### 6.2.3 Hole size equivalent to the impact damage

Different holes sizes up to 25.4 mm (1 inch) in diameter have been considered for the progressive failure analysis finalized to evaluate the hole diameter able to assure the same residual strength of the 50 joule impact test (138.21 kN, Table 6).

The following hole standard diameters have been considered sufficient to this investigation:

**19.05 mm (3/4 inch), 22.225 mm (7/8 inch), 25.4 mm (1 inch),** Figure 88.

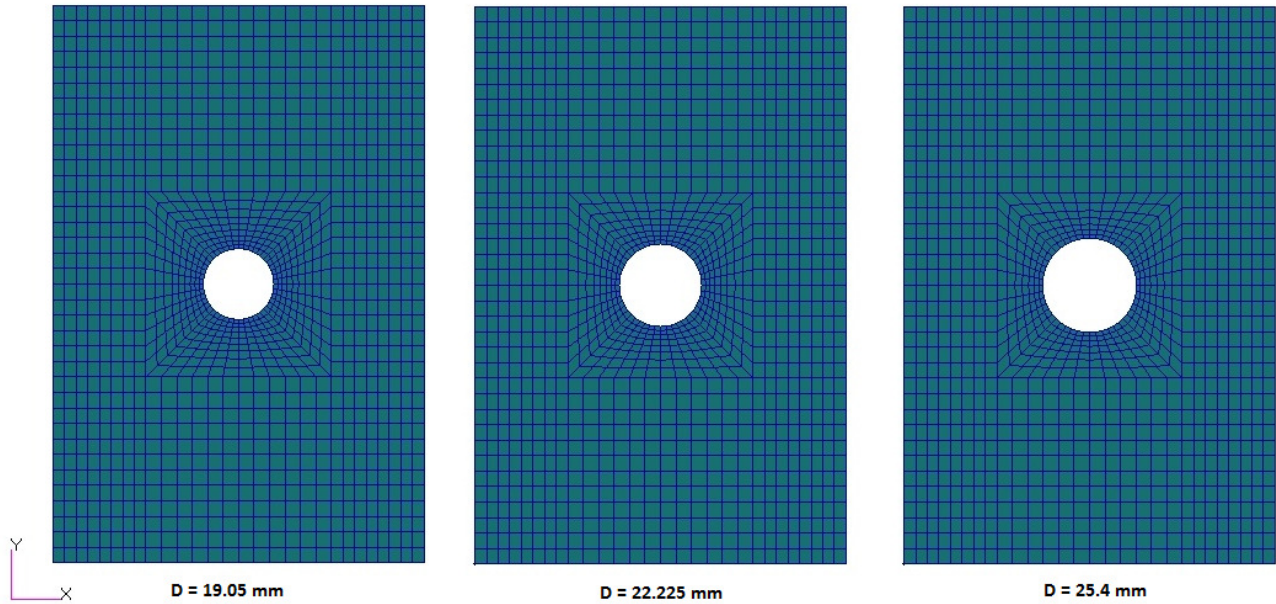
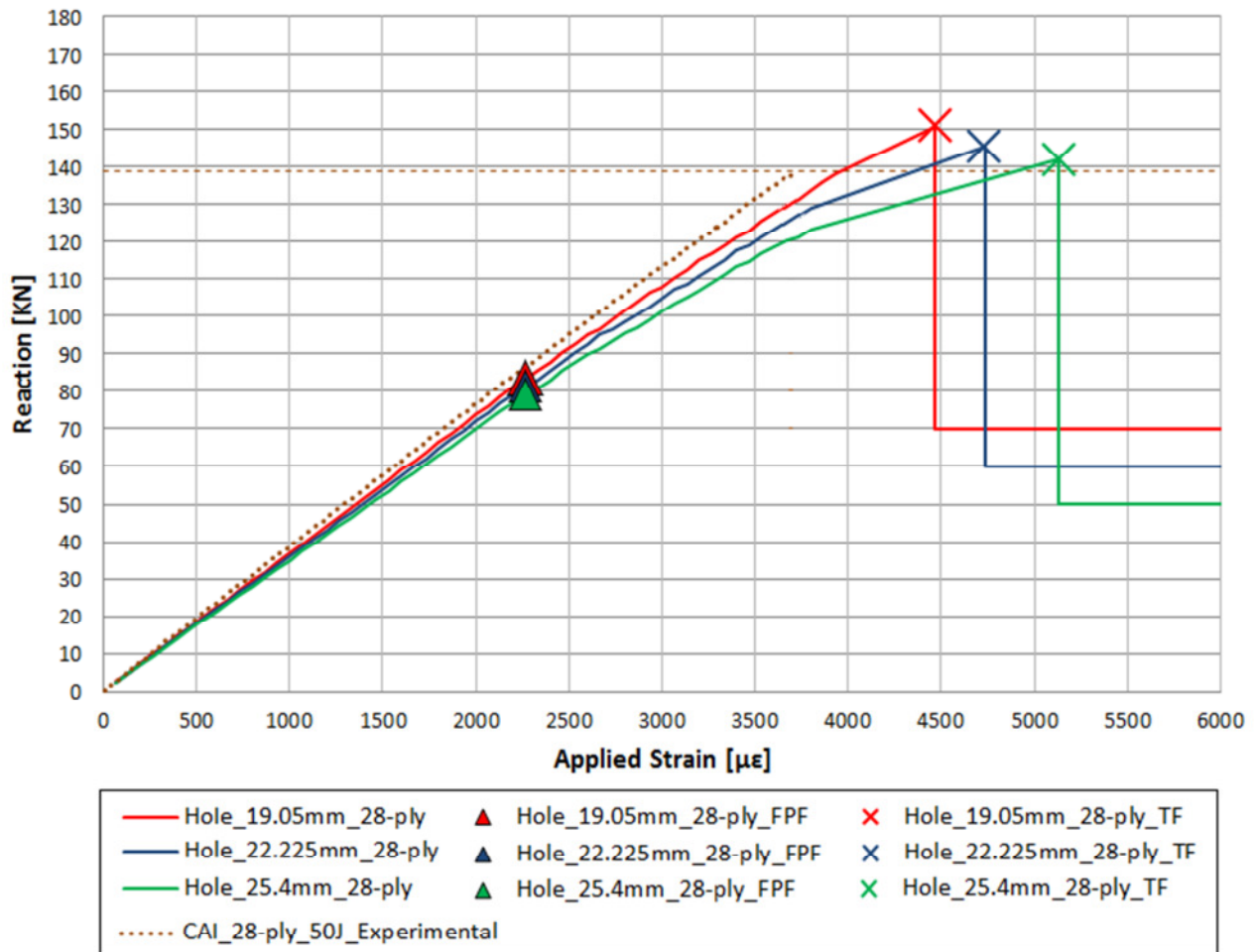


**Figure 88: hole diameters investigated**

Figure 89 compares the numerical results obtained by the different hole sizes and the experimental 50 J impact test in terms of Reaction Force vs Applied Strain; as expected the predicted stiffness of the notched coupons doesn't match that one of the impact test. Table 9 shows the comparison between the total failure loads of the notched coupons and that one experimental of the 50 J impact test, (138.21 kN, Table 6): the hole **25.4 mm** in diameter well correlates the residual strength of the 50 J impact test. This hole has been assumed equivalent to the BVID (cut-off energy level) of the 28-ply laminate (§ 6.1).



	FPF Load [kN]	FPF Strain [μϵ]	Total Failure [kN]	FAILURE Strain [μϵ]
Hole_19.05mm_28-ply	83.54	2266.67	150.87	4466.67
Hole_22.225mm_28-ply	81.59	2266.67	145.55	4733.33
Hole_25.4mm_28-ply	79.41	2266.67	141.97	5133.33

Figure 89: Reaction vs Applied Strain – laminate 28-ply with holes vs 50 joule impact test

		Total Failure [kN]	
<i>28-ply laminate</i>	<b>50 J impact test</b>	138.21	-
	Hole_19.05mm_28-ply	150.87	+ 9.16%
	Hole_22.225mm_28-ply	145.55	+ 5.31%
	Hole_25.4mm_28-ply	141.97	+ 2.73%

Table 9: numerical TF of notched CAI coupons vs 50 joule impact test

## 7 INFLUENCE ON THE CAPABILITY OF A STIFFENED PANEL IN PRESENCE OF AN IMPACT DAMAGE OBTAINED ON CAI COUPON

According to the new design approaches and criteria illustrated in § 2.2.3, the traditional use for the design of stiffened panels of the reduced allowable for BVID determined at coupon level, could be more conservative respect to what really happens in terms of residual strength if the impacted CAI coupon is part of the skin of a stiffened panel.

At this purpose a FE model of a 2-stringer panel has been built, in which the numerical 50 joule impact damage induced on 28-ply coupon (§ 6.2.1) *has been substituted to an equivalent portion of the skin of the panel*.

The impact damage has been substituted in the middle of the stringer bay as illustrated in Figure 90.

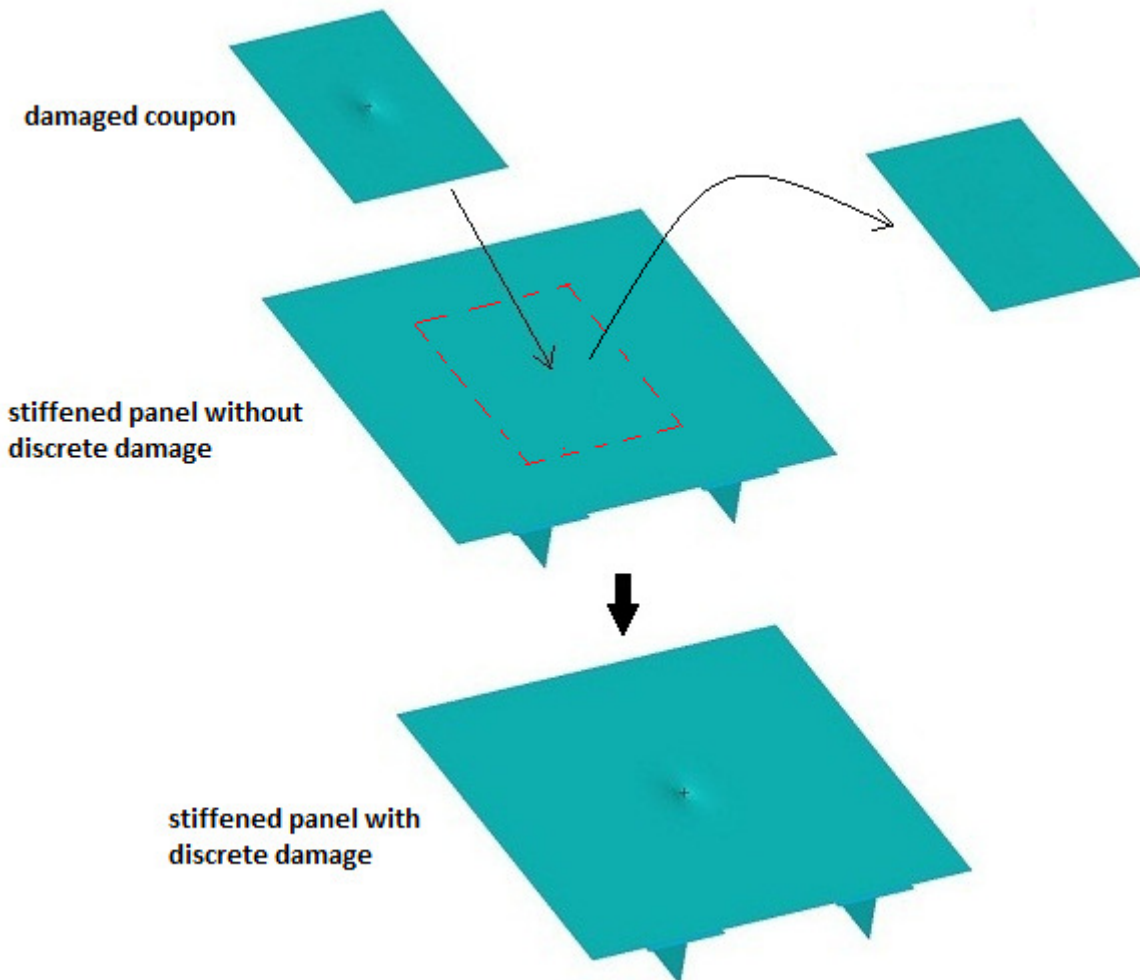


Figure 90: 50 joule impact damage introduction into 2-stringer skin panel

The panel geometry is a portion (stringer bay) of the panel with six stringers of § 5.1, as illustrated in Figure 91.



**Figure 91: 2-stringer panel**

Figure 92 shows the FE model of the panel, and Figure 93 the damaged elements.

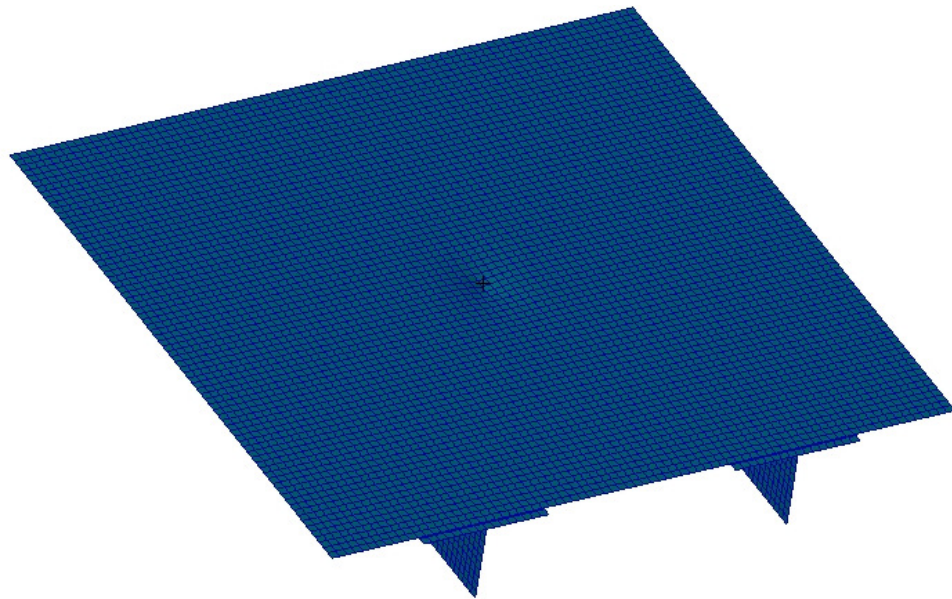


**Figure 92: FE model of the 2-stringer panel with 50 joule impact damage**

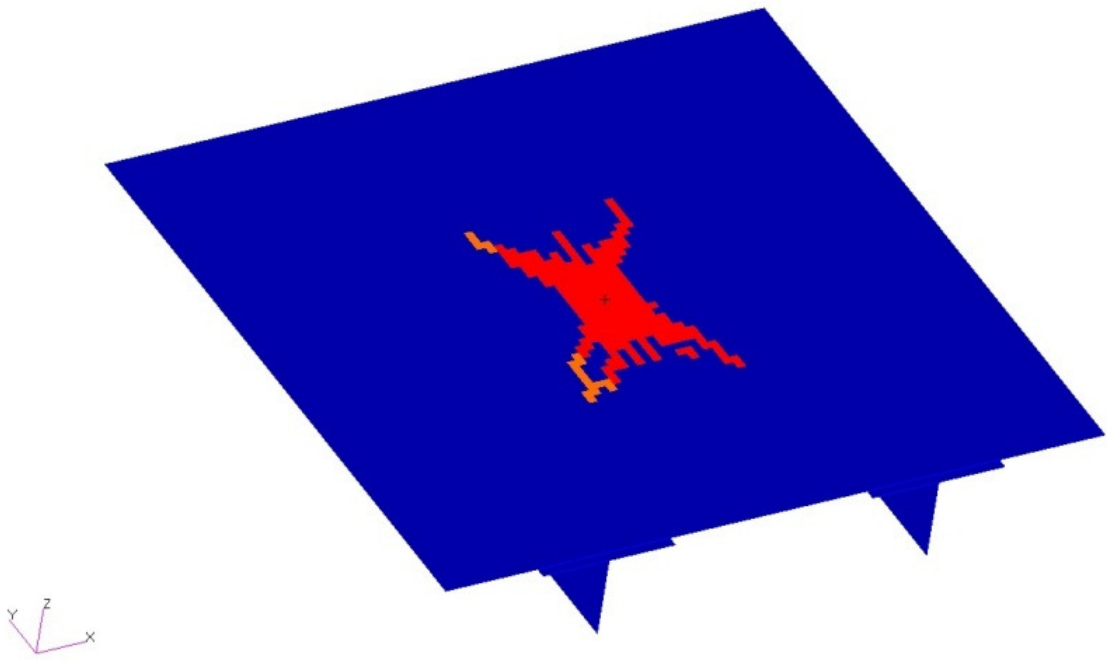


**Figure 93: 2-stringer panel – damaged elements**

In order to verify the equivalence BVID-hole, as found at coupon level (§ 6.2.3), also the 2-stringer panel with the central hole 25.4 mm in diameter has been considered, Figure 94.

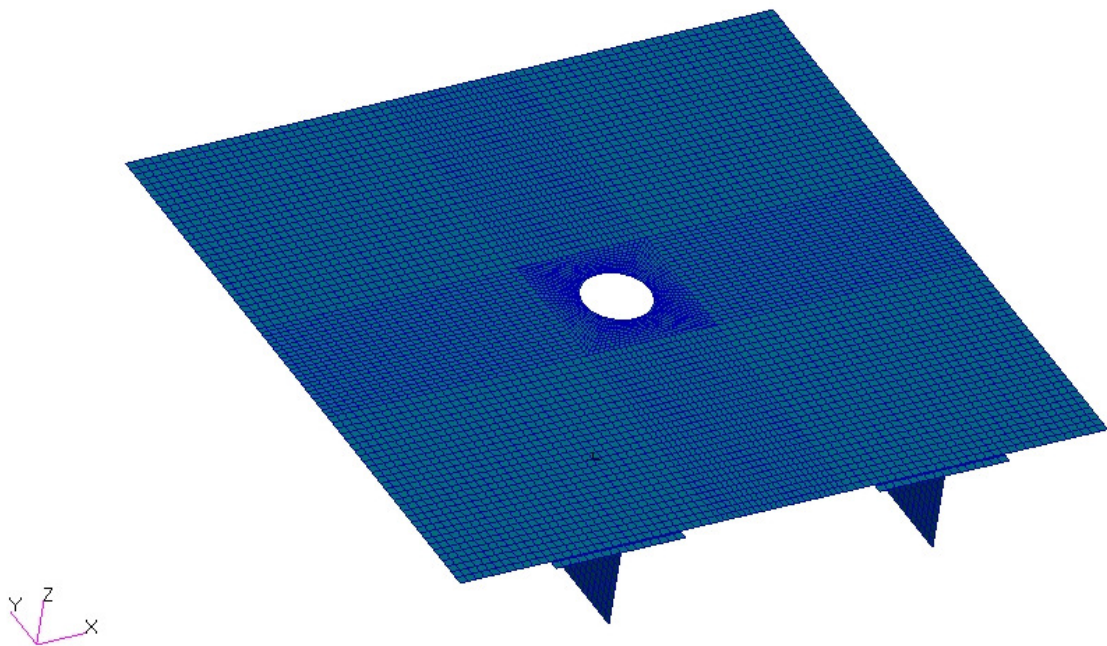


**Figure 94: 2-stringer panel with central hole 25.4 mm in diameter**

PFA analyses have been executed on the 2-stringer panel, according to the design criteria of § 2.2.3, in order to

- verify that the equivalence between the impact damage and the hole illustrated in § 6.2.3 remains valid also at panel level;
- compare the residual strength of the stiffened panel designed with reduced design allowable obtained at coupon level (50 joule/cut-off energy level), with that one of panel if the impacted CAI coupon is part of it at the middle of the stringer bay;
- further locations in the skin of this impact damage have been considered (very close to the cap of the stringer, under the cap of the stringer and at the edge of the cap of the stringer), in order to evaluate the residual strength of the panel for different damage scenarios.

The FE models are characterized by pristine mechanical strength properties of the material (no degradation for BVID, temperature, moisture and B-basis statistical reduction):  $\epsilon_{cu} = 6870 \mu\epsilon$  (Table 6).

### ***7.1.1 Comparison impact damage – hole at panel level***

The PFA has been performed on the 2-stringer panel with discrete damage of Figure 93, and on that one with the central hole 25.4 mm in diameter of Figure 94.

Figure 95 compares the Reaction Force vs the Applied Strain for the two panels and Table 10 shows the comparison between the total failure loads: the values are practically coincident (the difference is only 1%).

This result confirms that also at panel level, more complex structure, the hole 25.4 mm in diameter is equivalent in terms of collapse load to the 50 J impact damage, as already verified at coupon level (§ 6.2.3).

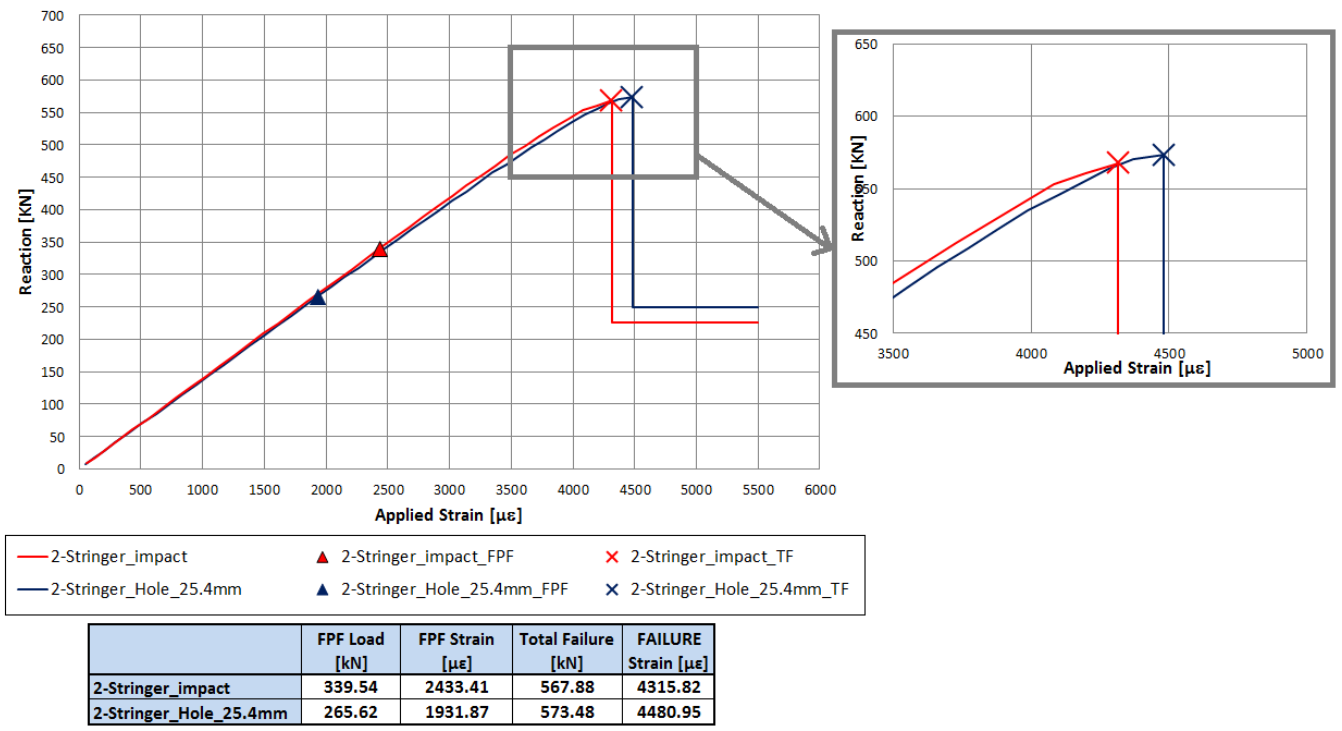


Figure 95: Reaction vs Applied Strain – 2-Stringer panel – impact damage vs hole 25.4 mm

		Total Failure [kN]	
<i>2-Stringer panel</i>	<b>50 J CAI in the skin</b>	567.88	-
	<b>Hole_ 25.4mm</b>	573.48	- 1%

Table 10: 2-Stringer panel – TF load comparison

### 7.1.2 Design at panel level

The traditional design approach of the 2-stringer panel is based on the use of the material design value in compression degraded for BVID using results obtained at coupon level (bottom level of the building block approach, Figure 2), in addition to the degradations for temperature, moisture and B-basis statistical reduction.

Regarding only the degradation for BVID, for the selected laminate the compressive allowable obtained by CAI tests in presence of the BVID (dent depth: 0.8-1 mm, § 2.1.1) or of the induced impact damage obtained at the cut-off energy level of 50 joule, is assumed as compressive design

value of the stiffened panel: *the whole panel is considered uniformly damaged* instead of considering a discrete damage model.

But according to the results illustrated in Figure 95 of § 7.1.1, the final failure strain of the 2-stringer panel, obtained by substituting the induced impact damage, obtained at coupon level, with an equivalent portion of its skin (discrete damage model),

- in the middle of the stringer bay,
- and with the pristine material strength properties,

is resulted **4270  $\mu\epsilon$ <sup>1</sup>**, and therefore higher than the design value used by the traditional design.

In detail, according to the CAI test results of Table 6 (§ 6.1), the longitudinal compressive strain ( $\epsilon_{cu}$ ) based on the results of the CAI tests is resulted equal to **3710  $\mu\epsilon$**  (50 J, cut-off energy level) against the value of 6870  $\mu\epsilon$  (pristine value). Consequently, the design of the 2-stringer panel assuming it uniformly damaged and with a material design value for compression,  $\epsilon_{cu}$ , equal to 3710  $\mu\epsilon$ , as expected by the traditional design approach, can lead to a not efficient structure in terms of weight and/or load carrying capability with respect to consider the material design value equal to 4270  $\mu\epsilon$  (+15%): this is the real residual strength of the stiffened panel with the discrete impact damage inserted in the skin.

Figure 96 summarises the above conclusions.

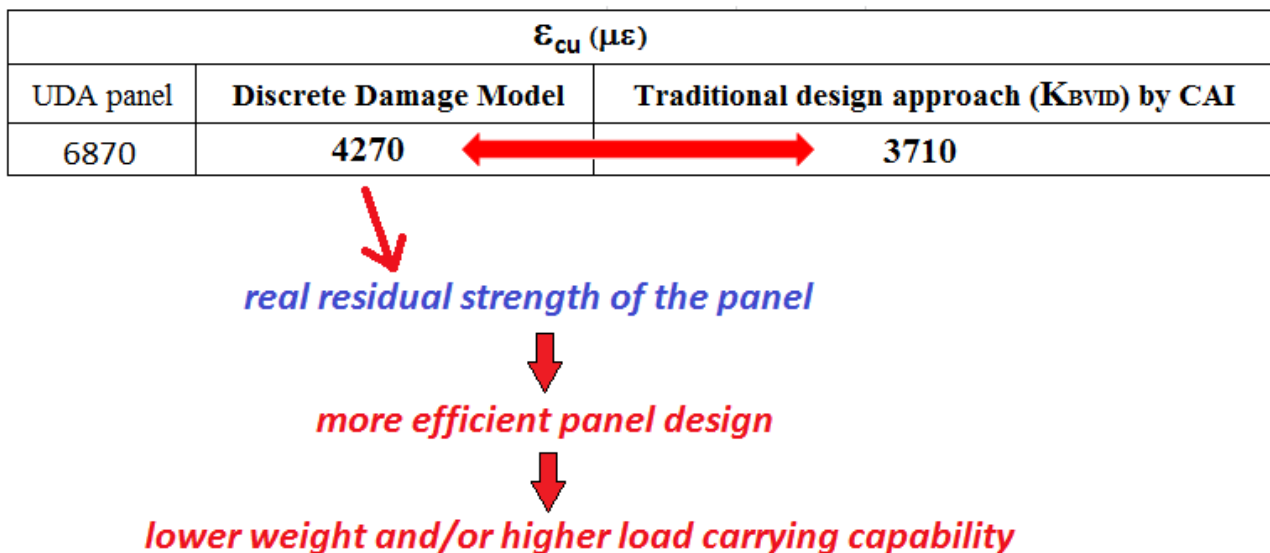


**Figure 96: design implications for the 2-stringer panel**

<sup>1</sup> This value is the analytical value. It has been evaluated as ratio between the experimental collapse load 567.88 kN and the analytical value EA of the panel.

A measure of the low weight reduction achievable can be appreciated considering that according to Figure 27 (weight vs compressive design value, § 3.2.2), the above panel designed by using as design value  $4270 \mu\epsilon$ , should have a weight lower of about **9%** than that one obtained by going to resize the panel but using the traditional allowable based on the material design value in compression degraded for BVID by using results obtained at the coupon level,  $3710 \mu\epsilon$ .

In addition to consider the impact damage in the middle of the stringer bay, also other different skin locations of this damage have been considered:

- under the cap of the stringer,
- at the edge of the cap of the stringer,
- very close to the cap of the stringer,

in order to evaluate the final capability of the panel for different damage scenarios.

Figure 97 illustrates a scheme of the different damage scenarios and Figure 98 the corresponding FE models.

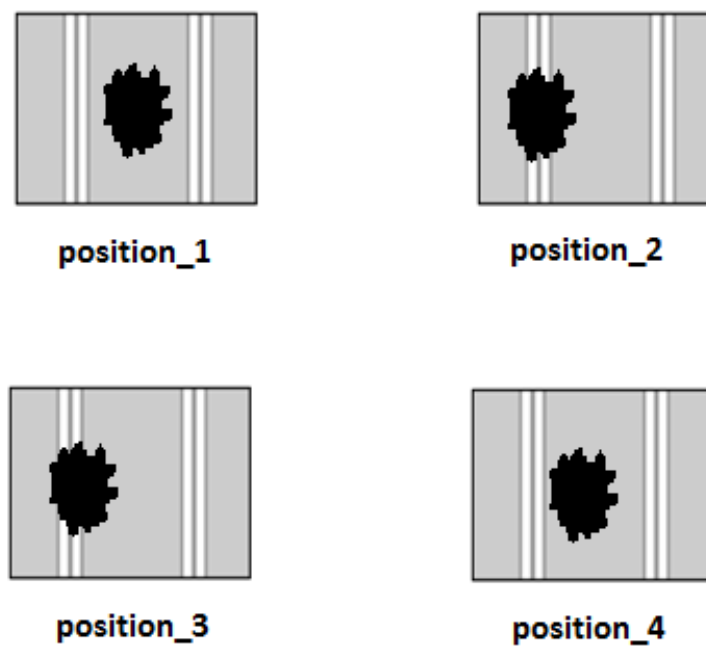


**Figure 97: scheme of the impact damage locations**

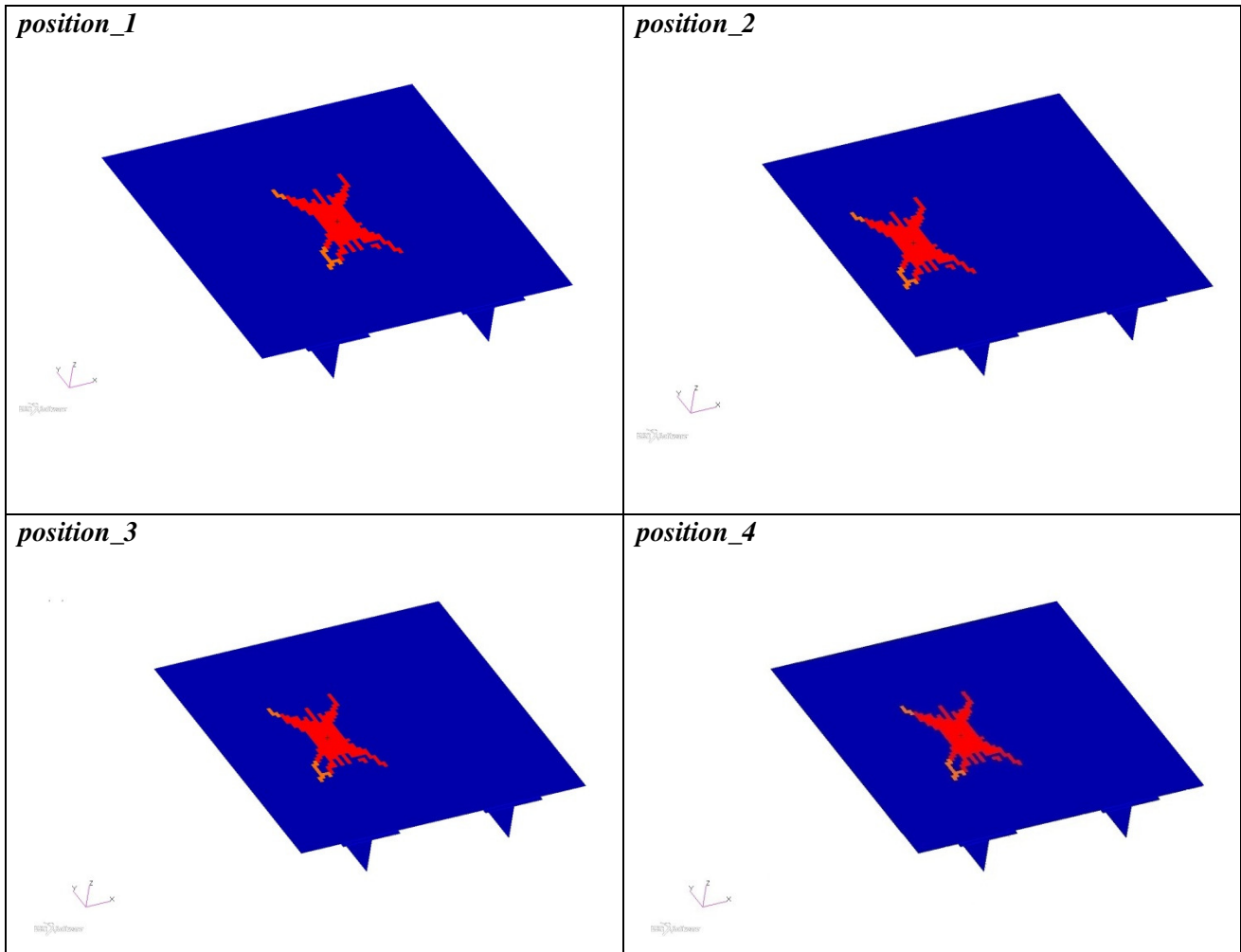


**Figure 98: FE models – different damage locations**

Figure 99 compares the Reaction Force vs the Applied Strain for the different damage locations.

The results of the PFA performed for all the four damage locations are very close to each other. The least critical cases are obtained for the *impact\_pos\_1* (damage in the middle of the stringer bay) and *impact\_pos\_2* (under the cap of the stringer): the TF loads are practically coincident. The lowest residual strength of the panel, most critical case, is that one corresponding to the damage located at the edge of the cap of the stringer (*impact\_pos\_3*).

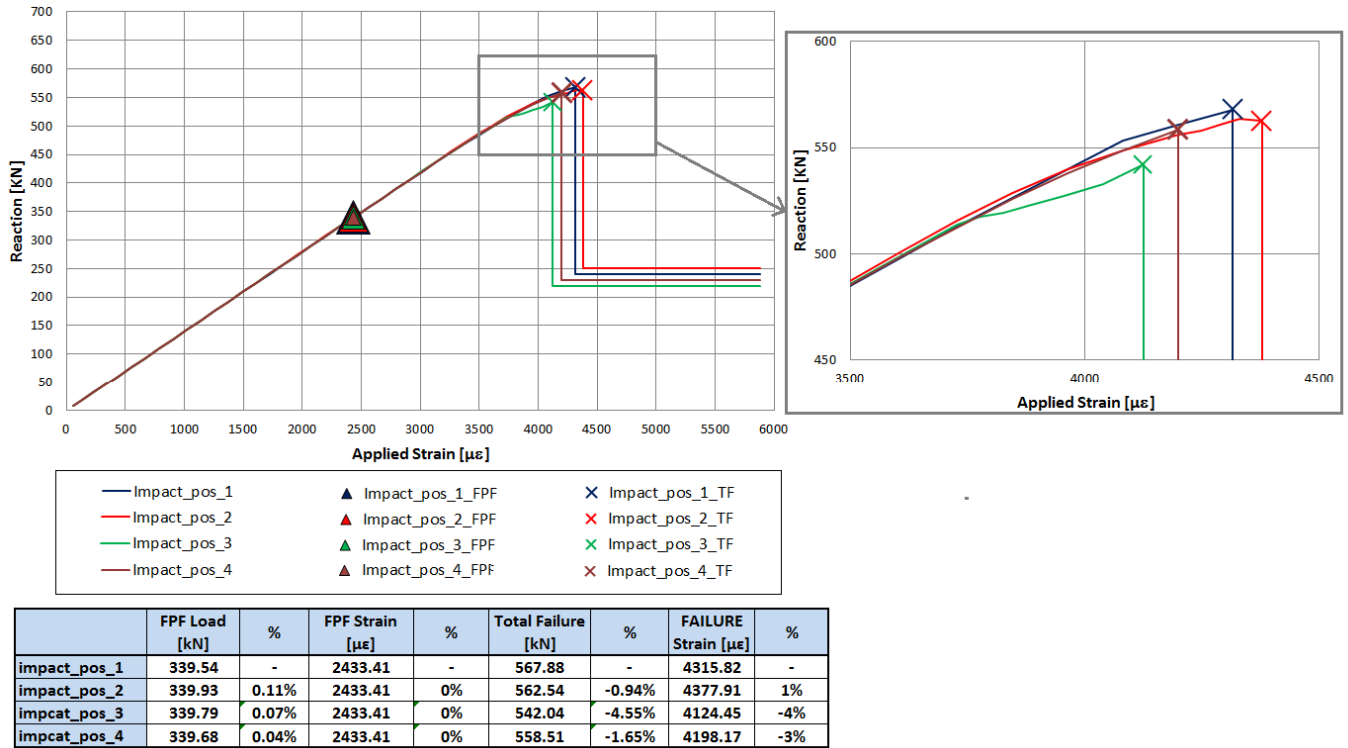


Figure 99: Reaction Force vs Applied Strain – for different damage locations

According to the above results, independently from the position of the impact damage in the skin of the panel, the residual strength of the 2-stringer panel with discrete damage, is always higher than that one obtained by the traditional design approach (3710 μϵ), based on the use of the material design value in compression degraded for BVID using results obtained at the coupon level (panel uniformly damaged). The lower value of the analytical failure compressive strain is that one related to the *position\_3*, 4075 μϵ, **+10%** with respect to 3710 μϵ.

According to Figure 27 (weight vs compressive design value, § 3.2.2), the above panel designed by using as design value 4075 μϵ, should have a weight lower of about **4%** than that one obtained by going to resize the panel but using as design value 3710 μϵ.

## 8 CONCLUSIONS AND FUTURE DEVELOPMENTS

This work has investigated new design criteria and approaches finalised to obtain composite stiffened panels lighter than those ones obtained by the traditional design approach for civil aircraft applications. In particular the work has evaluated the amount of the weight reduction that can be obtained releasing some traditional limitations and constraints used with the traditional design approach.

The design by supposing the presence of *SHM systems* has revealed that weight reductions are achievable thanks to the information given from this kind of systems. Consistent reductions could be obtained for the wing stiffened panels sized at strength instead of those ones critical at buckling. The work has also furnished the design requirements for the SHM systems in terms of which parts of the stiffened panel is necessary to monitor in order to obtain relevant weight reductions.

The application of the *progressive failure analysis methodology* has shown the effectiveness of this methodology to predict the real mechanical behaviour of the stiffened panels, demonstrating to be a valid design tool to investigate new design approaches by evaluating the residual strength of panels with discrete damages.

The analyses of the stiffened panels with impact discrete damages, simulated by holes 1/4 inch in diameter as suggested by design guidelines for the preliminary design phase, have given useful indications about the sensitivity of the residual strength of the panels respect to the densities of damages and different damage locations. These results will be useful tools to support in the future new design approaches. The results of the PFA have been obtained on two different stiffened panels with discrete damages: one panel critical at strength and the other one with buckling load lower than the failure load. Significant potential weight reductions, up to 30%, have been found respect to the traditional design. Further, the PFA has shown also the influence of the damage scenarios on the buckling onset and its shape.

*CAI tests* executed on the two laminates selected in this work, have shown that the hole 1/4 inch (6.35 mm) in diameter is representative of a less critical damage respect to the BVID. By means of the PFA, the hole equivalent to the BVID is resulted 1 inch in diameter.

The traditional use for the design of stiffened panels of the reduced allowable for BVID determined at coupon level, is resulted conservative respect to what really happens in terms of residual strength

if the impacted *CAI coupon is part of the skin of a stiffened panel*. The impact damage induced on coupon has been substituted to an equivalent portion of the skin of a 2-stringer stiffened panel; the residual strength of the panel is resulted higher of at least 10% respect to the traditional design and with a weight reduction of at least 4%.

For *further impacts on the design process* it is necessary *in the future* to enlarge the application of the progressive failure analysis considering

- more different hole diameters,
- different damage maps (with holes also on the web of the stringers),
- different layups and thicknesses,
- the presence of delaminations and skin-stringer disbondings,

and validate the numerical results with a dedicated test campaign.

## APPENDIX A: POST-BUCKLING ANALYSIS IN HYPERSIZER®

Figure 100 illustrates a typical load-strain curve for linear analysis and nonlinear analysis in post-buckling regime, by using Hypersizer® code. In this example, local buckling occurs at just under 50% limit load indicated by the orange triangle. From this point, the linear curve continues in a straight line until the failure is indicated with the blue star. In reality, the panel goes into post-buckling and the load-strain curve follows the black curve. The predicted failure along this curve is at the location of the red star which is substantially lower than the linear failure prediction.

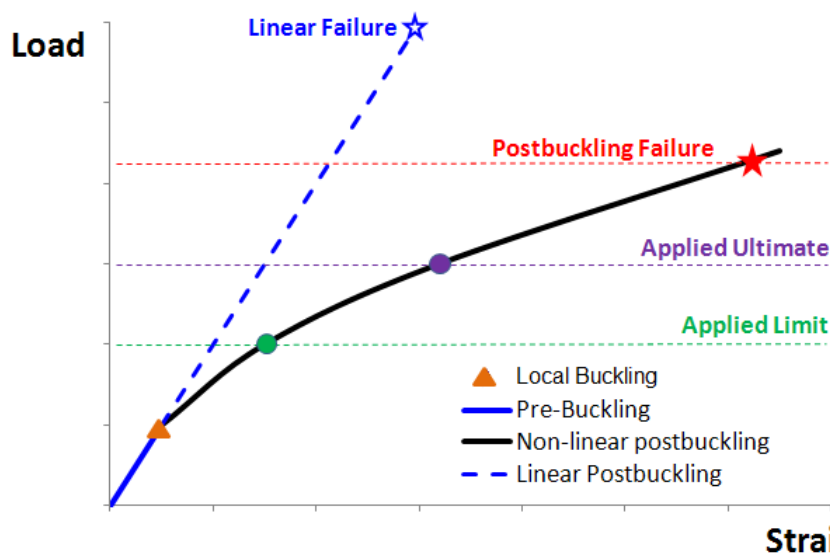


Figure 100: typical load-strain curve for nonlinear analysis in post-buckling regime

The main key features of the local post-buckling method implemented in Hypersizer® are the following ones:

- the margins of the panel in post-buckling regime are based on load redistribution into the remaining stable cross section;
- evaluation of the “Effective Width” at collapse (portion of panel that is capable of carrying post-buckling loads) to evaluate new ABD stiffness matrixes of the panel, Figure 101;
- the load in the “non-effective” part of the panel is held at the initial buckling load and the “effective” portion of panel carries additional load.

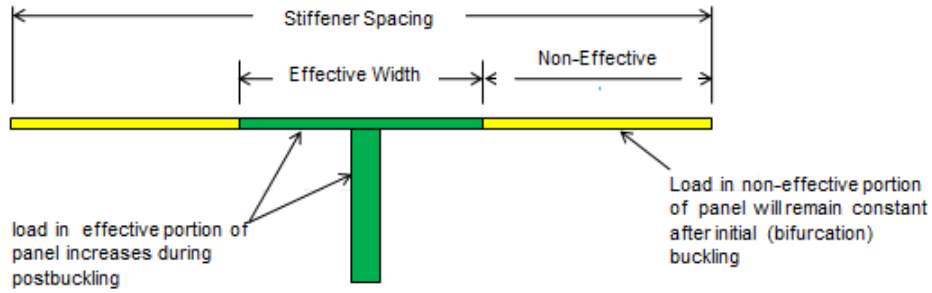


Figure 101: effective width of the panel

The “effective width” is found by the iteration.

At any load level below local buckling, the panel effective width is equal to the stiffener spacing. However, as the panel begins to postbuckle, the effective width becomes smaller and smaller, as illustrated for example in Figure 102.

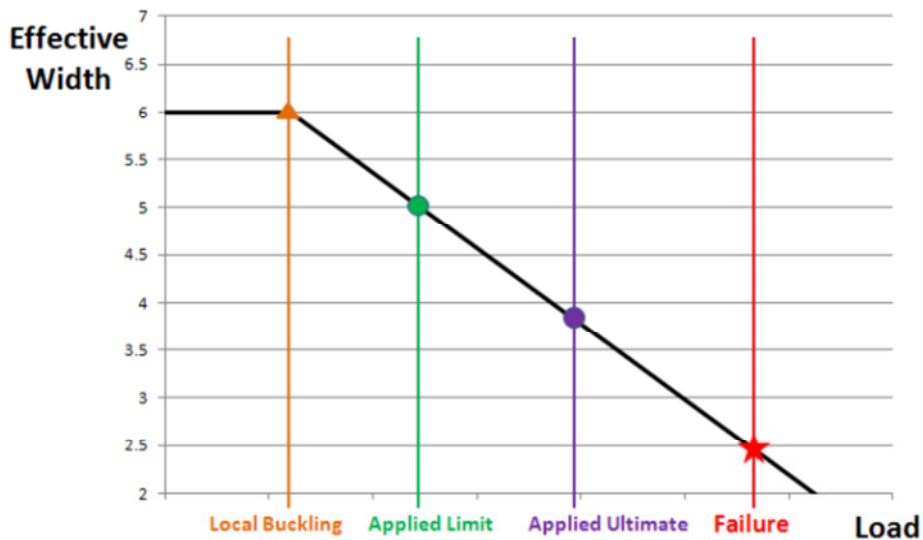


Figure 102: effective width of the panel vs load

---

**BIBLIOGRAPHY**

- [1] EASA AMC 20-29. Composite aircraft structure. 2010.
- [2] EASA CS-25. Certification specifications for large aeroplanes. 2010.
- [3] Hachenberg D. The role of advanced numerical methods in the design and certification of future composite aircraft structures. 5<sup>th</sup> world Congress on Computational Mechanics, WCCM V, Vienna, Austria, July 7-12, 2002.
- [4] Kassapoglou C. Design and analysis of composite structures with applications to aerospace structures. U.K.: John Wiley & Sons; 2010.
- [5] Baaran J. Visual inspection of composite structures. EASA Research Project. 2009.
- [6] ASTM D 7137/D 7137M – 07. Standard Test Method for Compressive Residual Strength Properties of Damaged Polymer Matrix Composite Plates.
- [7] Herszberg I, Bannister M K, Li H C H, Thomson R S, White C. Structural health monitoring for advanced composite structures in “Proceeding of 16th International Conference on Composite Materials”, Kyoto, Japan, (2007).
- [8] Kapoor H, Boller C, Giljohann S, Braun C. Strategies for structural health monitoring implementation potential assessment in aircraft operational life extension considerations in “Proceedings of 2nd International Symposium on NDT in Aerospace”, Hamburg, Germany, (2010).
- [9] Laveuve D M, Lehmann M, Erdmann K, Bütter A. SHM reliability demands on the multidisciplinary challenge of structural health monitoring in “Proceedings of 5th International Workshop of NDT Experts”, Prague, Czech Republic, (2009).
- [10] Lloyd P A. Structural Health Monitoring Systems - benefits and airworthiness issues. The Aeronautical Journal, 2008; 112: 285-289.
- [11] Boller C, Biemans C. Structural Health Monitoring in Aircraft - State of the Art, Perspectives and Benefits in “Structural Health Monitoring: Current Status and Perspectives”. Technomics Publishing company, Stanford, CA, U.S., 1997; 541-552.
- [12] ATA MSG-3. Operator/Manufacturer Scheduled Maintenance Development. 2003.
- [13] SAE International. Aerospace Recommended Practise. Guidelines for implementation of Structural Health Monitoring on Fixed Wing Aircraft. 2013.
- [14] Knight N F Jr, Rankin C C, Brogan F A. STAGS Computational Procedure for Progressive Failure Analysis of Laminated Composite Structures. International Journal of Non-Linear Mechanics, 2002; 37: 833-849.

- 
- [15] Sleight D W. Progressive Failure Analysis Methodology for Laminated Composite Structures. NASA Technical Paper, NASA/TP-1999-209107 (1999).
- [16] Moas E, Griffin O H Jr. Progressive Failure Analysis of Laminated Composite Structures. AIAA Journal, AIAA-97-1186, 1997; 2246-2256.
- [17] Puhui C, Zhen S, Junyang W. A new method for compression after impact strength prediction of composite laminates. J Compos Mater 2002; 36: 589–610.
- [18] Kassapoglou C, Jonas P J, Abbott R. Compressive strength of composite sandwich panels after impact damage: an experimental and analytical study. J Compos Technol and Res 1988; 10: 65–73.
- [19] Nyman T, Bredberg A, Schoen J. Equivalent damage and residual strength of impact damaged composite structures. J Reinforced Plast and Compos 2000; 19: 428–448.
- [20] Dost E F, Ilcewicz L B, Avery W B, Coxon B R. Effect of stacking sequence on impact damage resistance and residual strength for quasi-isotropic laminates. ASTM STP 1110, 476–500. 1991.
- [21] Xiong Y, Poon C, Straznicky P V, Vietinghoff H. A prediction method for the compressive strength of impact damaged composite laminates. Compos Struct 1993; 30: 357–367.
- [22] Kassapoglou C. Compression strength of composite sandwich structures after barely visible impact damage. J Compos Technol and Res 1996; 274–284.
- [23] Bailie J A, Ley R P, Pasricha A. A summary and review of composite laminate design guidelines. Northrop Grumman Report under NASA Contract NAS1-19347. 1997.
- [24] Collier Research Corporation. Hypersizer<sup>®</sup>, Software Package, Ver. 6.2.46. Hampton, VA, U.S., (2012). [www.hypersizer.com](http://www.hypersizer.com)
- [25] ASTM D 6484/D 6484M – 04. Standard Test Method for Open-Hole Compressive Strength of Polymer Matrix Composite Laminates.
- [26] Tan S C. A progressive failure model for composite laminates containing openings. J Compos Mater 1991; 25: 556-576.
- [27] Suemasu H, Takahashi H, Ishikawa T. On the failure mechanisms of composite laminates with an open hole subjected to compressive load. Compos Sci Technol 2006; 66: 634-641.
- [28] Lapczyk I, Hurtado J A. Progressive damage modeling in fiber-reinforced materials. Composites Part A 2007; 38: 2333-2341.
- [29] Xie D, Biggers S B. Postbuckling analysis with progressive damage modeling in tailored laminated plates and shells with a cutout. Compos Struct 2003; 59: 199-216.
- [30] Falzon B G, Apruzzese P. Numerical analysis of intralaminar failure mechanism in composite structures. Part II: applications. Compos Struct 2011; 93: 1047-1053.

- 
- [31] Tserpes K I, Labeas G, Papanikos P, Kermanidis T. Strength prediction of bolted joints in graphite/epoxy composite laminates. *Composites Part B Eng* 2002; 33: 521-529.
- [32] Aninfantis K N, Tsouvalis N G. Post buckling progressive failure analysis of composite laminated stiffened panels. *Appl Compos Mater* 2011; 1-18.
- [33] Orifici A C, de Zarate Alberdi I O, Thomson R S, Bayandor J. Compression and post-buckling damage growth and collapse analysis of flat composite stiffened panels. *Compos Sci Technol* 2008; 68: 3150-3160.
- [34] Schuecker C, Pettermann H E. Constitutive ply damage modeling, FEM implementation, and analyses of laminated structures. *Comput Struct* 2008; 86: 908-918.
- [35] Lin W P, Hu H T. Nonlinear analysis of fiber-reinforced composite laminates subjected to uniaxial tensile load. *J Compos Mater* 2002; 36: 1429-1450.
- [36] Borrelli R, Di Caprio F, Mercurio U, Romano F. Assessment of progressive failure analysis capabilities of commercial FE codes. *Int J Struct Integr* 2013; 4(3): 300-320.
- [37] Orifici A C, Herszberg I, Thomson R S. Review of methodologies for composite material modeling incorporating failure. *Compos Struct* 2008. 86: 194-210.
- [38] Reddy J N, and Pandey A. K. *A First-Ply Failure Analysis of Composite Laminates. Computers and Structures*, 1987; 25: 371-393.
- [39] Ochoa O, Reddy J N. *Finite Element Analysis of Composite Laminates. Kluwer Academic Publishers Dordreche, The Netherlands*, 1992.
- [40] Tsai S W, and Wu E M. A General Theory of Strength for Anisotropic Materials. *Journal of Composite Materials*, January 1971; 5: 58-80.
- [41] Tsai S W. *Strength Characteristics of Composite Materials. NASA CR-224*, 1965.
- [42] Hill R. A Theory of the Yielding and Plastic Flow of Anisotropic Metals. *Proceedings of the Royal Society of London, Series A*, 1948; 193: 281-297.
- [43] Azzi V D, Tsai S W. Anisotropic Strength of Composites. *Experimental Mechanics*, September 1965; 283-288.
- [44] Hoffman O. The Brittle Strength of Orthotropic Materials. *Journal of Composite Materials*, 1967; 1: 200-206.
- [45] Hashin Z. Failure criteria for unidirectional fiber composites. *J Appl Mech* 1980; 47: 329-334.
- [46] Murray Y, Schwer L. Implementation and verification of fiber-composite damage models. *Fail Criteria and Analysis in Dyn Response, ASME, AMD* 1990; 107: 21-30.
- [47] Petit P H, Waddoups M E. A method of predicting the nonlinear behavior of laminated composites. *J Compos Mater* 1969; 3: 2-19.

- [48] Nahas M N. Survey of failure and post-failure theories of laminated fiber-reinforced composites. *J Compos Technol and Res* 1986; 8(4): 138-153.
- [49] Hahn H T, Tsai S W. On the behavior of composite laminates after initial failures. *Astronautics and Aeronautics* 1983; 21: 58-62.
- [50] MSC Nastran<sup>®</sup>. Quick Reference Guide 2013.
- [51] ASTM D 7136/D 7136M – 07. Standard Test Method for Measuring the Damage Resistance of a Fiber-Reinforced Polymer Matrix Composite to a Drop-Weight Impact Event.
- [52] Borrelli R, Franchitti S, Di Caprio F, et all. A CAE based procedure to predict the low velocity impact response of a composite CAI specimen. *International CAE Conference* 2013. 21-22 October 2013.